SOME STUDIES ON ADDITIONAL SCALARS AT THE LHC

By

Ushoshi Maitra

(PHYS08201004001)

Harish-Chandra Research Institute, Allahabad

A thesis submitted to the

Board of Studies in Physical Sciences

In partial fulfillment of requirements

For the Degree of

DOCTOR OF PHILOSOPHY

of

HOMI BHABHA NATIONAL INSTITUTE

June, 2015

STATEMENT BY AUTHOR

This dissertation has been submitted in partial fulfillment of requirements for an advanced degree at Homi Bhabha National Institute (HBNI) and is deposited in the Library to be made available to borrowers under rules of the HBNI.

Brief quotations from this dissertation are allowable without special permission, provided that accurate acknowledgement of source is made. Requests for permission for extended quotation from or reproduction of this manuscript in whole or in part may be granted by the Competent Authority of HBNI when in his or her judgment the proposed use of the material is in the interests of scholarship. In all other instances, however, permission must be obtained from the author.

Ushoshi Maitra
(PhD Candidate)

DECLARATION

I, hereby declare that the investigation presented in the thesis has been carried out by me. The work is original and has not been submitted earlier as a whole or in part for a degree / diploma at this or any other Institution / University.

Ushoshi Maitra
(PhD Candidate)

List of Publications arising from the thesis

Journal

- An updated analysis of radion-Higgs mixing in the light of LHC data
  Nishita Desai, *Ushoshi Maitra*, and *Biswarup Mukhopadhyaya*
  Journal of High Energy Physics, **2013**, *Volume:2013, Issue:10, Article:093.*

- *Searching for an elusive charged Higgs at the Large Hadron Collider*
  Ushoshi Maitra, Biswarup Mukhopadhyaya, S. Nandi, S.K. Rai, and Ambresh Shivaji
  Physical Review D, ***2014***, *Volume:89, Issue:5, 055024-1-055024-12.*

- *Probing the light radion through diphotons at the Large Hadron Collider*
  Satyaki Bhattacharya, Mariana Frank, Katri Huitu, Ushoshi Maitra, Biswarup Mukhopadhyaya and S.K. Rai
  Physical Review D, ***2015***, *Volume:91, Issue:1, 016008-1-016008-11.*

List of other publications not related to this thesis

- Reconciling small radion vacuum expectation values with massive gravitons in an Einstein-Gauss-Bonnet warped geometry scenario
  Ushoshi Maitra, *Biswarup Mukhopadhyaya* and *Soumitra SenGupta*
  arXiv:1307.3018[hep-ph].

Ushoshi Maitra
(PhD Candidate)

Dedicated to

Baba and Ma

ACKNOWLEDGEMENTS

First of all I would like to express my gratitude towards my thesis supervisor Biswarup Mukhopdhyaya for involving me in the problems that are part of this thesis. I would also like to thank him for guiding me with all his patience.

I would like to thank all my collaborators Santosh Kumar Rai, Satyaki Bhattacharya, Soumitra SenGupta, Mariana Frank, Katri Huitu, Nishita Desai and Ambresh Shivaji for giving me the opportunity to work with them. I would like to thank Atri da for helping me out with various computational issues. I would like to thank Arindam, Arghya and Tanumoy for helpful discussions and suggestions

I would like to thank all my teachers who have encouraged me to pursue higher studies in physics.

I would like to thank all my friends of HRI especially Manoj da, Anushree di, Sabyasachi da, Sourav da, Sourabh da, Ujjal, Shankha, Nabarun, Maguni, Aritra, Dibyakanti, Juhi, Narayan and Taushif who have filled my journey of these five years with fun and laughter.

Finally I would like to thank my parents for supporting me and for bearing with my tantrums. I would like to thank my sister for everything. Without her presence it would not have been possible for me to complete this journey.

I would like to thank Arunabha for being there for me. I would like to thank him for clearing my doubts whenever I got stuck with something. I would also like to thank him for reading this thesis umpteenth time without complaining even once.

Finally, last but not the least, I would like to offer my sincere gratitude and thanks to everyone who had helped me in this endeavor whose names, unfortunately I failed to mention, inadvertently.

Contents

SYNOPSIS

The Standard model(SM) with gauge group $SU(3)_C \times SU(2)_L \times U(1)_Y$, is a unified framework of the elementary particles and the fundamental forces apart from gravity. The SM has two kind of fields: matter fields and gauge fields. The matter fields are three generation of quarks and leptons and the gauge fields are spin-1 particles that mediate the fundamental interactions. The mass of the gauge bosons as well as the fermions are generated by adding a SU(2) doublet of scalar fields. The potential of the doublet is chosen in such a way that its neutral component, known as the Higgs field, develops a vacuum expectation value (vev) which generates mass terms for the gauge bosons and the fermions. It involves spontaneously breaking the symmetry $SU(2)_L \times U(1)_Y \rightarrow U(1)_Q$. The $U(1)_Q$ as well as $SU(3)_C$ symmetry remain unbroken and hence, photons and gluons are massless.

Although the SM currently gives us the best description of subatomic world, it is unable to explain the disparity between the electroweak scale (of order 100 GeV) and the Planck scale (of order 10^{19} GeV), known as hierarchy problem. It doesn't have dark matter candidate and it lacks the explanation for the origin of flavor structure of fermions and baryon asymmetry. It is also a well established fact that neutrinos have tiny masses and SM is unable to explain that as well. The inadequacy of the SM to solve these problems, motivated particle physicists to look for a fundamental theory beyond SM, where some aspects of these puzzles can be incorporated. There are many scenarios embodying physics beyond Standard model (BSM), such as supersymmetry, extra dimensional models, multi-Higgs doublet models, that are capable of explaining hierarchy problem, origin of dark matter and flavor structure of fermions to varying degree of efficiency. Many of these BSM scenarios predict additional scalar sectors other than the SM Higgs. The parameters of SM, other than the Higgs, have been

precisely tested at Large Electron Positron collider(LEP), Tevatron and Large Hadron Collider(LHC). After the discovery of the scalar at 125 GeV at the LHC, the most natural question is whether it is the SM Higgs or imprint of some BSM scenario? Also, if we assume that the observed scalar comes from a BSM scenario, then to what extent this scenario is compatible with the existing experimental observables.

My thesis work includes constraining the parameter space of some of the BSM scenarios with the LHC 7+8 TeV data and finding efficient search strategies to discover additional scalars coming from various BSM scenarios, in the next run of LHC. In particular I have considered two BSM scenarios : The Randall-Sundrum(RS) model which is a warped extra dimensional model and two Higgs doublet model(2HDM).

The RS model has a non-factorizable geometry with an exponential warp factor. The additional dimension has an S_1/Z_2 orbifold symmetry, with two 3-branes residing at the orbifold fixed points. The SM fields are confined to one of the branes and gravity propagates in the bulk. When the warp-factor in the exponent has a value of about 35, mass parameters of the order of the Planck scale in the 'bulk' get scaled down to the TeV scale on the visible branch, thus providing a spectacular explanation of the hierarchy between the weak scale and the Planck scale. This model predicts TeV scale Kaluza-Klein(KK) graviton which can be detected in the colliders. However, LHC has not observed any signature of KK gravitons and its first KK mode has been excluded till 2.7 TeV.

Apart from the KK gravitons, the RS model has a canonically normalized modulus field, known as the radion. The radion gets its mass using the Goldberger-Wise mechanism, where a bulk scalar generates an effective 4-dimensional potential on the brane. Thus, mass of the radion is a free parameter and depends upon the mass of the bulk scalar. If we consider a light bulk scalar, then the mass of the radion can be lighter than TeV. The radion interacts with the matter via the trace of energy momentum tensor of the SM fields. Thus, even if we don't see the KK mode of gravitons and its bound increases, we still have a lighter signature of the RS model to probe at the colliders.

General covariance allows mixing between the Higgs and the radion. As a result, there are two states which are admixtures of both Higgs and radion. In the first project of this thesis I calculated the allowed parameter space of the Higgs-radion mixing from LHC $7 \oplus 8$ TeV data. We have constrained the Higgs-radion mixing in the parameter space of the mixing strength, mass of the scalars and the radion vev. We found that the LHC data rules out any possibility of the observed scalar to be a pure radion or radion-like state, but that it can be a Higgs-like state with a heavier or lighter radion-like state. A very light and a very heavy pure radion is allowed with the observed scalar being the SM Higgs. To make this analysis robust, we have considered the contribution from both the mass eigenstates in the WW^* channel to calculate the signal strength. The additional mass eigenstate gets affected differently by the cuts tuned for the SM Higgs of 125 GeV. To estimate this additional contribution, we have implemented cuts of ATLAS/CMS searches in WW^* channel. We showed that on considering contributions from both the masses for WW^* channel, we are able to rule out more parameter space. We have also considered the effect of interference of two states, when the two states are nearly degenerate i.e when they can not be distinguished by their mass peaks.

As a continuation of the earlier work, I developed search strategies for a very light pure radion of mass about 60 GeV in my second project. A light radion is allowed by LEP, Tevatron and LHC 7+8 TeV data. We found that the diphoton channel will be the best decay mode to study such a light radion. In spite of having relatively low branching ratio, it is possible to have a clean mass reconstruction in diphoton channel. After carrying out a detailed simulation, considering specific experimental issues and taking into account diphoton, single photon and dijet backgrounds, we found that on using (a) an improved isolation technique and (b) relatively stronger $\mathrm{p_T}$ cut on the final state photon we can observe a light radion at nearly 5σ significance for an integrated luminosity of $3000 fb^{-1}$. Thus, a radion as light as 60 GeV, having vev of 2 TeV can be probed in the next run of LHC. It was observed that a radion having mass of the order of 100 GeV can be probed at much lower luminosity.

After exploring the radion in my thesis extensively, we wanted to consider the status of other additional scalars coming from some other BSM scenarios. The simplest extension of the SM that conserves ρ parameter is addition of another $SU(2)$ doublet, more commonly known as two Higgs doublet model (2HDM). There are many motivation behind 2HDM for e.g, supersymmetry, axion model and baryon asymmetry.

I have studied the phenomenology of a charged Higgs in a neutrinophillic two Higgs doublet model as a part of my thesis work. This model was first proposed by Gabriel and Nandi, where they have three right handed neutrinos in addition to two Higgs doublets. Along with that there is an additional Z_2 symmetry. The SM particles are Z_2 even whereas the right handed neutrinos and the additional Higgs doublet are Z_2 odd. The essential point is that the neutrinos have Dirac masses and hence, lepton number is conserved. The neutrino mass are much lighter as compared to the other fermions because they couple with the second doublet. However, the Yukawa coupling is of the order of one, and the smallness of neutrino mass is an artifact of small vev (of order eV), for the second doublet. This small vev is achieved by spontaneously breaking the Z_2 symmetry. Thus, the charged Higgs of this model has distinct phenomenology as compared to the normal 2HDMs. The charged Higgs couple weakly to quarks and therefore the leptonic decay mode is the most promising one.

In this project we have performed a cut-flow based analysis for searching the charged Higgs. On considering the bounds from the recent astrophysical data, we found that the vev of the second doublet can not be lower than keV. As a result, the charged Higgs in this case becomes fermiophobic and hence, the only decay mode allowed is to W boson and a very light scalar, σ. We studied the pair production of the charged Higgs decaying to W and σ. We found that although the SM background overwhelms the signal coming from the charged Higgs at 8 TeV, at 14 TeV one can still have sufficient signal significance on using the combination of (a) p_T cut on the final state leptons and (b) cut on azimuthal angle between the leptons and the missing energy vector. We found that at 14 TeV a charged Higgs of mass about 150 GeV can be observed at

$3000 fb^{-1}$ with nearly 5σ significance.

List of Figures

List of Tables

Chapter 1

Introduction

1.1 The Standard Model

The standard model(SM) explains the interactions of the elementary particles upto nearly the TeV energy scale, as mediated by three of the four fundamental forces, namely, the strong, electromagnetic and weak forces. Gravitational interactions among the elementary particles are very weak at this energy regime and thus, can be neglected. The matter sector of the SM is made up of spin-1/2 particles called the fermions. The fermions are further classified into three generations of the quarks and leptons. The Lagrangian representing the interaction among the fermions should be invariant under local $SU(3)_C \times SU(2)_L \times U(1)_Y$ transformations. This is made possible by introducing vector fields, known as the gauge fields. The quanta of the gauge fields are the mediators of the fundamental forces and are known as the gauge bosons. The strong interactions among the quarks are mediated by the gluons and is based on the $SU(3)_C$ gauge group [10, 11, 12]. The electromagnetic interactions are mediated by the photons and the weak interactions are mediated by the weak bosons, namely $W^{\pm}$ and Z. The electromagnetic and weak interactions among the fermions are described in a unified way, by the electroweak theory [13, 14, 15] based on the gauge group $SU(2)_L \times U(1)_Y$. The three generators of the group $SU(2)_L$ are called the isospin op-

erators $T^i(i = 1, 2, 3)$. The isospin operators are proportional to the Pauli matrices $\tau^i(i = 1, 2, 3)$. The eight generators of the group $SU(3)_C$ are called the color operators and they are proportional to the Gell-Mann matrices λ^i where i = (1-8). Y is the generator of the U(1) gauge group and is called weak hypercharge operator. Y, T_3 and the electric charge Q are connected by the Gell-Mann Nishijima relation

$$Q = T_3 + \frac{Y}{2}. \tag{1.1.1}$$

The transformations and the eigenvalues of the first generation of the fermions under the gauge group $SU(3)_C \times SU(2)_L \times U(1)_Y$ are tabulated in 1.1.

Fermion	$SU(3)_C$	**Hypercharge, Y**	**Isospin**	T_3	EM charge, Q
d_R	3	$\frac{-2}{3}$	0	0	$\frac{-1}{3}$
u_R	3	$\frac{4}{3}$	0	0	$\frac{2}{3}$
$Q_L = \begin{pmatrix} u_L \\ d_L \end{pmatrix}$	3	$\frac{1}{3}$	1/2	+1/2, -1/2	$\frac{2}{3}$, $\frac{-1}{3}$
e_R	1	-2	0	0	-1
$L_L = \begin{pmatrix} \nu_L \\ e_L \end{pmatrix}$	1	-1	1/2	+1/2, -1/2	0, -1

Table 1.1: The eigenvalues and the transformations of the first family of quarks and leptons

The second and third generations of the fermions are exact replicas of the first generation except that masses increase progressively with generation number. The quark fields transform as a triplet under the $SU(3)_C$ gauge group whereas leptons are singlet. Thus, quarks participate in the strong interaction whereas leptons do not. Similarly, the left-handed fermions participate in the weak interaction. In the SM, the neutrinos are massless and do not have their right handed components. A gauge field is associated for each of the generators. Thus, we have eight gluon fields $G_\mu^{1,\ldots,8}$ corresponding to the color operators , three weak fields $W_\mu^{1,2,3}$ corresponding to the isospin operators

and B_μ corresponding to the generator Y. The field strengths are given by

$$\begin{aligned} G^a_{\mu\nu} &= \partial_\mu G^a_\nu - \partial_\nu G^a_\mu + g_s f^{abc} G^b_\mu G^c_\nu \\ W^a_{\mu\nu} &= \partial_\mu W^a_\nu - \partial_\nu W^a_\mu + g_2 \epsilon^{abc} W^b_\mu W^c_\nu \\ B_{\mu\nu} &= \partial_\mu B_\nu - \partial_\nu B_\mu \end{aligned} \tag{1.1.2}$$

where g_s,g_2 and g_1 are the coupling constants of $SU(3)_c$, $SU(2)_L$ and $U(1)_Y$ group respectively. f^{abc} and ϵ^{abc} are the structure constants of $SU(3)_c$ and $SU(2)_L$ gauge group respectively. A matter field ψ having isospin T and hypercharge Y interacts with the gauge fields via the covariant derivative D_μ given by

$$D_\mu = \partial_\mu - i g_s G^a_\mu \frac{\lambda^a}{2} - i g_2 W^a_\mu T^a - i g_1 \frac{Y}{2} B_\mu. \tag{1.1.3}$$

The kinetic part of the SM Lagrangian can be written as

$$\begin{aligned} \mathcal{L} &= \frac{-1}{4} W^a_{\mu\nu} W^{a\mu\nu} - \frac{1}{4} G^a_{\mu\nu} G^{a\mu\nu} - \frac{1}{4} B_{\mu\nu} B^{\mu\nu} \\ &+ \bar{L}_L i\gamma^\mu D_\mu L_L + \bar{Q}_L i\gamma^\mu D_\mu Q_L + \bar{e}_R i\gamma^\mu D_\mu e_R + \bar{d}_R i\gamma^\mu D_\mu d_R. \end{aligned} \tag{1.1.4}$$

Because of the non abelian nature of SU(2) and SU(3) gauge groups, G^a_μs and W^i_μs have self interaction terms present in the Lagrangian. Note that we haven't added mass terms for the fermions and gauge bosons yet. In the case of strong interaction, gluons are massless. In the electroweak theory, addition of the mass terms for the gauge bosons or the fermions spoils the invariance of the Lagrangian $\mathcal{L}$ under the $SU(2)_L \times U(1)_Y$ symmetry group. The mass of the fermions and the gauge bosons are generated by the Higgs mechanism [16, 17, 18, 19, 20] which is outlined briefly in the next section.

1.2 The Higgs mechanism

In the Higgs mechanism, an SU(2) doublet Φ of complex scalar fields is introduced with a scalar potential V_Φ. The scalar potential is chosen such that it has degenerate minima. The neutral component of the scalar field then develops a vacuum expectation value(vev) which spontaneously breaks the gauge symmetry $SU(2)_L \times U(1)_Y$ to the gauge symmetry of electromagnetism $U(1)_{em}$. The phenomena of spontaneous breakdown of the SM gauge symmetry generates masses for the gauge bosons and fermions. The doublet Φ with hypercharge +1 is defined as

$$\Phi = \begin{pmatrix} \Phi^+ \\ \\ \Phi^0 \end{pmatrix} \tag{1.2.5}$$

where $\Phi^+ = \sqrt{\frac{1}{2}}(\Phi_1 + i\Phi_2)$ and $\Phi^0 = \sqrt{\frac{1}{2}}(\Phi_3 + i\Phi_4)$. The Lagrangian density of Φ is given by $\mathcal{L}_\Phi$,

$$\mathcal{L}_\Phi = |(\partial_\mu - ig_2 W_\mu^a T^a - ig_1 \frac{Y}{2} B_\mu)\Phi|^2 - V_\Phi(\Phi^\dagger \Phi), \tag{1.2.6}$$

where $V_\Phi(\Phi^\dagger\Phi) = \mu^2\Phi^\dagger\Phi + \lambda(\Phi^\dagger\Phi)^2$. The interactions of the charged leptons with the scalar doublet Φ is given by $\mathcal{L}_\Phi^F$,

$$\mathcal{L}_\Phi^F = -y_l \bar{L}_L \Phi l_R. \tag{1.2.7}$$

When $\mu^2 < 0$, the potential has degenerate minima given by the condition

$$\Phi^\dagger\Phi = \frac{-\mu^2}{2\lambda} \equiv \frac{v^2}{2}.$$

Taking advantage of the gauge freedom one can chose the vacuum expectation value(vev) of the Φ doublet in such a way that only the neutral component exist with

a value v,

$$\langle\Phi\rangle_0 \equiv \langle 0|\Phi|0\rangle = \begin{pmatrix} 0 \\ \\ \frac{v}{\sqrt{2}} \end{pmatrix}, \tag{1.2.8}$$

where $v = \sqrt{\frac{-\mu^2}{\lambda}}$. The scalar doublet Φ can be expanded about its vev as

$$\Phi(x) = e^{\frac{i\xi^a\tau^a}{2v}} \begin{pmatrix} 0 \\ \\ \frac{v+H(x)}{\sqrt{2}} \end{pmatrix} \tag{1.2.9}$$

where $\xi_1(x), \xi_2(x), \xi_3(x)$ and $H(x)$ have zero vevs. On removing the phase factor of the doublet by a suitable SU(2) transformation, the Φ can be written as,

$$\begin{pmatrix} 0 \\ \\ \frac{v+H(x)}{\sqrt{2}} \end{pmatrix},$$

where $H(x)$ is called the Higgs field. This act of preferring a vacuum over the other degenerate vacua break the $SU(2)_L \times U(1)_Y$ invariance. The covariant derivative can be expressed as,

$$\begin{aligned} |D_\mu\Phi|^2 &= |(\partial_\mu - ig_2 W_\mu^i \frac{\tau^i}{2} - ig_1 \frac{1}{2} B_\mu)\Phi|^2 \\ &= \frac{1}{2}(\partial_\mu H)^2 + \frac{1}{8} g_2^2 (v+H)^2 |W_\mu^1 + iW_\mu^2|^2 + \frac{1}{8}(v+H)^2 |g_2 W_\mu^3 - g_1 B_\mu|^2. \end{aligned} \tag{1.2.10}$$

In (1.2.10), the fields B_μ and W_μ^3 mix in such a manner that to obtain the physical mass eigenstates A_μ and Z_μ, one has to rotate them by an angle known as the Weinberg angle $\theta_W = \tan^{-1}(g_1/g_2)$. If the new fields are defined as

$$W_\mu^\pm = \frac{1}{\sqrt{2}}(W_\mu^1 \mp W_\mu^2), Z_\mu = \frac{g_2 W_\mu^3 - g_1 B_\mu}{\sqrt{g_2^2 + g_1^2}} \text{ and } \mathrm{A}_\mu = \frac{\mathrm{g_2 W_\mu^3 + g_1 B_\mu}}{\sqrt{\mathrm{g_2^2 + g_1^2}}},$$

then the Lagrangian $\mathcal{L}_\Phi$ in terms of the new fields becomes,

$$\begin{aligned}\mathcal{L}_\Phi &= \frac{1}{2}\partial_\mu H \partial^\mu H + \frac{1}{4}g_2^2 W_\mu^+ W^{\mu-}(v+H)^2 + \frac{1}{8}(g_2^2+g_1^2)(v+H)^2 Z_\mu Z^\mu \\ &+ \frac{\lambda v^2}{2}(v+H)^2 - \frac{\lambda}{4}(v+H)^4. \end{aligned} \tag{1.2.11}$$

The masses of the gauge bosons are given by

$$M_W = \frac{1}{2}g_2 v \text{ and } M_Z = \frac{1}{2}g^{'}v = \frac{1}{2\cos\theta_W}g_2 v \tag{1.2.12}$$

where $g^{'} = \sqrt{g_2^2+g_1^2}$. As the electromagnetism $U(1)_{em}$ symmetry and $SU(3)_C$ color symmetry are unbroken, the photon and gluons are massless.
Due to the spontaneous symmetry breaking of $SU(2)_L \times U(1)_Y \rightarrow U(1)_{em}$, the couplings are related by the relation

$$g_1 \cos\theta_w = g_2 \sin\theta_w = e$$

where e is the electromagnetic coupling constant.
Similarly, fermion masses are obtained from the Lagrangian L_Φ^F where

$$L_\Phi^F = \frac{-1}{\sqrt{2}}\lambda_l \bar{L}_R \begin{pmatrix} 0 \\ v+H \end{pmatrix} l_R - \frac{1}{\sqrt{2}}\lambda_d \bar{Q}_L \begin{pmatrix} 0 \\ v+H \end{pmatrix} d_R - \frac{1}{\sqrt{2}}\lambda_u \bar{Q}_L i\tau_2 \begin{pmatrix} 0 \\ v+H \end{pmatrix} u_R. \tag{1.2.13}$$

The masses of the fermions are given by

$$m_l = \frac{1}{2}\lambda_l v \text{ and } m_q = \frac{1}{2}\lambda_q v. \tag{1.2.14}$$

The standard model is the theory of $SU(3)_C \times SU(2)_L \times U(1)_Y$ with the inclusion of electroweak symmetry breaking. The electroweak phenomena have been tested at various colliders such as the Tevatron, Large electron positron(LEP) collider and Large

Hadron collider(LHC). Till now, no serious deviations have been observed from the predictions of the SM apart from existence of the neutrino mass. However, discovery of the Higgs has all along been the litmus test for validating the SM. On the 4th of July 2012, the LHC has observed a scalar with mass close to 125 GeV [21, 22]. The properties of the discovered scalar are close to the SM Higgs predictions. However, there are discrepancies and the next run of the LHC will help us to probe the scalar further. In spite of the success of the SM in explaining most of the electroweak processes, it is unable to explain some of existing puzzles in the frontier of particle physics. This motivated us to look for a fundamental theory whose low energy behaviour corresponds to the SM. The existing puzzles as well as some of the BSM scenarios offering plausible solutions are discussed in the following sections.

1.3 Why beyond the Standard Model?

Some of the issues that can not be explained within the SM are:

- **Neutrino mass generation:** It is now a well established fact that neutrinos have small masses, of the order of eV, which can not be accommodated within the described structure of the SM. The neutrino mass can be accommodated with the inclusion of right-handed neutrinos in the SM. However, to generate the neutrino masses using the Dirac mass term with the Higgs doublet, left-handed SU(2) doublet leptons and right-handed SU(2) singlet neutrinos, the Yukawa coupling should be 10^{-12} times smaller than the top coupling y_t. This is a highly fine tuned scenario which raises concerns over the validation of the SM [9, 23, 24, 25, 26].

- **Dark matter candidate:** The rotation curves of spiral galaxies first indicated the presence of dark matter. The cosmological and astrophysical observations predicted that the total matter density of the universe is $\Omega_M h^2 = 0.1358$ where h is the Hubble parameter. The measurement on the abundances of the light chemical elements estimated the baryonic density $\Omega_B h^2$ of about 0.02. The rest

of the matter in the universe is made up of non-baryonic and non-luminous materials. The SM lacks explanation of the dark matter present in the universe [27, 28, 29, 30, 31].

- **Flavor structure of the fermions:** The SM does not explain why there should be only three generations of the fermions. Also, SM is incapable of explaining the hierarchy among the masses of the fermions. It does not even explain why mixing matrix of quarks and leptons are so drastically different from each other.

- **Baryon asymmetry:** Our universe is baryon dominated i.e there is excess of baryons over antibaryons. The SM is unable to explain such matter antimatter asymmetry [32, 33].

- **Naturalness Problem:** The Higgs mass is sensitive under quantum corrections. If the coupling of the SM Higgs with the fermion f is given by $\lambda_f \bar{f} f H$, then the correction received by the Higgs mass from the fermionic loop is

$$\Delta M_H^2 = -\frac{|\lambda_f|^2}{8\pi^2}\Lambda_{UV}^2 \tag{1.3.15}$$

  where Λ is the cut-off energy scale till which the SM is valid. If we assume that the SM is valid till the Planck scale, then the correction of the Higgs mass is huge. For the Higgs below TeV, the counter term has to be adjusted order by order in a fine-tuned manner. Thus, one has to rely on an unnatural phenomena to obtain Higgs at the weak scale. This is also known as the hierarchy problem [34, 35].

- **No clue to further unification:** In the SM, the running of the electroweak and strong couplings are such that it is difficult to achieve unification of all couplings at high scale. Also the gravitational force is completely outside the scope of all dimensions. Thus, one may consider a fundamental theory which unifies four fundamental forces instead of just two.

These aforementioned problems motivated people to look for a fundamental theory where some (if not all) of them can be explained. My thesis is based on the phenomenology of additional scalars that arises from scenarios beyond the Standard model. Some of the new physics scenarios predicting additional scalars are briefly discussed in the next section.

1.4 Additional scalars coming from new physics

The scalar structure of the SM is intimately connected with a parameter known as ρ-parameter. The ρ-parameter is defined as the relative strength of the weak neutral current with respect to the weak charged current. Thus,

$$\rho = \frac{M_W^2}{M_Z^2 \cos^2\theta_W}. \tag{1.4.16}$$

If we have a $SU(2)_L \times U(1)_Y$ gauge theory, with n scalar multiplets Φ_i having weak isospin T_i, weak hypercharge Y_i and vev of the neutral component of the scalar multiplet v_i, then the ρ-parameter at tree level is

$$\rho = \Sigma_{i=1}^{n} \frac{[4T_i(T_i+1) - Y_i^2]\, v_i^2}{\Sigma_i 2Y_i^2 v_i^2}. \tag{1.4.17}$$

The experimentally measured value of the ρ-parameter is $1.0004^{+0.0003}_{-0.0004}$. Thus, the value of ρ-parameter controls the way one can extend the scalar sector of the SM. One can achieve the experimental value of ρ-parameter with the following scalar structures:

- **Only one SU(2) doublet:** In the SM, we have one SU(2) doublet (T = 1/2, Y = 1) where the neutral component gets the vev v, then

$$\rho = \frac{(4(1/2)(1/2+1) - 1)v^2}{2 \times 1 \times v^2} = 1.$$

- **One SU(2) doublet and one SU(2) singlet:** If we have an SU(2) doublet(T = 1/2) with vev v(Y = 1) and an SU(2) singlet with vev v_s and hypercharge $y_s = 0$ then

$$\rho = \frac{(4 \times 1/2(1/2+1) - 1)v^2 + (4y_s^2 v_s^2)}{2v^2 + 2y_s^2 v_s^2} = 1.$$

In general, ρ-parameter remains unity at the tree-level for an arbitrary number of SU(2) doublet and singlet scalar. However, this is not true when higher representations of SU(2) are involved in electroweak symmetry breaking.

Some of the models predicting a singlet scalar along with the SM Higgs are

– **Randall-Sundrum model:** The Randall-Sundrum model is a warped extra dimensional model where along with the SM fields there exist a scalar metric fluctuation, known as the radion [36, 37, 38]. The radion couples to the trace of the energy-momentum tensor. We will discuss the RS model and the radion phenomenology thoroughly in chapter 2 and 3.

– **Dilatonic models:** Dilaton is a pseudo-Nambu Goldstone boson that arises from spontaneous symmetry breaking of the conformal symmetry. If the scale of conformal symmetry breaking f is higher than the electroweak scale v, then the theory predicts a dilaton having mass of the order of weak scale along with the SM Higgs. The dilaton couples with SM particles through the trace of the energy momentum tensor. The couplings of the dilaton are similar to the couplings of the SM Higgs with vev of the SM-Higgs replaced by the scale f. The massless gauge bosons couple via the trace anomaly terms which are proportional to the β-functions [39, 40, 41]. One may note that the coupling of the radion and dilaton are exactly the same.

– **Higgs portal models:** In these models, there are particles which are not charged under the SM group and commonly referred as the hidden sector [42]. There are several possibilities for the structure of the hidden sector.

* One of them is used as a solution for the dark matter problem [43, 44]. There is an additional real scalar field S which is uncharged under the SM gauge group. A Z_2 discrete symmetry is added under which the scalar field S is odd. S can couple with the SM Higgs in the gauge invariant way via $y_s S^2 H^\dagger H$. The scalar S can be considered as the dark matter candidate. The relic density has been calculated as a function of the various parameter m_s and y_s keeping the SM Higgs mass at 125 GeV. The scalar S doesn't get any vev and the Z_2 symmetry remains unbroken. Thus, the scalar S can not mix with the SM Higgs but contributes to the invisible decay width of the SM Higgs. The invisible branching ratio of the SM Higgs further constrain the parameter space.

* Another possibility is that the particles of the hidden sector are charged under a U(1) symmetry group [45]. This is known as the hidden abelian Higgs model where there is an additional U(1) symmetry group along with the SM gauge group. In the SM, there are two gauge invariant operators with mass dimension less than 4 which are $B_{\mu\nu}$ and $|\Phi_{SM}|^2$. These operators can couple to the hidden sector abelian gauge boson X and Higgs Φ_H in a gauge invariant way via the terms $X_{\mu\nu}B^{\mu\nu}$ and $|\Phi_H|^2|\Phi_{SM}|^2$. Once $U(1)_X$ is broken by the vev of the hidden scalar Φ_H, we have two CP even scalars that are admixtures of the SM Higgs and the hidden Higgs. An additional neutral gauge boson $Z^{'}$ comes from the term involving kinetic mixing. The couplings of the CP scalars and $Z^{'}$ to the SM particles are used to explore the hidden world. If there are fermions in the hidden sector that are charged under the $U(1)_X$ then the lightest fermion can be considered as the dark matter candidate. There is an accidental Z_2 symmetry that ensures the stability of the dark matter candidate [46].

- **Two SU(2) doublets:** If we have two SU(2) doublets with hypercharge $Y = \pm 1$ then $T(T+1) = 3/4Y^2$ i.e ρ-parameter remains always 1. There are wide classes of models having two SU(2) doublets which are commonly known as the two Higgs doublet models. The two Higgs doublet models are used to solve various problems of the SM [47]. An interesting motivation for two Higgs doublets is found in the minimal supersymmetric standard model(MSSM) where an additional doublet is required [34]. Axion models also predict two Higgs doublets. Peccei and Quinn observed that a small CP-violating term in the QCD Lagrangian can be rotated away by using a global U(1) symmetry. The U(1) can be incorporated in the presence of two Higgs doublets [48]. Also a single SU(2) doublet is unable to produce the required baryon asymmetry [49]. Two Higgs doublet models can be used to generate the required asymmetry because of additional CP violating term present in the Lagrangian. We will discuss two Higgs doublet models in details in chapter 5. A variation of such models can be used to generate small neutrino masses. The charged Higgs of this neutrino mass model offers a peculiar signature that can be probed at the colliders. We have discussed some implications of this model in chapter 6.

  There are models with further extended scalar structure involving singlets and doublets. For example, two two Higgs doublets coexisting with one SU(2) singlet scalar is the next to minimal supersymmetric standard model(NMSSM) [34]. This model not only can explain the naturalness of the Higgsino mass parameter, but also provides a good fit for the scalar mass around 125 GeV.

- **One SU(2) doublet and one SU(2) triplet:** A combination of one SU(2) doublet with hypercharge $Y = \pm 1$ and an SU(2) triplet can preserve the ρ parity if,

  - the hypercharge Y of the triplet is 0 and the vev of the triplet is negligible as compared to the vev of the SU(2) doublet.

– the hypercharge Y of the triplet is 2 and ratio of the vev of the triplet to vev of the doublet is less than 2 %. For example, the type-II seesaw model [50, 51] predicts an $SU(2)_L$ triplet scalar field $\overrightarrow{\Delta} = (\Delta^{++}, \Delta^{+}, \Delta^{0})$ known as messenger field along with the SM Higgs doublet. A nonzero vev of the SU(2) doublet induces a non zero vev to the neutral component of the triplet which generates Majorana mass term for the neutrinos. In this model, there are seven scalar mass eigenstates; two doubly charged Higgs, two singly charged Higgs, two CP-even scalars and one CP-odd scalar.

– Another variation of the type-II seesaw model is called the Georgi-Machacek model [52, 53, 54] where along with one SU(2) doublet, two SU(2) triplets with hypercharge Y = 0 and Y = 2 are added. The electroweak scale is generated by the doublet and triplets. If the vev of the neutral component of both the triplets are same then the ρ-parameter remains at unity at the tree level. Thus, in contrast to the type-II seesaw model, even sizeable vev of the triplet preserves the value of ρ-parameter.

After discussing the SM and its incapability to address some of the issues, it is necessary to discuss the machine with which these scalars can be probed i.e colliders. I'll be presenting a brief review of the LHC and status of the Higgs searches at the LHC in the following sections.

1.5 The Large Hadron Collider

The Large Hadron Collider is the hitherto largest particle accelerator that has been devised to probe TeV scale interactions [55, 56]. It is situated at CERN and is approximately buried 100 m underground. It is placed inside a circular tunnel of 27 km circumference containing superconducting magnetic materials. There are accelerating electric fields that enhance the energy of colliding particles in bunches. It is a proton proton collider that has been designed to produce highest centre of mass energy

of 14 TeV. Apart from protons, the LHC has also been built to collide lead ions for studying heavy ion physics. The beams are maintained on their circular tracks with magnetic fields, and accurate focussing is done with the help of an array of magnetic quadrupoles. The two high energy particle beams travel in opposite directions in separate beam pipe. The beams inside the LHC are made to collide at four major particle detectors:

- **ATLAS(A Toroidal LHC Apparatus):** The detector has been designed to study the electroweak phenomena of the SM as well as to look for exotic particles that may arise from various scenarios beyond the SM(BSM). The ATLAS detector is the largest particle detector constructed till date. It is 46m long, 25m high and 25m wide. It weighs about 7000 tonne.

- **CMS(Compact Muon Solenoid):** The scientific goals of the detector are similar to that of the ATLAS. The CMS is constructed around a huge solenoid magnet. It is 21m long, 15 m wide and 15 m high. It appears as a cylindrical coil of superconducting cable which generates magnetic field of about 4 Tesla. The magnetic field is confined by a steel yoke. Due to the yoke present inside CMS, it weighs about 14,000 tonne.

- **LHCb(Large Hadron Collider beauty):** The detector has been developed to study matter-antimatter asymmetry using b-quarks.

- **ALICE(A Large Ion Collider Experiment):** It is a heavy ion detector that has been designed to study quark gluon plasma.

Apart from these four detectors, there are two smaller detectors: **TOTEM**(Total elastic and diffractive cross section measurement) and **LHCf**(Large Hadron Collider Forward). These two detectors are designed to study forward particles i.e the particles which pass each other during the collision. These two detectors are positioned on the either side of ATLAS and CMS. TOTEM detectors are placed across half a kilometer

around the interaction point of the CMS.TOTEM is designed to study protons emerging from collisions at small angles. The LHCf is situated at 140 m on either side of the ATLAS collision point. The LHCf uses particles thrown forward by ATLAS collisions and simulates cosmic ray in laboratory conditions.

Unlike electron-positron colliders such as LEP, in a hadron collider, only a fraction of total centre of mass energy is used to probe the physics scale. This fraction of energy is carried by the quarks and gluons, known together as partons. Thus, in spite of 14 TeV centre of mass energy, scales upto a few TeV can be probed at the LHC. Another important parameter is the instantaneous luminosity, defined as the number of particles passing each other per unit time per unit transverse area at the interaction point. If there are n_1 number of particles in beam 1 and n_2 number of particles in beam 2, then the instantaneous luminosity L is fn_1n_2/a where f is the crossing frequency and a is the transverse area. The designed luminosity of the LHC is $10^{34}cm^{-2}s^{-1}$ which is expressed as $10nb^{-1}s^{-1}$. This value of instantaneous luminosity is equivalent to integrated luminosity of $100fb^{-1}/year$.

The accumulation of data at the LHC has been divided into three major runs. The LHC run-1 started with 7 TeV centre of mass energy. During the year 2012, the machine was upgraded to 8 TeV and collected 30 fb^{-1} of data. During this period ATLAS and CMS has independently confirmed the existence of a scalar around 125 GeV. After LHC-run 1, there was a shutdown for the span of two years. LHC has again started at 13 TeV in March, 2015. The plan is that the machine will be upgraded to 14 TeV. During 2018-19, there will be a shutdown for two years and the machine is expected to collect $300fb^{-1}$ of data afterwards. The machine is expected to collect $3000fb^{-1}$ of data by 2025.

1.6 Some basic kinematics of LHC

The laboratory(lab) frame of the collider is defined as the centre of mass frame of the proton system. However, partons participating in the hard scattering carry fraction of

the proton momentum and hence their centre of mass frame is longitudinally boosted with respect to the lab frame. The proton beam direction is considered as the longitudinal direction (z-axis) and the two mutually perpendicular directions constitute the transverse plane. It is convenient to write the 4-momentum of the particle(E, p_x, p_y, p_z) using the variables that transform in a simplified way under the longitudinal boost. The magnitude of the transverse component of the momentum and azimuthal angle ϕ are invariant under the longitudinal boost. The rapidity y of the particle with 4-momentum p^μ is defined as

$$y = \frac{1}{2} \ln \frac{E + p_z}{E - p_z}. \tag{1.6.18}$$

In effect, rapidity is a measure of the boost of the parton centre-of-mass frame with respect to the laboratory frame. Rapidities are additive in nature, under longitudinal boosts [56]. Also, the difference between two rapidities i.e Δy is an invariant quantity under any such boosts. The 4-momentum of a particle can also expressed as

$$p^\mu = (E_T \cosh y, p_T \cos\phi, p_T \sin\phi, E_T \sinh y) \tag{1.6.19}$$

where $E_T = \sqrt{p_T^2 + m^2}$ is the transverse energy. In the massless limit where $E >> p_z$,

$$y \to \ln \cot \frac{\theta}{2} \equiv \eta \tag{1.6.20}$$

where η is known as pseudorapidity and has one to one correspondence to the polar angle θ. The separation between two objects in the transverse plane is realized by a boost invariant quantity $\Delta R = \sqrt{\Delta\eta^2 + \Delta\phi^2}$.

At a collider, any SM or BSM process is characterized by the interaction of the particles present in the final states with the materials of the collider. The short lived particles such as massive particles like $W^\pm$, Z and top decay instantaneously and they can be identified by reconstructing the kinematic variables of the mother particle from daughter particles i.e the decay products. One of the kinetic variable which plays a pivotal

role in identifying the mother particle for the s-channel process is the invariant mass m_{inv} defined by

$$m_{inv} = \sqrt{(p_{d1} + p_{d2})^2} \tag{1.6.21}$$

where p_{d1} and p_{d2} are the 4-momentum of the daughter particles. During resonant production of the mother particle, invariant mass coincides with the mass of the mother particle. The leptons, jets and photons are identified through their interactions with the materials of the detectors. If a particle is stable i.e it does not participate in strong and weak interaction or is long lived, then the particle escapes detection at the LHC. The stable particles can be identified through the missing transverse energy ($\not{E}_T$). The missing transverse energy is quantified as the net momentum imbalance in the transverse plane,

$$\overrightarrow{\not{E}}_T = -\Sigma_{n=i}\overrightarrow{p_T}^i \tag{1.6.22}$$

where i sums over all visible final states, including jets, leptons, photons and the so called 'unclustered components' which do not satisfy the triggers for either of the above. However, if there are more than one stable particle in the process, then the variables of the invisible decay products can not reconstructed.

1.7 Particle detection at the LHC

In this thesis, we are interested in the search of additional scalars coming from various scenarios beyond the standard model at the ATLAS and CMS. I'll be discussing the basic structure of these two detectors. A typical detector is made up of charge tracking system, electromagnetic calorimeter, hadronic calorimeter and muon chamber.

- **Tracker:** Tracking chamber determines the trajectory of the charged particles. The rapidity coverage for the tracking chamber for ATLAS and CMS is $|\eta| < 2.5$. In presence of the magnetic field(B), the curvature of the trajectory κ is used to

calculate momentum of the charged particle using the relation,

$$\kappa = \frac{QB}{p}, \tag{1.7.23}$$

where Q is the electric charge. Once momentum of the particle is known, velocity is calculated by using the energy loss measurement. The energy loss by excitations and ionisation of the charged particle can be scaled in a mass independent way with the charge to velocity ratio,

$$\frac{dE}{dx} = (\frac{Q}{\beta})^2.$$

The mass of the particle can then be deduced from the momentum and velocity. If the charge of the particle is not known, then one has to rely on some additional measurements such as time of flight.

The calorimeters are designed to measure energy loss of the particles as it passes through it. Generally, calorimeters absorb most of particles coming from the hard process. There are two types of calorimeters:

- **Electromagnetic Calorimeter(ECAL):** The electromagnetic calorimeter surrounds the tracking chamber. Electrons and photons interact with the material of th electromagnetic calorimeter and produces cascade of electromagnetic showers due to brehmsstralung and pair production. The number of particles created in the cascade increases exponentially with the depth of the material. The incident energy measured by the electromagnetic calorimeter is proportional to the number of particles created. The rapidity coverage of ECAL for ATLAS and CMS is $|\eta_{e,\gamma}| \sim 3$. ATLAS uses liquid Argon calorimeter where CMS uses $PbWO_4$ scintillating crystal.

- **Hadron Calorimeter(HCAL):** The HCAL is located outside ECAL. In the HCAL, high energy hadrons interact with the HCAL material and produce showers of

hadrons. The rapidity coverage of the HCAL is $|\eta| \sim 5$ for ATLAS and CMS. HCAL measures the incident energy of the hadrons.

- **Muon chamber:** The muon chamber is located outside the HCAL. The high energy muons interact weakly with the materials of calorimeters and travel longer distance before decaying. Hence, muons are detected at the outermost chamber where the transverse momentum of the muon is measured precisely. For both detectors, the rapidity coverage of muon chamber is $|\eta| < 2.7$.

1.8 Higgs searches at the LHC

One of the most important scientific goals of the LHC has been to discover the SM Higgs and to probe its properties. In this section I'll briefly discuss the status of the Higgs searches at the LHC [6, 7, 57] At the LHC, Higgs is produced mainly via

- Associated Production with W,Z: $q\bar{q} \rightarrow V + H$
- vector boson fusion: $qq \rightarrow V^*V^* \rightarrow qq + H$
- gluon-gluon fusion: $gg \rightarrow H$
- associated production with the heavy quarks: $gg, q\bar{q} - > Q\bar{Q} + H$.

Out of them, the gluon fusion channel is the dominant production mode for the SM Higgs. For a heavy Higgs ($m_H > 800GeV$), the production cross section of the vector boson fusion channel is comparable to the gluon fusion mode. The other associated production processes are suppressed by several order of magnitudes. The vector boson fusion channel is characterized by two forward jets with high invariant mass that can be used as a discriminating 'tag' for identifying the signal.
The Higgs searches are divided into

- **Low mass region:** The promising channels for a low mass Higgs($M_H < 150GeV$) are its decay to pair of photons, $b\bar{b}$ and $\tau^+\tau^-$. In spite of low branching ratio,

the $H \to \gamma\gamma$ channel offers clean mass reconstruction and is the main detection channel for $M_H < 135GeV$. On demanding a narrow invariant mass peak of diphoton system, one can get rid of the continuous diphoton and single photon backgrounds. Other than diphoton channel, the SM Higgs has been searched in WW^* and ZZ^* channels. The ATLAS and CMS have also probed associated production of Higgs and its decay to $b\bar{b}$ and $\tau\tau$ channels.

- **Intermediate mass region** When Higgs lies in the mass range $120 < M_H < 2 \times M_Z$, $H \to WW^* \to ll\nu\nu$ is the most promising channel for its detection. Since, Higgs mass can not be reconstructed in this channel, one should apprehend the signal by calculating the excess over the background. The most important backgrounds are the continuum W pair production and top pair production. The WW background can be reduced by exploiting the spin correlations in $H \to WW^* \to ll\nu\nu$. The leptons should be collinear, i.e the azimuthal separation between two lepton peak over small values for the signal than the background.

- **High mass region:** In the mass region where $M_H > 2M_Z$, the decay $H \to ZZ \to 4l$ is considered as the "gold plated mode" and can be used to probe SM Higgs up to TeV mass scale. The channel has negligible background that can be removed using cuts on the transverse momentum of the leptons. One can reconstruct the Higgs from the invariant mass of the four lepton system.

A summary of the search results for the discovered scalar in terms of the signal strength is given in figure 1.1.

My thesis is divided into two parts. The first part includes chapters 2, 3 and 4 where I have given a brief introduction of the warped extra dimension scenario and also discussed the phenomenology of the radion at the LHC. The second part is comprised of chapters 5 and 6 where I have summarized two Higgs doublet models and discussed the phenomenology of a charged Higgs at the LHC, in the rather unusual case where

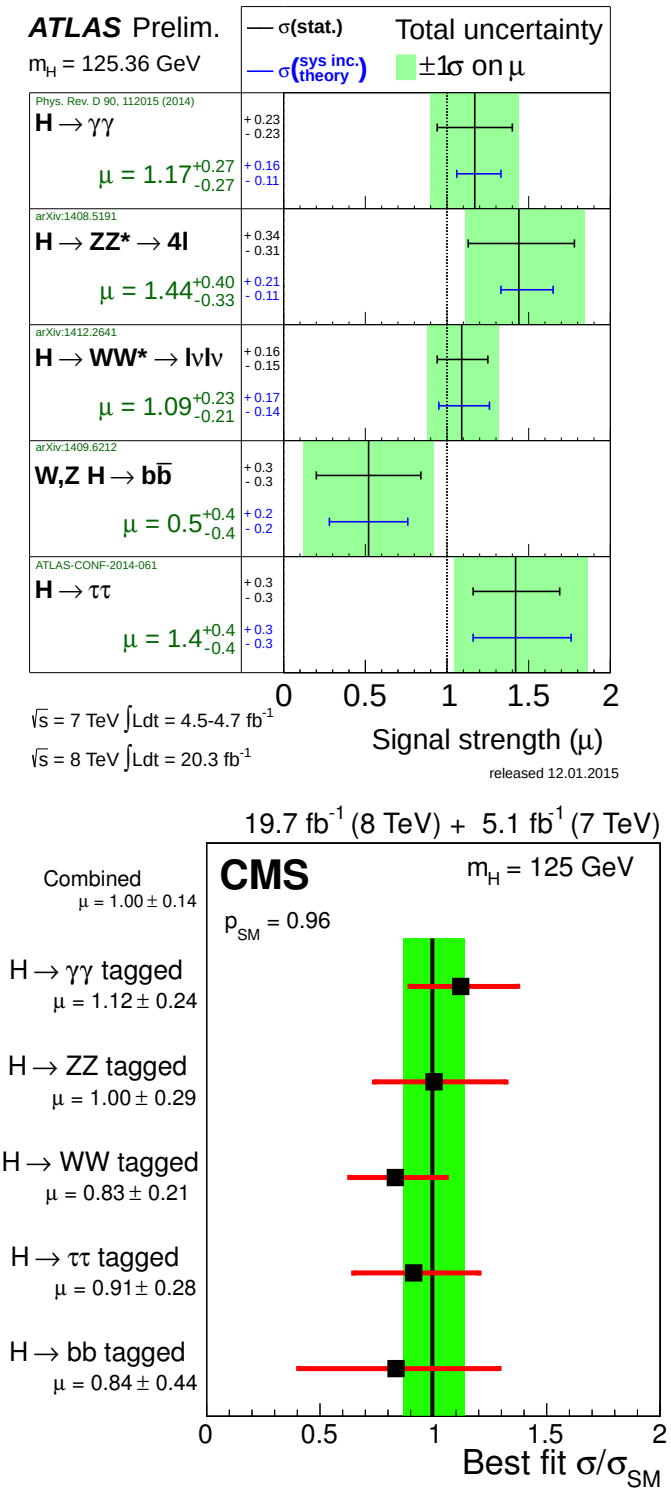

Figure 1.1: Signal strength$(\sigma_{observed}/\sigma_{SM})$ of the observed scalar for each of the search channels at ATLAS(top) and CMS(bottom) [1, 2].

one doublet gives masses to neutrinos alone. After that, I have concluded my thesis.

Chapter 2

Warped Geometry: The Randall-Sundrum model and the radion

Scenarios where extra space-like compact dimensions exist, with implications in TeV scale physics, have been widely explored over the last two decades. Scenarios with flat extra dimensions include the so called ADD models [58] as well as those with UED models [59]. However, such scenarios require large compactification radii, whose stability introduces a fresh naturalness problem. Such problems are largely avoided in theories of warped extra dimensions. The Randall-Sundrum(RS) model is the most popular example of such theories.

2.1 The minimal Randall-Sundrum model

Randall and Sundrum proposed a scenario where the hierarchy between the Planck scale and the weak scale is generated from a five dimensional non-factorizable geometry. The model elides on a slice of AdS_5 space-time. The additional space-like dimension is S_1/Z_2 orbifolded. One further postulates the existence of two 3-branes

with opposite tensions, which are placed at the orbifold fixed points, namely $\phi = 0, \pi$, where ϕ is the angular coordinate parameterizing the extra dimension. One also expresses the co-ordinate along this dimension as $y = r_c\phi$, where r_c is the radius of the compactification. Gravitation propagates in the entire 5-dimensional 'bulk', peaking at the 'hidden' or 'Planck' brane $(\phi = 0)$, whereas the standard model (SM) fields are confined to the 'visible' brane $(\phi = \pi)$. The action for the aforementioned configuration is given by [36]

$$\begin{aligned} S &= S_{gravity} + S_v + S_h, \\ S_{gravity} &= \int d^4x \int_{-\pi}^{\pi} d\phi \sqrt{-G} \left(-\Lambda + 2M_5^3 R\right), \\ S_v &= \int d^4x \sqrt{-g_v} \left(\mathcal{L}_v - V_v\right) \text{ and} \\ S_h &= \int d^4x \sqrt{-g_h} \left(\mathcal{L}_h - V_h\right) \end{aligned} \tag{2.1.1}$$

where the subscripts v and h refer to the visible and the hidden branes respectively, G is the determinant of the five dimensional metric G_{MN}. The metrics on the visible and hidden branes are given by

$$g^v_{\mu\nu}(x^\mu) \equiv G_{\mu\nu}(x^\mu, \phi = \pi), g^h_{\mu\nu}(x^\mu) \equiv G_{\mu\nu}(x^\mu, \phi = 0), \tag{2.1.2}$$

where the greek indices are the representation of (1+3) dimensional coordinates on the visible (hidden) brane. M_5 is the five dimensional Planck mass and Λ is the bulk cosmological constant. V_v and V_h are the brane tensions of the visible and the hidden branes respectively.

If the solution respects four dimensional Poincare symmetry, then the metric is

$$ds^2 = e^{-2\sigma(\phi)}\eta_{\mu\nu}dx^\mu dx^\nu - r_c^2 d\phi^2. \tag{2.1.3}$$

On plugging the ansatz form of the metric in the Einstein's equation (2.1.2), we get

$$\begin{aligned} \frac{6\sigma'^2}{r_c^2} &= \frac{-\Lambda}{4M_5^3} \\ 3\frac{\sigma''}{r_c^2} &= \frac{V_h}{4M_5^3 r_c}\delta(\phi) + \frac{V_v}{4M_5^3 r_c}\delta(\phi-\pi). \end{aligned} \tag{2.1.4}$$

On applying the orbifolding condition and solving (2.1.4), we get

$$\sigma = r_c|\phi|\sqrt{\frac{-\Lambda}{24M_5^3}}. \tag{2.1.5}$$

Thus, the bulk metric becomes

$$ds^2 = e^{-2k|y|}\eta_{\mu\nu}dx^\mu dx^\nu - dy^2 \tag{2.1.6}$$

where, $k = \sqrt{\frac{-\Lambda}{24M_5^3}}$ and

$$V_h = -V_v = 24M_5^3 k. \tag{2.1.7}$$

On comparing the curvature term of the effective four dimensional action, we get the following relation between the five dimensional Planck mass M_5 and the four dimensional reduced Planck mass $\bar{M}_{Pl}$

$$\bar{M}_{Pl}^2 = \frac{M_5^3}{k}[1 - e^{-2kr_c\pi}] \tag{2.1.8}$$

where, $\bar{M}_{Pl} = M_{Pl}/\sqrt{8\pi}$.

The five dimensional curvature of the metric is $R_5 = 20k^2$. The classical solution for the bulk metric can be trusted for $R_5 < M_5$. As a result, $k/\bar{M}_{Pl}$ can not be too large ($k/\bar{M}_{Pl} \sim 0.2$).

2.2 Hierarchy problem revisited

Let us consider the Higgs field on the visible brane ($\phi = \pi$),

$$S_{vis} = \int d^4x\sqrt{-g_v}\left(g_v^{\mu\nu}D_\mu H^\dagger D_\nu H - \lambda(H^2 - v_0^2)^2\right). \tag{2.2.9}$$

On using the expression for the induced metric($g^v_{\mu\nu} = e^{-kr_c\pi}\bar{g}_{\mu\nu}$) on the visible brane given in (2.1.2), (2.2.9) takes the form of

$$S_{vis} = \int d^4x\sqrt{-\bar{g}}e^{-4kr_c\pi}\left(\bar{g}^{\mu\nu}e^{2kr_c\pi}D_\mu H^\dagger D_\nu H - \lambda(H^2 - v_0^2)^2\right). \tag{2.2.10}$$

After redefining H ($H \rightarrow He^{-kr_c\pi}$), we get

$$S_{vis} = \int d^4x\sqrt{-\bar{g}}\left(\bar{g}^{\mu\nu}D_\mu H^\dagger D_\nu H - \lambda(H^2 - e^{-2kr_c\pi}v_0^2)^2\right). \tag{2.2.11}$$

Thus, effectively the mass parameter v_0 in (2.2.9) is replaced by $v_0e^{-kr_c\pi}$ in (2.2.11). The five dimensional metric consists solely of mass parameters whose values are around the Planck scale. For the choice of $kr_c \simeq 12$, which requires barely an order of disparity between the scales k and $1/r_c$, the mass parameters on the visible brane are suppressed with respect to the Planck scale by the exponential factor $e^{kr_c\pi} \simeq 10^{16}$, thus offering a rather appealing explanation of the hierarchy between the Planck and TeV scales.

2.3 Signatures of the RS model

When we are studying 4-dimensional physics on the visible brane, the extra dimension is integrated out, or compactified. Consequently, a tower of Kaluza-Klein (KK) states of any bulk field should appear on the visible brane. The first excitation of the RS graviton (G^*) is the readiest object of investigation in the quest of phenomenolgical signatures of this scenario. Another particle that can be of interest is the radion, arising out of a modulus field introduced to stabilise the radius of the fifth dimension. Both the graviton excitation(s) and the radion may lead to signals of the RS model. Such potential signals have been probed extensively in the recent and present high-energy

colliders. They are reviewed in the following sections.

2.4 KK graviton

The Kaluza-Klein (KK) decomposition of the graviton on the visible brane leads to a discrete tower of states, with one massless graviton and a series of TeV-scale spin-2 particles. [60, 61, 62].

Let us parametrize the tensor fluctuation $h_{\alpha\beta}$ by considering the linear expansion of the flat metric about its Minkowski value,

$$G_{\alpha\beta} = e^{-2\sigma}\left(\eta_{\alpha\beta} + K^* h_{\alpha\beta}\right) \tag{2.4.12}$$

where K^* is the expansion parameter.

One can expand $h_{\alpha\beta}$ in terms of the KK modes of the graviton,

$$h_{\alpha\beta}(x,\phi) = \Sigma_{n=0}^{\infty} h^n_{\alpha\beta}(x)\frac{\chi^n(\phi)}{\sqrt{r_c}} \tag{2.4.13}$$

where $h^n_{\alpha\beta}(x)$ corresponds to the n^{th} KK mode of the graviton about the Minkowski space on the 3-brane.

In the gauge where $\eta^{\alpha\beta}\partial_\alpha h^n_{\beta\gamma}(x) = \eta^{\alpha\beta}h^n(x)_{\alpha\beta} = 0$, the equation of motion of the n^{th} mode of the KK graviton having mass m_n is given by

$$\left(n_{\alpha\beta}\partial^\alpha\partial^\beta - m_n^2\right) h_{\mu\nu}(x) = 0. \tag{2.4.14}$$

On plugging the KK expansion of $h^n_{\alpha\beta}(x,y)$ in the Einstein's equation and using the equation of motion (2.4.14), we obtain the following differential equation for $\chi^n(\phi)$,

$$\frac{-1}{r_c^2}\frac{d}{d\phi}\left(e^{-4\sigma}\frac{d}{d\phi}\chi^n\right) = m_n^2 e^{-2\sigma}\chi^n. \tag{2.4.15}$$

The solutions for $\chi^n(\phi)$ are given by

$$\chi^n(\phi) = \frac{e^{2\sigma}}{N_n}\left[J_2(z_n) + \alpha_n Y_2(z_n)\right] \tag{2.4.16}$$

where J_2 is the Bessel function of order 2 and Y_2 is the Neumann function of order 2, $z_n(\phi) = m_n e^{\sigma(\phi)}/k$, N_n is the wave function normalization and α_n are constant coefficients.

The continuity of the first derivative of $\chi(\phi)$ at the orbifold fixed points leads to $J_1(z_n(\pi)) = 0$ and $\alpha_n \sim x_n^2 e^{-2kr_c\pi}$. Thus, $z_n(\pi) = x_n$, where x_n are the roots of the Bessel functions of order 1.

As a result, the mass of the n^{th} KK mode of the graviton is given by

$$m_n = k x_n e^{-kr_c\pi}. \tag{2.4.17}$$

For $x_n << e^{kr_c\pi}$, the second term of (2.4.15) is negligible. Hence, the normalization, N_n becomes

$$N_n \simeq \frac{e^{kr_c\pi}}{\sqrt{kr_c}} J_2(x_n); n > 0, \tag{2.4.18}$$

and the normalization of the zero mode is $N_0 = 1/\sqrt{kr_c}$.

Using the solutions for χ^n, we can derive the interactions of the KK graviton $h^n_{\alpha\beta}$ with the matter fields on the visible brane. The interaction Lagrangian in the 4-D effective theory has the form of

$$\mathcal{L} = -\frac{1}{M_5^{3/2}} T^{\alpha\beta}(x) h_{\alpha\beta}(x, \phi = \pi) \tag{2.4.19}$$

where $T^{\alpha\beta}$ is the energy momentum tensor of the matter fields.

Expanding the graviton wavefuntion in terms of the KK towers and using the normalization of (2.4.18), we obtain the interaction of the KK modes of graviton with the

matter fields on the visible brane

$$\mathcal{L} = \frac{-1}{\bar{M}_{Pl}} T^{\alpha\beta}(x) h(x)^0_{\alpha\beta} - \frac{1}{\Lambda_\pi} T^{\alpha\beta}(x) \Sigma_{n=1}^{\infty} h(x)^n_{\alpha\beta}(x) \tag{2.4.20}$$

where $\Lambda_\pi = \bar{M}_{Pl} e^{-kr_c\pi}$, The massless graviton couples to all matter fields with strength $\sim 1/\bar{M}_{Pl}$, whereas the corresponding couplings for the massive modes receive an exponential enhancement and is suppressed by TeV scale. As a result, the possibility of observing signals of the massive gravitons in TeV-scale experiments opens up.

2.4.1 Status of the KK gravitons at the colliders

The first KK excitation of RS graviton(G*) is produced resonantly at hadron colliders through the process of quark-antiquark annihilation or gluon-gluon fusion. Due to small gluon parton distribution function at large momentum fraction, the quark-antiquark annihilation dominates over the gluon fusion production cross-section for the KK graviton. Inspite of its universal coupling to all SM particles, it decays predominantly to quarks and gluons because of their high multiplicity to color, spin and flavor states. However, these channels are difficult to probe at the hadron colliders due to large QCD backgrounds. Although the decay width of KK gravitons to dilepton is suppressed because of its spin-2 nature, the dilepton channel offers a clean signal for KK graviton search.

$k/\bar{M}_{Pl}$ and the mass of the first KK mode of graviton (m_1) are considered as free parameters in the KK graviton sector. The mass of n^{th} KK mode can be expressed in terms of m_1.

$$m_n = (x_n/x_1) m_1 \tag{2.4.21}$$

For the first KK mode, the total decay width is given by

$$\Gamma_1 = \rho m_1 x_1^2 (k/\bar{M}_{Pl})^2 \tag{2.4.22}$$

where ρ is a constant that depends on number of SM channels available.

Thus, limits at 95% CL on total cross-section for G^* decaying to dilepton are compared to the theoretical value for the total cross-section. This results are used to set lower limits on m_1 at a given value of $k/\bar{M}_{Pl}$. Current experimental limits from the LHC rule out any mass for the lowest graviton excitation below $1.15(2.47)$ TeV for $k/M_{Pl} \leq 0.01(0.1)$ [63].

2.5 The radion

How does the chosen value of r_c, the radius of compactification arise, and why is it stable at $r_c \sim 12/k$? In order to answer this question, there has been an attempt to view r_c as the vacuum expectation value (vev) of a ϕ-independent field, known as modulus field or the radion. This field is parametrized by a scalar fluctuation about the background geometry. Thus, the metric is

$$ds^2 = e^{-2k|\phi|T(x)}\bar{g}_{\mu\nu}(x)dx^\mu dx^\nu - T^2(x)d\phi^2. \tag{2.5.23}$$

The KK reduction of the five dimensional Einstein-Hilbert action using the metric of (2.5.23) leads to the following effective action for $T(x)$ and $\bar{g}_{\mu\nu}(x)$

$$S = 2M_5^3 \int d^4x d\phi \sqrt{-\bar{g}} e^{-2k|\phi|T} \left[6k|\phi|\partial_\mu T \partial^\mu T - 6k^2|\phi|^2 T \partial_\mu T \partial^\mu T + TR\right] \tag{2.5.24}$$

where R is the Ricci scalar constructed from $\bar{g}_{\mu\nu}(x)$.

After integrating out the additional coordinate ϕ, we have the following four dimensional effective action involving the modulus field $T(x)$ and the induced metric $\bar{g}_{\mu\nu}$(x)

$$S = \frac{2M_5^3}{k}\int d^4x\sqrt{-\bar{g}}(1-e^{-2k\pi T})R + \frac{3M_5^3}{k}\int d^4x\sqrt{-\bar{g}}\partial_\mu(e^{-k\pi T})\partial^\mu(e^{-k\pi T}). \quad (2.5.25)$$

To make the kinetic term of the (2.5.25) canonical, the modulus field is redefined to $\varphi(x) = \Lambda_\varphi e^{-k\pi(T(x)\,-\,r_c)}$ with $\Lambda_\varphi = \sqrt{6M_5^3/k}e^{-kr_c\pi}$. Hence, we arrive at

$$S = \frac{2M_5^3}{k}\int d^4x\sqrt{-\bar{g}}(1-(\varphi/f)^2)R + \frac{1}{2}\int d^4x\sqrt{-\bar{g}}\partial_\mu\varphi\partial^\mu\varphi \quad (2.5.26)$$

where $f = \sqrt{6M_5^3/k}$.

The effective four dimensional action (2.5.26) contains a massless scalar $\varphi(x)$. However, to solve the hierarchy problem, there should be some additional dynamics that will stabilize the $\varphi(x)$ and give $T(x)$ its desired vev, r_c. The vev of the field $\varphi(x)$ is Λ_φ. The stabilization procedure was first proposed by Goldberger-Wise [37, 38] and is briefly reviewed here.

Let us consider a scalar field Φ propagating in the bulk, having interaction terms on the visible and the hidden branes (v_v and v_h respectively).

$$\begin{aligned} S_b &= \frac{1}{2}\int d^4x\int_{-\pi}^{\pi} d\phi\sqrt{G}(G^{AB}\partial_A\Phi\partial_B\Phi - m^2\Phi^2) \\ S_h &= -\int d^4x\sqrt{-g_h}\lambda_h(\Phi^2 - v_h^2)^2 \\ S_v &= -\int d^4x\sqrt{-g_v}\lambda_v(\Phi^2 - v_v^2)^2. \end{aligned} \quad (2.5.27)$$

The terms on the branes cause the scalar field Φ to develop a ϕ-dependent vev which is determined classically by solving the equation of motion of the action in (2.5.27). Inserting the general solution of $\Phi(\phi)$ into the bulk scalar field action and

integrating over ϕ yields an effective potential for $\varphi(x)$ of the form

$$\begin{aligned} V_\varphi(r_c) &= k\epsilon v_h^2 + 4ke^{-4kr_c\pi}(v_v - v_h e^{-\epsilon kr_c\pi})^2(1+\epsilon/4) \\ &- k\epsilon v_h e^{-(4+\epsilon)kr_c\pi}(2v_v - v_h e^{-\epsilon kr_c\pi}) \end{aligned} \tag{2.5.28}$$

where we have assumed $\epsilon \equiv m^2/4k^2 \ll 1$. After neglecting the terms of order ϵ and working in large λ limit, we get

$$V(\varphi) = \frac{k^3}{144M_5^6}\varphi^4(v_v - v_h(\frac{\varphi}{f})^\epsilon)^2. \tag{2.5.29}$$

The potential of (2.5.29) has a minima at

$$\frac{<\varphi>}{f} = (\frac{v_v}{v_h})^{1/\epsilon} \tag{2.5.30}$$

or

$$kr_c = k < T >= \frac{1}{\pi\epsilon} ln(v_h/v_v). \tag{2.5.31}$$

From the relation given in (2.5.31) we can see that $kr_c \sim 12$ can be generated without any kind of extreme fine tuning of the parameters. Also, (2.5.29) gives us the mass of the radion

$$m_\varphi^2 = \frac{\partial^2 V}{\partial\varphi^2}_{|<\varphi>} = \frac{k^2 v_v^2}{3M_5^3}\epsilon^2 e^{-2kr_c\pi}. \tag{2.5.32}$$

If we assume that the effective potential is generated by a light bulk scalar, then, due to the suppression by ϵ, the mass of radion is smaller than TeV. As a result, it becomes the first clear signal of RS model.

As the radion arises from the gravitational degree of freedom, its couplings to the matter fields on the visible brane should be governed by the principle of general covariance. The induced metric on the visible brane is defined by $g_{v\mu\nu} = (\varphi/\Lambda_\varphi)^2\eta_{\mu\nu}$. This term generates a direct coupling of the radion to the matter fields on the visible brane.The radion does not couple directly to the matter fields present in the hidden

brane. The linear coupling of the radion to the matter [64, 65] on the visible brane can be obtained from

$$\varphi \frac{\partial S_{SM}}{\partial \varphi}_{|\Lambda_\varphi} = \varphi \frac{\partial S_{SM}}{\partial g_{v\mu\nu}} \frac{\partial g_{v\mu\nu}}{\partial \varphi}_{|\Lambda_\varphi} = \frac{\varphi}{\Lambda_\varphi} T_\mu^{\mu SM}. \tag{2.5.33}$$

where $T_\mu^{\mu SM}$ is the trace of energy momentum tensor of the SM and is given by

$$T_\mu^\mu = m_h^2 h^2 + \Sigma_f m_f \bar{f} f - 2M_W^2 W_\mu^+ W^{-\mu} - M_Z^2 Z_\mu Z^\mu. \tag{2.5.34}$$

Thus, the couplings of radion with massive gauge bosons, fermions and Higgs [3] are given by

$$\begin{aligned}
\Gamma(\varphi \to f\bar{f}) &= \frac{N_c m_f^2 m_\varphi}{8\pi\Lambda_\varphi^2}(1-x_f)^{3/2}, \\
\Gamma(\varphi \to W^+W^-) &= \frac{m_\varphi^3}{16\pi\Lambda_\varphi^2}\sqrt{1-x_W}\Big(1-x_W+\frac{3}{4}x_W^2\Big), \\
\Gamma(\varphi \to ZZ) &= \frac{m_\varphi^3}{32\pi\Lambda_\phi^2}\sqrt{1-x_Z}\Big(1-x_Z+\frac{3}{4}x_Z^2\Big), \\
\Gamma(\varphi \to hh) &= \frac{m_\varphi^3}{32\pi\Lambda_\varphi^2}\sqrt{1-x_h}\Big(1+\frac{1}{2}x_h\Big)^2.
\end{aligned} \tag{2.5.35}$$

The symbol f denotes all quarks and leptons. The variable x_i is defined as $x_i = 4m_i^2/m_\varphi^2$ $(i = t, f, W, Z, h)$.

Since, the gluon and the photon are massless. The radion does not have any tree level coupling to them. The couplings of the radion with the gluon(photon) are generated from the following terms:

- There are triangle diagrams involving the W-boson and the top quark. These terms are analogous to that of the SM Higgs.

- The running of the gauge couplings in QCD and QED breaks the scale invariance and generates the following trace anomaly term,

$$T_\mu^{\mu\ anomaly} = \frac{\beta_a(g_a)}{2g_a} F^{\mu\nu a} F^a_{\mu\nu} \tag{2.5.36}$$

where

$$\begin{aligned}\frac{\beta_{QCD}}{2g_s} &= -\frac{\alpha_s}{8\pi}b_3 \\ \frac{\beta_{QED}}{2g_f} &= -\frac{\alpha_e}{8\pi}(b_2+b_y)\end{aligned} \tag{2.5.37}$$

where $b_3 = 7$ is the QCD β-function coefficient and $b_2 = 19/6$ and $\mathrm{b_Y} = -41/6$ are the SM $SU(2)_L \times U(1)_Y$ β-function coefficients. The trace anomaly contribution enhances the φgg and $\varphi\gamma\gamma$ amplitudes, with the same Lorentz structures as for loop diagrams and these terms are responsible for supplementing rates in $\gamma\gamma$ and gg channels. On adding the above contributions, we get

$$\Gamma(\varphi \to gg) = \frac{\alpha_s^2 m_\varphi^3}{32\pi^3\Lambda_\varphi^2}\left|b_3 + x_t\left\{1+(1-x_t)f(x_t)\right\}\right|^2, \tag{2.5.38}$$

$$\begin{aligned}\Gamma(\varphi \to \gamma\gamma) = \frac{\alpha_{\rm EM}^2 m_\varphi^3}{256\pi^3\Lambda_\varphi^2}\Bigg|b_2 + b_Y - \left\{2+3x_W+3x_W(2-x_W)f(x_W)\right\} \\ +\frac{8}{3}x_t\left\{1+(1-x_t)f(x_t)\right\}\Bigg|^2,\end{aligned} \tag{2.5.39}$$

$$\begin{aligned}\Gamma(\varphi \to Z\gamma) = \frac{\alpha_{\rm EM}^2 m_\varphi^3}{128\pi^3 s_{\rm w}^2\Lambda_\varphi^2}\left(1-\frac{m_Z^2}{m_\varphi^2}\right)^3 \\ \times\left|\sum_f N_f\frac{Q_f}{c_{\rm W}}\hat{v}_f\, A_{1/2}^\varphi(x_f,\lambda_f) + A_1^\varphi(x_W,\lambda_W)\right|^2\end{aligned} \tag{2.5.40}$$

where $x_i = 4m_i^2/m_\varphi^2$ $(i = t, f, W, Z, h)$, and $\lambda_i = 4m_i^2/m_Z^2$ $(i = f, W)$. The gauge couplings for QCD and QED are given by α_s and $\alpha_{\rm EM}$, respectively. The factor N_f is the number of active quark flavors in the 1-loop diagrams and N_c is 3 for quarks and 1 for leptons. Q_f and $\hat{v}_f$ denote the electric charge of the fermion and the reduced vector coupling in the $Zf\bar{f}$ interactions $\hat{v}_f = 2I_f^3 - 4Q_f s_W^2$, where I_f^3 denotes the weak isospin and $s_W^2 \equiv \sin^2\theta_W,\ c_W^2 = 1 - s_W^2$.

The form factors $A^{\varphi}_{1/2}(x,\lambda)$ and $A^{\varphi}_{1}(x,\lambda)$ are given by

$$A^{\varphi}_{1/2}(x,\lambda) = I_1(x,\lambda) - I_2(x,\lambda)\,, \tag{2.5.41}$$
$$A^{\varphi}_{1}(x,\lambda) = c_W\left\{4\left(3-\frac{s_W^2}{c_W^2}\right)I_2(x,\lambda) + \left[\left(1+\frac{2}{x}\right)\frac{s_W^2}{c_W^2} - \left(5+\frac{2}{x}\right)\right]I_1(x,\lambda)\right\}.$$

The functions $I_1(x,\lambda)$ and $I_2(x,\lambda)$ are

$$I_1(x,\lambda) = \frac{x\lambda}{2(x-\lambda)} + \frac{x^2\lambda^2}{2(x-\lambda)^2}[f(x^{-1}) - f(\lambda^{-1})] + \frac{x^2\lambda}{(x-\lambda)^2}[g(x^{-1}) - g(\lambda^{-1})]\,,$$
$$I_2(x,\lambda) = -\frac{x\lambda}{2(x-\lambda)}[f(x^{-1}) - f(\lambda^{-1})]\,, \tag{2.5.42}$$

where the loop functions $f(x)$ and $g(x)$ in ((2.5.38)), ((2.5.39)) and ((2.5.42)) are given by

$$f(x) = \begin{cases} \left\{\sin^{-1}\left(\dfrac{1}{\sqrt{x}}\right)\right\}^2 & , \quad x \geq 1 \\ -\dfrac{1}{4}\left(\log\dfrac{1+\sqrt{1-x}}{1-\sqrt{1-x}} - i\pi\right)^2 & , \quad x < 1 \end{cases}, \tag{2.5.43}$$

$$g(x) = \begin{cases} \sqrt{x^{-1}-1}\,\sin^{-1}\sqrt{x} & , \quad x \leq 1 \\ \dfrac{\sqrt{1-x^{-1}}}{2}\left(\log\dfrac{1+\sqrt{1-x^{-1}}}{1-\sqrt{1-x^{-1}}} - i\pi\right) & , \quad x > 1 \end{cases}. \tag{2.5.44}$$

The radion mass m_φ and the vev Λ_φ constitute the set of free parameters of the theory in the radion sector, which now has the distinction of 'naturally' generating a TeV-scale vev on the visible brane. Since, the radion mass is below a TeV, the detection of radion becomes somewhat easier than that of the first KK mode of the graviton [37, 38].

2.5.1 Phenomenology of the radion

The radion can be produced at hadron colliders in the gluon fusion channel, vector boson fusion channel and in association with the vector bosons and $t\bar{t}$. However, because of the enhancement factor coming from the trace anomaly term, the gluon fusion becomes the prime channel for production of radion. The other production channels are relatively suppressed by the vev of radion. The production of radion in gluon fusion channel has two times larger cross-section than the other production channels. The cross-section of the radion produced via gluon fusion channel at a hadronic collider with centre of mass energy ($\sqrt{s}$) is given by

$$\sigma(s) = \int_{\frac{m_\varphi^2}{s}}^{1} \frac{dx}{x} g(x) g(\frac{m_\varphi^2}{sx}) \frac{\alpha_s^2}{256\pi\Lambda_\varphi^2} \frac{m_\varphi^2}{s} |b_3 + x_t(1 + (1 - x_t) f(x_t))|^2 \tag{2.5.45}$$

where g(x) is the gluon parton distribution function at a given momentum fraction x.

At electron-positron collider, the radion can be produced in association with W, Z bosons or in association with $\nu\bar{\nu}$ (e^+e^-) via W(Z) fusion.

The striking difference between the decay of low mass radion and SM Higgs is in their decay to pair of gluons(figure 2.1). A light radion, due to the boost coming from trace anomaly, decays mostly to gluon-gluon whereas a SM Higgs of the same mass decays to pair of bottom quarks. After the radion crosses WW threshold, it decays predominantly to a pair of Ws. If kinematically allowed, a heavier radion can also decay to a pair of SM Higgs. A heavier radion (m_φ > 350 GeV) decays to WW* mostly, whereas an SM-like second Higgs if exist, decays mostly into $t\bar{t}$.

2.5.2 Status of the radion at the colliders

The radion has been studied extensively in the LEP, Tevatron and LHC. As most of the decays of radion are similar to the SM Higgs, so searches of the SM Higgs has been used to constraint the parameter space of the radion. Apart from the SM Higgs search,

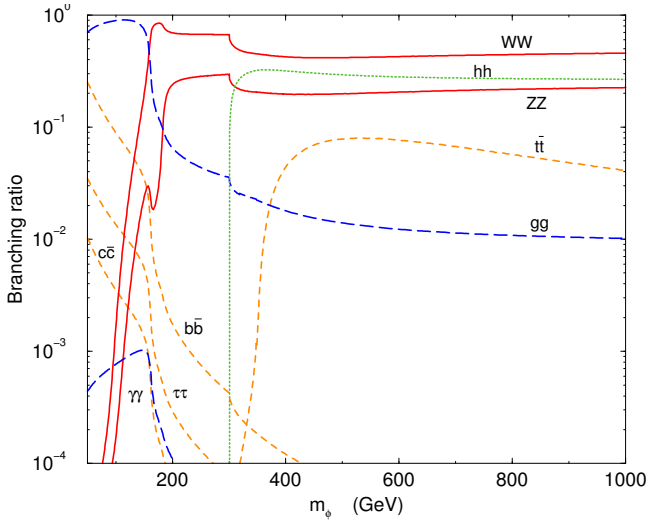

Figure 2.1: Branching ratio of the radion for all possible decay channels [3]. ϕ denotes the radion.

searches on the RS graviton excitations also put a lower bound on the vev of radion.

$$\Lambda_\varphi = \frac{\sqrt{6} m_1}{k/\bar{M}_{Pl} x_1} \tag{2.5.46}$$

As the RS solution is valid for $k/\bar{M}_{Pl} < 1$, absence of the first excitation of RS graviton(G*) till 2.6 TeV excludes radion vev till 1.8 TeV. The radion can mix with the SM Higgs because of the presence of a curvature term. After the discovery of the scalar at 125 GeV at LHC, speculations have been made on whether the observed 125-126 GeV state, instead of being a pure SM Higgs, could instead be the radion, or a mixture of the two. A number of studies have already taken place in this direction, based on both the 'pure radion' and 'radion-Higgs mixing' hypotheses [66, 67, 68, 69, 70, 71, 72, 73, 74, 75, 76, 77, 78, 79, 80, 81, 82, 83, 84, 85, 86, 87, 88, 89]. The Higgs-radion mixing scenario has been discussed thoroughly in chapter 3. The next chapter comprises of the study that we carried out in the paper [90]. We have restricted the available parameter space of the Higgs-radion mixing using the results of LHC run-1. We found that the LHC run-1 data has constrained the space made up of mass of the mixed scalar and the mixing parameter with vev of the order of 1-5 TeV.

Once the vev of the radion increases beyond 5 TeV, the production cross-section of the radion becomes too small and hence, run-1 data is unable to put any limit on it. We showed that the discovered scalar can not be a radion. However, the scenario where a very heavy ($m_\varphi >= 500GeV$) or a very light radion (m_φ<= 100 GeV) exist along with the SM Higgs, is still allowed by the LHC run-1 data. The gluon fusion production cross section of the heavy radion decreases. The cross section gets further suppression once Λ_φ increases. Thus, a heavy radion with vev of the order of 3-5 TeV is still allowed by the LHC data. The LHC run-2 will be able to shed light on the allowed regions in the parameter space of the scenario involving Higgs-radion mixing. The phenomenology of a light radion($\sim$ 100 GeV) is also very interesting. At LEP, a light radion could have been produced via $e^+e^- \to Z\varphi$. The production mode in this channel is however found to be suppressed for $\Lambda_\varphi > 1.0$ TeV and hence, a radion as light as 50 – 100 GeV with $\Lambda_\varphi \simeq 2 - 3$ TeV, is still allowed by the LEP data as well as by the LHC searches [91, 92, 93]. The distinct signature of a light radion is its decay to two gluon. However, due to immense QCD background at the LHC, the gluonic channel is impossible to study. We have found that the diphoton channel can be used as a probe for discovering the radion [94]. Because of the limited luminosity at 8 TeV run of LHC, signals coming from the light radion were masked by huge diphoton background. However, with proper signal background analysis one can discover such a light radion at 14 TeV run of LHC with high luminosity. The detailed phenomenology of such a light radion is the topic of discussion in chapter 4.

There exist various modifications over the minimal RS model, for example, including gauge fields and fermions in the bulk [95, 96, 97, 98, 99, 100, 101, 102], that explain the SM flavor structure as well. As the SM fermions receive masses from the Higgs, one can explain the fermion mass hierarchy by localizing the light fermions relatively away from the TeV brane or 'visible' brane. The third family fermions, on the other hand, peak close to the 'visible' brane. The SM Higgs is localized on the TeV brane. All the fermions have O(1) Yukawa couplings in the 5D theory. The varying degrees

of overlap affect Yukawa coupling on the TeV brane and generate the flavor hierarchy. In this chapter, I have discussed the minimal version of the RS model, where the SM particles are on the visible brane and only gravity propagates in the bulk.

Chapter 3

Radion-Higgs mixing at LHC

3.1 Introduction

This chapter is based on our work done in [90]. In this work, we have considered the mixing of radion with Higgs. We have performed a global analysis of the available data, assuming that both of the physical states arising from radion-Higgs mixing contribute to the event rates in various channels. Using both the 2011 and 2012 data, we found the best fit points in terms of the parameters of the model. Furthermore, we have obtained the 95% confidence level contours in the parameter space, which indicate the extent to which new physics can be accommodated in the light of the available results. Side by side, we identify the regions which are disallowed by data in one or more channels, as obtained from the published 95% C.L. exclusion limits on the signal strength, defined as $\mu = \sigma/\sigma_{SM}$, where σ is the predicted cross-section in the relevant channel for a specific combination of the model parameters, and σ_{SM} is the corresponding prediction for the SM Higgs boson. The region that is left after such exclusion can be treated as one where the presence of a radion-like (Higgs-like) scalar is compatible with the data as of now. A comparison of this region with the 95% C.L. contours around the best fit values of the parameters indicates the viability (or otherwise) of this particular new physics scenario.

Our work improves upon other recent studies based on LHC data [87, 85, 86, 89] in a number of ways. This is the first global analysis, following a χ^2-minimization procedure, of radion-Higgs mixing, using the latest available data from 7 and 8 TeV LHC runs to obtain best fit parameters and significance contours. We include the possibility of an additional scalar mass eigenstate coexisting with the 125 GeV state, with both of them contributing to the final states looked for, subject to event selection criteria pertaining to the 125 GeV Higgs. While it is unlikely that the contribution from the additional scalar will be confused with the signal of a 125 GeV scalar in the $\gamma\gamma$ and $ZZ^{(*)}$ final states (as the reconstructed invariant mass will point to two distinct resonances), it cannot *a priori* be ruled out for the $WW^{(*)}$ channel. The presence of two neutrinos in the di-lepton final state makes it impossible to reconstruct the mass of the parent particle and one would therefore expect some enhancement to the signal strength due to the extra contribution from the second state which must be estimated by simulating the effect of the selection cuts used by the corresponding experimental analyses. This makes the best-fit regions different from what one finds with the assumptions that the entire contribution in every channel comes from one scalar resonance only.

Secondly, we also use the strategy of simulating the full cut-based analysis in restricting the allowed regions from the available upper limit on σ/σ_{SM} for an addition scalar with different mass, demanding not only (a) the extra contribution at 125 GeV be smaller than the current upper limit, but also (b) the combined contribution using cuts corresponding to the SM Higgs search at the mass of the extra resonance be smaller than the upper limit at that mass. Again, this makes a difference mainly in the $WW^{(*)}$ channel. The contribution here (as also in the case of global fits) is the sum of those from two distinct mass eigenstates, so that the acceptance of the cuts does not factor out when taking the ratio to expected SM cross section.

Thirdly, we have taken into account the interference between processes mediated by radion-Higgs mixed mass eigenstates whenever they are close to each other. And finally, we have explicitly included processes where a relatively heavy, radion(Higgs)-

dominated state decays into two Higgs(radion)-dominated scalars at 125 GeV, each of which can go to the decay channels searched for. In a way, this leads to an additional production mechanism of the 125 GeV state, which we have felt should be included in a full analysis.

3.1.1 Radion-Higgs mixing

In addition to the action in Eqn[2.1.1], general covariance also allows a Higgs-radion mixing term [103], parametrized by the dimensionless quantity ξ. Such a term couples the Higgs field to the Ricci scalar of the induced metric (g_{ind}) on the visible brane

$$S = -\xi \int d^4x \sqrt{-g_{ind}} R(g_{ind}) H^\dagger H \tag{3.1.1}$$

where $H = [(v+h)/\sqrt{2}, 0]$ with $v = 246$ GeV

The radion couples with trace of the energy momentum tensor(chapter 2). For phenomenological purpose, we are interested in terms in T^μ_μ, which are bilinear in the SM fields. Retaining such terms only, one has

$$T^\mu_\mu = T^{(1)\mu}_\mu + T^{(2)\mu}_\mu \tag{3.1.2}$$

with

$$\begin{aligned} T^{(1)\mu}_\mu &= 6\xi v \Box h \\ T^{(2)\mu}_\mu &= (6\xi - 1)\partial_\mu h \partial^\mu h + 6\xi h \Box h + 2m_h^2 h^2 + m_{ij}\bar{\psi}_i\psi_j - M_v^2 V_{A\mu} V_A^\mu \end{aligned} \tag{3.1.3}$$

$T^{(1)\mu}_\mu$ induces a kinetic mixing between φ and h. After shifting φ with respect to its vacuum expectation value Λ_φ we obtain

$$\mathcal{L} = -\frac{1}{2}\varphi(\Box + m_\varphi^2)\varphi - \frac{1}{2}h(\Box + m_h^2)h - 6\xi\frac{v}{\Lambda_\varphi}\varphi\Box h \tag{3.1.4}$$

We confine our study to a region of the parameter space where the radion vev Λ_φ is well above the vev of the SM Higgs. Besides, it is phenomenologically safe not to consider ξ with magnitude much above unity, since a large value may destabilize the geometry itself through back-reaction. Thus one can make the further approximation $6\xi\frac{v}{\Lambda_\varphi} << 1$. In this approximation, the kinetic energy terms acquire a canonical form under the basis transformation from (φ, h) to $(\varphi^{'}, h^{'})$, such that

$$\begin{aligned} \varphi &= (\sin\theta - \sin\rho\cos\theta)h^{'} + (\cos\theta + \sin\rho\sin\theta)\varphi^{'} \\ h &= \cos\rho\cos\theta h^{'} - \cos\rho\sin\theta\varphi^{'} \end{aligned} \tag{3.1.5}$$

where

$$\tan\rho = 6\xi\frac{v}{\Lambda_\varphi}, \quad \tan 2\theta = \frac{2\sin\rho m_\varphi^2}{\cos^2\rho(m_\varphi^2 - m_h^2)} \tag{3.1.6}$$

and one ends up with the physical masses

$$m^2_{\varphi^{'},h^{'}} = \frac{1}{2}\left[(1+\sin^2\rho)m_\varphi^2 + \cos^2\rho m_h^2 \pm \sqrt{\cos^4\rho(m_\varphi^2 - m_h^2)^2 + 4\sin^2\rho m_\varphi^4}\right] \tag{3.1.7}$$

The interactions of $\varphi^{'}$ and $h^{'}$ with fermions (f) and massive gauge bosons (V) is given by

$$\mathcal{L}_1 = \frac{-1}{v}(m_{ij}\bar{\psi}_i\psi_j - M_v^2 V_{A\mu}V_A^\mu)(A_h h' + \frac{v}{\Lambda_\varphi}A_\varphi\varphi^{'}) \tag{3.1.8}$$

As has been mentioned in 2, the coupling of φ to a pair of gluons also includes the trace anomaly term. Taking it into account, the gluon-gluon couplings for both of the mass eigenstates are given by

$$\mathcal{L}_2 = \frac{-1}{v}\frac{\alpha_s}{16\pi}G_{\mu\nu}G^{\mu\nu}(B_h h^{'} + \frac{v}{\Lambda_\varphi}B_\varphi\varphi') \tag{3.1.9}$$

while the corresponding Lagrangian for the photon is

$$\mathcal{L}_3 = \frac{-1}{v}\frac{\alpha_{EM}}{8\pi}F_{\mu\nu}F^{\mu\nu}(C_h h^{'} + \frac{v}{\Lambda_\varphi}C_\varphi \varphi^{\prime}) \tag{3.1.10}$$

where

$$\begin{aligned}
a_h^1 &= \frac{v}{\Lambda_\varphi}(\sin\theta - \sin\rho\cos\theta), \\
a_h^2 &= \cos\rho\cos\theta, \\
a_\varphi^1 &= \cos\theta + \sin\rho\sin\theta, \\
a_\varphi^2 &= \frac{\Lambda_\varphi}{v}(\cos\rho\sin\theta), \\
A_h &= a_h^1 + a_h^2, \\
A_\varphi &= a_\varphi^1 - a_\varphi^2,
\end{aligned}$$

$$\begin{aligned}
B_h &= A_h F_{1/2}(\tau_t) - 2b_3 a_h^1, \\
B_\varphi &= A_\varphi F_{1/2}(\tau_t) - 2b_3 a_\varphi^1, \\
C_h &= A_h(\frac{4}{3}F_{1/2}(\tau_t) + F_1(\tau_W)) - (b_2 + b_y)a_h^1, \\
C_\varphi &= A_\varphi(\frac{4}{3}F_{1/2}(\tau_t) + F_1(\tau_W)) - (b_2 + b_y)a_\varphi^1 \\
\tau_t &= \frac{4m_t^2}{q^2}, \\
\tau_W &= \frac{4m_W^2}{q^2}, \\
b_3 &= 7,\ b_2 = 19/6,\ b_Y = -41/6.
\end{aligned} \tag{3.1.11}$$

where $q^2 = m_{h^{'}}^2(m_{\varphi^{'}}^2)$ depending on $h^{'}(\varphi^{'}) \to gg, \gamma\gamma$. b_2, b_3 and b_Y are the SM β-function coefficients in $SU(3)$ and $SU(2) \times U(1)_Y$ respectively. $F_1(\tau_W)$ and $F_{1/2}(\tau_t)$ are the form

factor for W and top loop respectively. The form of these functions are

$$\begin{aligned} F_{1/2}(\tau) &= -2\tau[1+(1-\tau)f(\tau)], \\ F_1(\tau) &= 2+3\tau+3\tau(2-\tau)f(\tau), \\ f(\tau) &= [\sin^{-1}(\frac{1}{\sqrt{\tau}})]^2, \quad if \ \ \tau \geq 1 \\ &= \frac{1}{4}[ln(\frac{\eta_+}{\eta_-})-\imath\pi]^2, \quad if \ \ \tau < 1 \\ \eta_\pm &= 1 \pm \sqrt{1-\tau}. \end{aligned} \tag{3.1.12}$$

The coupling of φ to h depends on the Goldberger-Wise stabilization potential $V(\varphi)$. On assuming the self-couplings of φ in $V(\varphi)$ to be small, we have

$$\Gamma(\varphi^{'} \to h^{'}h^{'}) = \frac{m^3_{\varphi'}}{32\pi\Lambda^2_\varphi}[1-6\xi+2\frac{m^2_{h'}}{m^2_{\varphi'}}(1+6\xi)]^2\sqrt{[1-4\frac{m^2_{h'}}{m^2_{\varphi'}}]} \tag{3.1.13}$$

Obviously, all interactions of either physical state are now functions of $m_{\varphi'}, m_{h'}, \Lambda_\varphi$ and ξ. In our subsequent calculations, we use these as the basic parameters, obtaining in each case the quantities m_φ, m_h by inverting (Eqn. 3.1.7). Requiring that the discriminant in (Eqn. 3.1.7) to remain positive implies a restriction on the parameter ξ as a function of the remaining three parameters. This constitutes a "theoretically allowed" region in ξ for given ($m_{h'}$, $m_{\phi'}$, Λ_φ). Within this region, we have two solutions corresponding to $m_\varphi > m_h$ and $m_\varphi < m_h$ in (Eqn. 3.1.7). In the first case we have $m_{\varphi'} \to m_\varphi$ and $m_{h'} \to m_h$ in the limit $\xi \to 0$. Exactly the opposite happens in the other case, with $m_{\varphi'} \to m_h$ and $m_{h'} \to m_\varphi$ as ξ approaches zero. A further constraint on ξ follows when one requires $m_\varphi > m_h$. This is because one has in that case,

$$m^2_\varphi - m^2_h = \frac{\sqrt{D} - \sin^2\rho(m^2_{\varphi'}+m^2_{h'})}{1-\sin^4\rho} \tag{3.1.14}$$

where,

$$D = (m^2_{\varphi'}+m^2_{h'})^2 - 4(1+\sin^2\rho)m^2_{\varphi'}m^2_{h'} \tag{3.1.15}$$

One thus ends up with the condition $\sqrt{D} > \sin^2\rho(m^2_{\varphi'} + m^2_{h'})$, thus yielding an additional constraints on ξ.

In the other case described above one has

$$m^2_{\varphi} - m^2_h = -\frac{\sqrt{D} + \sin^2\rho(m^2_{\varphi'} + m^2_{h'})}{1 - \sin^4\rho} \tag{3.1.16}$$

which trivially ensures $m_\varphi < m_h$.

We now define the convention for our analysis. (Eqn. 3.1.7) implies that the lightest state will always be h'. Thus, when $m_\varphi < m_h$, h' becomes the radion-dominated state i.e. $m_{h'} \to m_\varphi$ when $\xi \to 0$. On the other hand, when $m_\varphi > m_h$, we have $m_{h'} \to m_h$ when $\xi \to 0$. Let us label $\varphi^{'}(h^{'})$ as the mixed radion state (R) if, on setting $\xi = 0$, one recovers $m_{\varphi'} = m_\varphi$ $(m_{h'} = m_\varphi)$. The other state is named the mixed Higgs state (H).

Basically, the two interchangeable limits of the states $h^{'}$ and $\varphi^{'}$ for $\xi = 0$ in the two cases arise from the fact that the angle θ in (Eqn. 3.1.6) is 0 or $\pi/2$, depending on whether $m_\varphi > m_h$ or $m_\varphi < m_h$. Both of the above mass inequalities are thus implicit in (Eqn. 3.1.7, 0).

3.2 Strategy for analysis

We propose to scan over the parameter space in terms of masses of the observable physical eigenstates m_H and m_R for all allowed values of the mixing parameter ξ for a given Λ_φ. Since one scalar has been discovered at the LHC, two possibilities arise — viz. we identify the resonance near 125 GeV with either H or R. To cover both these, we present two scenarios based on the conventions defined in the previous section. In the first case, we will fix mass of the mixed Higgs state ($m_H = 125$ GeV) and scan over the mass of the mixed radion state (m_R) from 110 to 600 GeV. Exactly the opposite is done in the other case. We describe our analysis using the first case with the understanding that the identical arguments apply when m_R is held fixed at 125 GeV. To improve the efficiency of our scan, we restrict it to two parameters viz. (m_R, ξ) and take snapshot

values of Λ_φ at 1.5, 3, 5 and 10 TeV.

While it is possible to constrain Λ_φ further using either heuristic arguments or from searches for KK excitation of the RS graviton [104], we refrain from doing so to examine whether the current Higgs search data can provide a complementary method for constraining the parameters of the RS model. Thus we start our study with the lowest value radion vev at 1.5 TeV. Taken together with the mass limits on the first excitation of the RS graviton, this might imply values of the bulk cosmological constant well into the trans-Planckian region where quantum gravity effects may in principle invalidate the classical RS solution. However, it may also be possible to reconcile a low radion vev with rather large gravition masses in some extended scenarios, such as one including a Gauss-Bonnet term in the 5-dimensional action [105, 106, 107, 108, 109].

We simulate the kinematics of the signal (Higgs production and decay) using Pythia 8.160 [110] and reweighting according to the changed couplings. In the region where the second resonance lies between 122-127 GeV, we use Madgraph 5 [111] to calculate the full cross section for $pp \to X \to WW^{(*)}/ZZ^{(*)}/\gamma\gamma$ to include interference from both states. The SM rates are taken from [112, 113].

3.2.1 The overall scheme

In this study, we ask two questions: first, what fraction of the radion-Higgs mixing parameter space survives the observed exclusion limits on signal strengths in various search channels for the SM Higgs; and second, if a radion-Higgs scenario can explain the current data with a better fit than the SM?

Having framed these questions, we compare the theoretical predictions with observed data in various channels, namely, $\gamma\gamma$, $ZZ^{(*)} \to 4\ell$, $WW^{(*)} \to 2\ell + MET$, $b\bar{b}$ and $\tau\bar{\tau}$. Each channel receives contribution from both of the states H and R. Since the production channels for both H and R are same as the SM Higgs (denoted henceforth as h_{SM}), albeit with modified couplings to SM particles, the production cross section of a given scalar can be written in terms of the SM Higgs production cross section mul-

tiplied by a function of the modified couplings. We denote this function by $p^{R,H}_{mode}$, e.g. in the gluon-fusion mode,

$$p^R_{gg}(m) = \left.\frac{\sigma(gg \to R)}{\sigma(gg \to h_{SM})}\right|_{m_R=m_h=m} = \frac{B(R \to gg)}{B(h_{SM} \to gg)} \tag{3.2.17}$$

In general, we expect the acceptance of the cuts to depend on (a) the production mode, and (b) mass of the resonance. Let us denote the acceptance of cuts applied for a candidate mass m by the experimental analysis in a given channel as $a(m)_{prod-channel}$. Thus the predicted signal strength at a particular mass $\mu(m) = \sigma/\sigma_{SM}(m_{h_{SM}} = m)$ in any given decay channel c is given by

$$\mu(m;c) = \sum_{j=gg,VBF,VH} \left\{ p^H_j \frac{a(m;H)_j}{a(m;h_{SM})_j} \frac{\mathrm{B}(H \to c)}{\mathrm{B}(h_{SM} \to c)} + p^R_j \frac{a(m;R)_j}{a(m;h_{SM})_j} \frac{\mathrm{B}(R \to c)}{\mathrm{B}(h_{SM} \to c)} \right\} \tag{3.2.18}$$

In this analysis, we will be assuming that the state discovered at the LHC is the Higgs-like H ($m_H = m_{h_{SM}} = 125$ GeV) for the first case and the radion like state R ($m_R = m_{h_{SM}} = 125$ GeV) for the second. Therefore, we expect the acceptances to cancel for one of the terms but not for the other where the second physical state has a different mass. For the rest of this section, we derive the formulae assuming the first case with the understanding that the expressions for the second case can be obtained merely by switching m_R and m_H.

For channels where the resonance is fully reconstructible viz. $\gamma\gamma$, $b\bar{b}$ and $ZZ^{(*)}$, the analyses use reconstructed mass to identify the resonance and therefore contribution from the second state are negligible if the resonance is narrow. Furthermore, by restricting the number of jets in the final state, it is possible to restrict contribution to the dominant production mode. Since the Lorentz structure of the couplings of R or H is the same as the SM Higgs h_{SM}, the acceptances also factor out. Therefore, for $\mathrm{h}+0\,\mathrm{jets}$,

in $\gamma\gamma$ and $ZZ^{(*)}$ channels, $\mu = \sigma/\sigma_{SM}$ takes the simplified form

$$\mu(c) = p_{gg}^{H} \frac{\mathrm{B}(H \to c)}{\mathrm{B}(h_{SM} \to c)} = \frac{\mathrm{B}(H \to c)\mathrm{B}(H \to gg)}{\mathrm{B}(h_{SM} \to c)\mathrm{B}(h \to gg)} \tag{3.2.19}$$

However, in the $WW^{(*)}$ channel, the final state is not fully reconstructible and therefore we need to consider contributions from both the scalar physical states. Even on restricting to zero- and one-jet final states (which are largely due to gg fusion), we still have

$$\begin{aligned} \mu(m; WW) &= p_{gg}^{H} \frac{a(m; H)}{a(m; h_{SM})} \frac{\mathrm{B}(H \to WW)}{\mathrm{B}(h_{SM} \to WW)} \\ &+ p_{gg}^{R} \frac{a(m; R)}{a(m; h_{SM})} \frac{\mathrm{B}(R \to WW)}{\mathrm{B}(h_{SM} \to WW)} \end{aligned} \tag{3.2.20}$$

The branching fraction $R \to WW^{(*)}$ reaches its maximal value when its mass passes the threshold $m_R = 2m_W$. At this point, the largest contribution to the dilepton final state can come from decay of R rather than H. Therefore, even with fixed mass of H at 125 GeV, the presence of another state that can contribute to the signature results in much stronger bounds on the radion-Higgs mixed scenario. To estimate the effect of this, we have implemented the kinematical cuts on the leptons, jets and missing energy as described by the respective ATLAS [5] and CMS [114] analyses. We verify that our simulation of these analyses reproduce the expected number of signal events for a SM Higgs within the errors quoted by the respective analyses.

In the $\mathrm{h} + 2$ jets channel, the requirement of two well-separated jets means the dominant contribution comes to VBF instead of gg fusion. However, the gluon-fusion contribution is still a significant fraction and therefore, the correct estimate would require simulation of the kinematics of $gg \to R(H) + 2\,\mathrm{jets}$ to high accuracy as well as full detector simulation. A possible way out is to use the gg-fusion subtracted numbers as have been reported by ATLAS. However, to extract this contribution the ATLAS analysis uses the estimate of gluon fusion production for SM Higgs as a background which

requires, by definition, to assume the SM. We have therefore neglected the VBF mode in our study.

Another important effect arises when the mass of both the scalar eigenstates is close to each other. In such cases, the interference effects cannot be neglected. We have therefore calculated the full interference effects when $122 < m_R < 127$ GeV. As we shall see in the next section, this has important effects both on exclusions as well as on the global best-fit regions.

In addition, there is the possibility that the branching ratio for the decay $\varphi^{'} \rightarrow h^{'}h^{'}$ can be substantial in certain regions of the parameter space, resulting in an enhancement even in fully reconstructible channels. Such signals are relatively suppressed for the $WW^{(*)}$ channel because of various vetos on additional leptons and jets. However they contribute to the $ZZ^{(*)}$ and $\gamma\gamma$ channels where the analysis is by and large inclusive. We have included this kind of processes whenever the resultant enhancement is more than 5% of the direct production rate i.e. $\sigma(pp \longrightarrow \varphi^{'}) \times B(\varphi^{'} \longrightarrow h^{'}h^{'}) \geq 0.05\sigma(pp \longrightarrow h^{'})$ for the sake of completeness.

We end this subsection by reiterating the parameters used in our scan. They are Λ_φ, ξ and mass of either of the mixed radion state m_R (or the mixed Higgs state m_H), with the other fixed at 125 GeV. We use four representative values of Λ_φ, namely 1.5 TeV, 3 TeV, 5 TeV and 10 TeV. ξ is varied over the entire theoretically allowed region according to the criteria discussed earlier.

3.2.2 Allowed regions of the parameter space

First, we remember that the experiments have provided 95% upper limits on the signal strength in each channel, which can be used to rule out regions of our parameter space incompatible with observed data. For the $\gamma\gamma$ and $ZZ^{(*)}$ channel-based exclusions, we make use of the simplified formula given in (Eqn. 3.2.19) for the entire range of m_R.

The case for $WW^{(*)}$ is more complicated in the region where m_R lies in the range 110 - 160 GeV since contribution from both the eigenstates are of comparable magnitude.

Therefore, we add the contributions from both states (Eqn. 3.2.20). For example, for calculating the cross section at say 150 GeV, we consider the contribution from $m_R = 150$ GeV as well as the contribution from $m_H = 125$ GeV to cuts designed for the 150 GeV analysis. As m_R approaches 160 GeV, the contribution from the 125 GeV state becomes smaller and smaller till after 160, it is dominated entirely by m_R. After this point, we continue with the simple ratio treatment viz.

$$\mu(125; WW) = \frac{\mathrm{B}(R \to WW)\mathrm{B}(R \to gg)}{\mathrm{B}(h_{SM} \to WW)\mathrm{B}(h \to gg)} \tag{3.2.21}$$

A second source of upper limits comes from demanding that the total signal strength at 125 GeV does not exceed the upper limit at that mass. The cuts based on transverse mass e.g. the ATLAS cut on transverse mass demanding $0.75m_H < m_T < m_H$ cuts off part of the contribution from m_R state.

$$\mu(WW) = p_{gg}^{H} \frac{\mathrm{B}(H \to WW)}{\mathrm{B}(h_{SM} \to WW)} + p_{gg}^{R} \frac{a(125; R)}{a(125; h_{SM})} \frac{\mathrm{B}(R \to WW)}{\mathrm{B}(h_{SM} \to WW)} \tag{3.2.22}$$

In the ATLAS analysis, the kinematical cuts for Higgs search up to mass of 200 GeV are identical excepting the transverse mass cut. In the CMS analysis, the cuts vary continuously with mass. We refer the reader to the relevant papers [4, 5, 114] for details of the cuts used.

3.2.3 Best fit contours

To answer the second question posed at the beginning of Sec. 3.2.1, we wish to obtain the best fit values for ξ and the varying scalar mass (m_R or m_H) for each value of Λ_ϕ. We primarily use data in the $\gamma\gamma$, $ZZ^{(*)}$ and $WW^{(*)}$ channels, which are the most robust. We also use $\tau\bar{\tau}$ data, however, we find that the error bars for these are so large its role in deciding the favoured region of the parameter space is somewhat inconsequential. For the $b\bar{b}$ final state, we use data in the associated production channels WH, ZH [8].

Channel	ATLAS	CMS	Tevatron
WW^*	1.0 ± 0.3	0.68 ± 0.20	
ZZ^*	1.5 ± 0.4	0.92 ± 0.28	
$\gamma\gamma$	1.6 ± 0.3	0.77 ± 0.27	
$\tau\tau$	0.8 ± 0.7	1.10 ± 0.41	
$b\bar{b}$ (Tevatron)			1.97 ± 0.71

Table 3.1: Best-fit values of signal strength used for global fits [6, 7, 8].

We do not use the data from LHC in this channel as its error bars are larger even than the $\tau\bar{\tau}$ channel and therefore do not restrict any of the parameter space.

To find the best fit, our task is to scan the parameter space and find the values of $m_{\varphi'}$ and ξ for any Λ_ϕ, which minimize

$$\chi^2 = \sum_i \frac{(\mu_i - \hat{\mu}_i)^2}{\bar{\sigma_i}^2} \tag{3.2.23}$$

where $\mu_i = \sigma/\sigma_{SM}$ is the signal strength at 125 GeV as calculated in the ith channel, $\hat{\mu}_i$ denotes the experimental best fit value for that channel, and $\bar{\sigma}_i$ being the corresponding standard deviation. Changing ξ and m_R affect the signal strength of H even though m_H is held fixed at 125 GeV. Again, we use the simple ratio-based formulae for $\gamma\gamma$, $ZZ^{(*)}$, $b\bar{b}$ and $\tau\bar{\tau}$ (using associated production instead of gluon fusion for $b\bar{b}$). For $WW^{(*)}$, the formula (Eqn. 3.2.22) is used. The data points used for performing global fit are summarized in Table 3.1.

The 68% and 95 % contours are determined using

$$\chi^2 = \chi^2_{min} + \Delta\chi^2 \tag{3.2.24}$$

where $\Delta\chi^2$ values corresponding to the confidence levels for seven degrees of freedom (8.15, 14.1) are used. Since the best-fit values reported by the experiments are based on combination of 7 and 8 TeV runs, we combine our signal strengths at 7 and 8 TeV weighted by the luminosity.

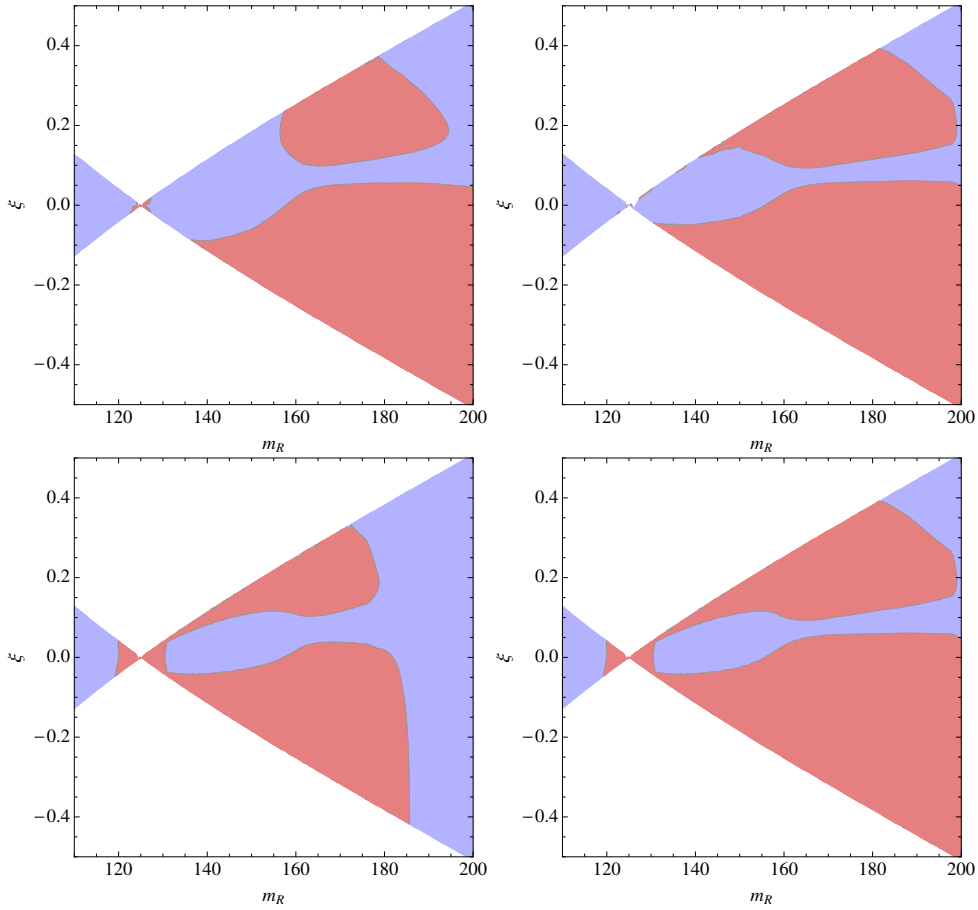

Figure 3.1: The effect on the excluded parmeter space (shown in red) from various contributions. The top-left panel shows the excluded region using ratios of branching fractions of m_R alone. The top-right panel is the exclusion when contribution from both states are taken into account. The bottom-left panel shows the exclusion from applying the limit on signal strength at 125 GeV. Finally, the bottom-right panel shows the total excluded parameter space. This illustration uses $\Lambda_\varphi = 3$ TeV and 95% CL limits from the ATLAS collaboration.

Since the upper limits are based on signal strength mainly due to the second resonance whereas the best-fit requires the correct signal strength at 125 GeV, there may be regions with a small chi-squared that are already ruled out due to constraints on signal from the second resonance. We therefore also perform the best fit in the region left out after the exclusion limits are applied. However, to avoid overconstraining the parameter space, we do not include the exclusions arising from upper limit on the signal strength at 125 GeV as given by (Eqn. 3.2.22) while performing the chi-squared minimization.

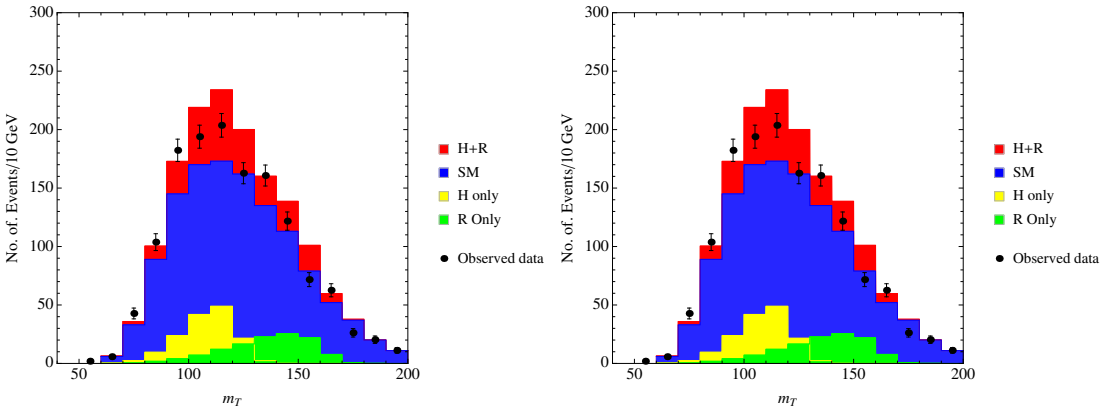

Figure 3.2: Comparison of m_T distribution after contribution from both scalars is taken into account for a parameter point that is ruled out and one that is not by the ATLAS limits. The parameters for illustration are $\xi = 0.045$ (left; disallowed) and $\xi = 0.065$ (right; allowed), $m_H = 125$ GeV, $m_R = 164$ GeV and $\Lambda_\varphi = 3$ TeV. The label "SM" refers to the total SM background as extracted from [4, 5].

3.3 Results and discussions

The most recent CMS and ATLAS search results exclude the Standard Model Higgs in the mass range 128 to 600 GeV at 95% CL [6, 7]. In this section we present the regions of the RS parameter space that allow the presence of an extra scalar consistent with observed upper limits.

We illustrate the effect of taking signal contributions from both states in Fig. 3.1. The top-left panel shows the excluded region when the upper limits are placed on signal strength of the extra R state alone using only the multiplicative correction of Eqn. 3.2.19. This was the approach used e.g. in [87]. However, the presence of two states means there are two sources of limits — firstly, we require the total signal strength at 125 GeV to be less than the observed upper limit at 125 GeV (bottom-left panel) and secondly, we also require that the combined signal strength be smaller than the observed limit at the mass of the radion-like resonance m_R (top-right panel). Finally we show the effects of both these taken together to give the full exclusion (bottom-right panel).

A caveat in the above result is that the likelihood function used by the experiments

to place limits makes use of not just on the total number of events but also the shape of certain distributions like the lepton invariant mass $m_{\ell\ell}$ or the transverse mass m_T.[1]

The presence of a shoulder, in e.g. the m_T distribution, can be indicative of a second state and could possibly lead to stronger exclusions in the region where $m_R > m_H$. For a fixed ξ, the branching fraction $R \to WW^*$ reaches it's maximum value for about 160 GeV. For masses greater than this threshold, the change in total signal strength is governed mainly by the change the production cross section. However, since the production cross section decreases with increasing m_R, the distortion in m_T distribution from the extra state also becomes smaller with increasing m_R and is maximal around 160 GeV.

We present the m_T distribution showing extra contribution from R for $m_R = 164$ GeV in Fig. 3.2 for two nearby values of ξ viz. 0.045 and 0.065. Our calculation of the m_T distribution is superimposed over the estimated background reported by ATLAS [5]. There are in principle, regions of parameter space where the contribution at 125 GeV from R even exceeds that from H. However, we find that the current upper limits on signal strength in WW channel are so strong that this always results in a very large total signal strength at m_R and is consequently ruled out. This is illustrated in Fig. 3.2 where the point with $\xi = 0.045$ shows a significant contribution from R but we find is already disallowed by the 95% upper limits on signal strength at 164 GeV.

This observation justifies our assumption that the distortion in the m_T distribution is not too large even for $m_R \gtrsim 160$ GeV. We therefore present our results with the assumption that the upper limits on total signal strength give a reasonably good approximation of the true exclusion limits even though in principle it corresponds to a limit on the overall normalization of the distribution only.

[1]The transverse mass variable is defined as $m_T = \sqrt{(E_T^{\ell\ell} + \not{E}_T)^2 - |(p_T^{\ell\ell} + \not{E}_T)|^2}$, where $E_T^{\ell\ell}$ is the transverse energy of the leptonic system, p_T^{ll} is the total transverse momentum of the leptonic system and $\not{E}_T$ is the missing energy.

3.3.1 Exclusion of the Parameter Space

We show the regions of parameter space ruled out from current ATLAS and CMS data in Fig. 3.3. As expected, the allowed parameter space for low Λ_φ is more restricted than for higher values. We find that barring a small sliver close to $\xi = 0$, almost the entire parameter space is ruled out for $\Lambda_\varphi = 1.5$ TeV. For $\Lambda_\varphi = 3,\ 5$ TeV, the exclusion is less severe. However, the region with nearly degenerate R and H states is ruled out. At large m_R, the most stringent limits come from ZZ. We therefore find regions where a significant branching fraction $R \to t\bar{t}$ reduces the constraints after $m_R > 350$ GeV. However limits are still restrictive for negative ξ values as the production via gluon fusion is enhanced in this region.

We also find that CMS constraints are much stronger than ATLAS. This is expected in $WW^{(*)}$ since CMS has provided limits based on the full 7 and 8 TeV dataset whereas ATLAS has provided only partial results [114, 5]. We list here the corresponding conference notes from ATLAS that have been used for determining the ATLAS limits. Both experiments give limits in ZZ channel based on the full dataset [115, 116].

The $\gamma\gamma$ limits are available only in the range 110-150 GeV [117, 118], presumably since the SM Higgs decays into the diphoton channel becomes negligibly small beyond this range. However, since there can be enhancements to this rate in the radion-Higgs mixed scenario, it may be useful to have the limits in the full range. Taking interference of both states when their masses lie between 122 and 127 GeV pushes the predicted signal strength beyond the observed upper limits thus ruling out the degenerate region entirely. The $b\bar{b}$ limits, from ATLAS, CMS or Tevatron are found to not affect the extent of the region of exclusion.

Whenever the limits are based on combined datasets, we combine our calculated signal strength at 7 and 8 TeV with the luminosities serving as weights. For $\Lambda_\varphi = 10$ TeV, we do not find any significant exclusions.

A natural question to follow this analysis is what happens if the boson found at 125

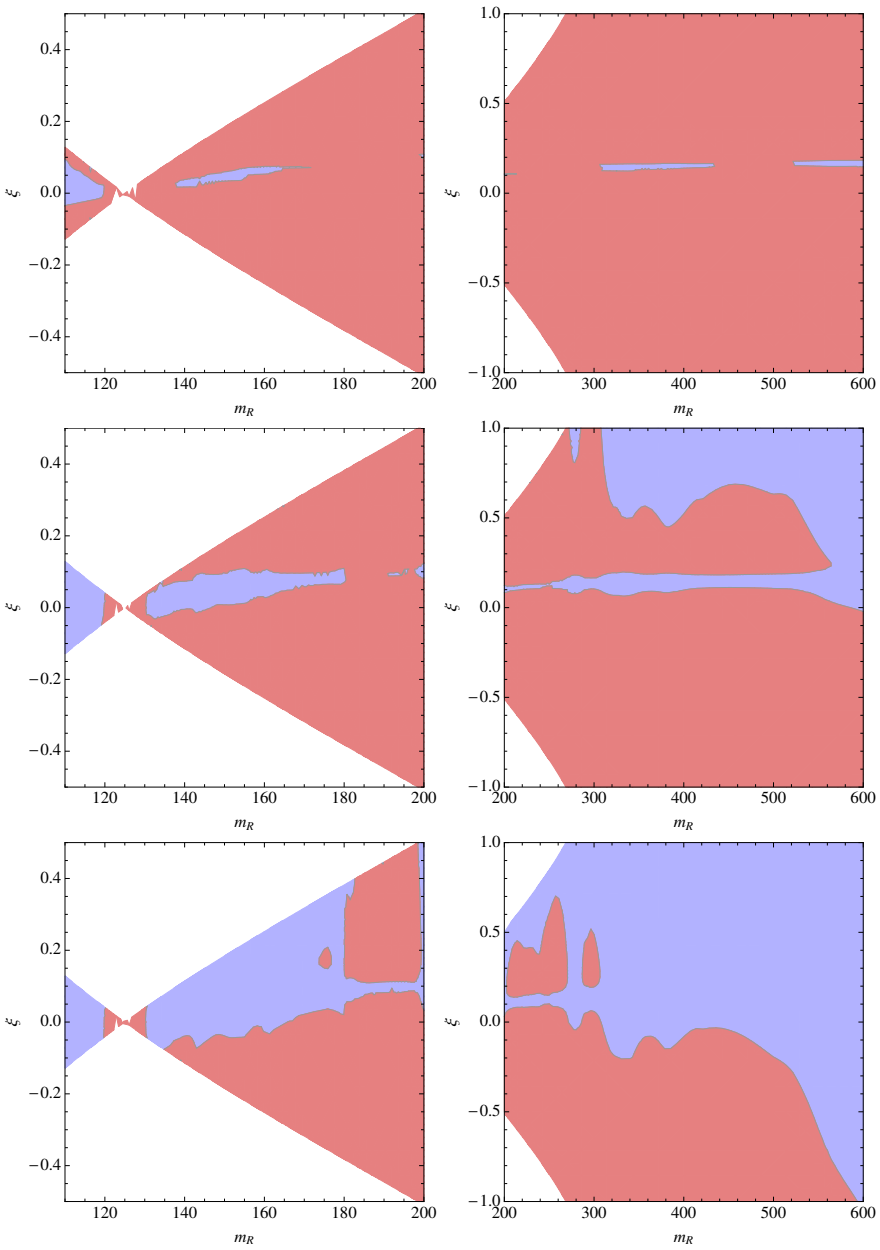

Figure 3.3: Excluded parameter space for the case with $m_H = 125$ GeV (shown in red) using 95% CL limits from the ATLAS and CMS. This illustration uses Λ_φ =1.5 TeV(top), 3 TeV(mid) and 5 TeV(bottom).

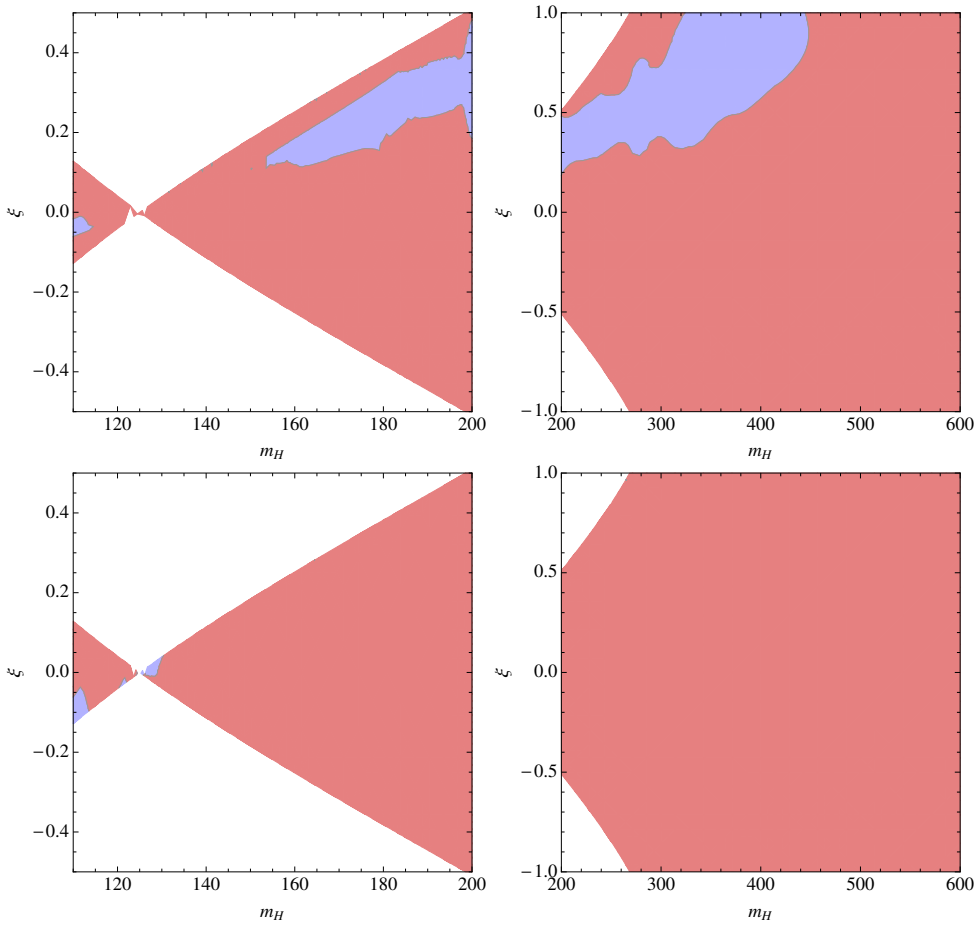

Figure 3.4: Excluded parameter space (shown in red) for the case with $m_R = 125$ GeV using 95% CL limits from the ATLAS and CMS. This illustration uses Λ_φ =1.5 TeV(top) and 3 TeV (bottom). Almost the entire parameter space is excluded for Λ_φ =5 TeV and higher.

GeV is the m_R state and not the m_H one. The exclusions resulting from reversing our analysis in accord with this change is shown in Fig. 3.4. We find here that larger values of Λ_φ have larger exclusions with almost the entire parameter space being excluded for $\Lambda_\varphi > 5$ TeV. This is in accordance with [78] where they show that a pure radion at 125 GeV is already ruled out. As Λ_φ increases, H becomes more and more like the SM Higgs (and equivalently R becomes a pure radion). As the limits on SM Higgs already rule it out in most of the mass range, we find that nearly the entire parameter space is ruled out too. In performing the reverse analysis, we have not considered the interference from both states, therefore the small allowed region near 125 GeV should be taken with a pinch of salt. Since the result should not change from the earlier case as $m_R \simeq m_H$ in this region and we may assume that it will be ruled out if a full calculation with interference is made.

3.3.2 Regions of best-fit with the data

Using the chi-squared analysis outlined in the Sec. 3.2.3, we perform a global fit using the values of signal strength shown in Table 3.1. We also perform the same exercise after removing the regions excluded by the upper limits. Of course, while doing so, we do not apply the upper limit on signal strength at 125 GeV. So the only exclusions considered are those resulting from limits on signal from m_R only. For illustration, we show the results at $\Lambda_\varphi = 3$ TeV in Fig. 3.5. The first panel shows the regions that agree with the data within 68% and 95%. The second panel shows the reduction in the best-fit region when the exclusions reported in Fig. 3.3 are imposed as well. The bottom panel shows the best-fit region after exclusions for the reverse case where $m_R = 125$ GeV and m_H is varied.

The chi-squared value for the SM is 10.93 for nine degrees of freedom. We find that in the first case with $m_H = 125$ GeV, there is always a small region of parameter space that fits with a similar χ^2/dof as the SM. For $\Lambda_\varphi = 1.5$ TeV, the minimum chi-squared value found is 9.06 without exclusions and 11.57 with exclusions at point

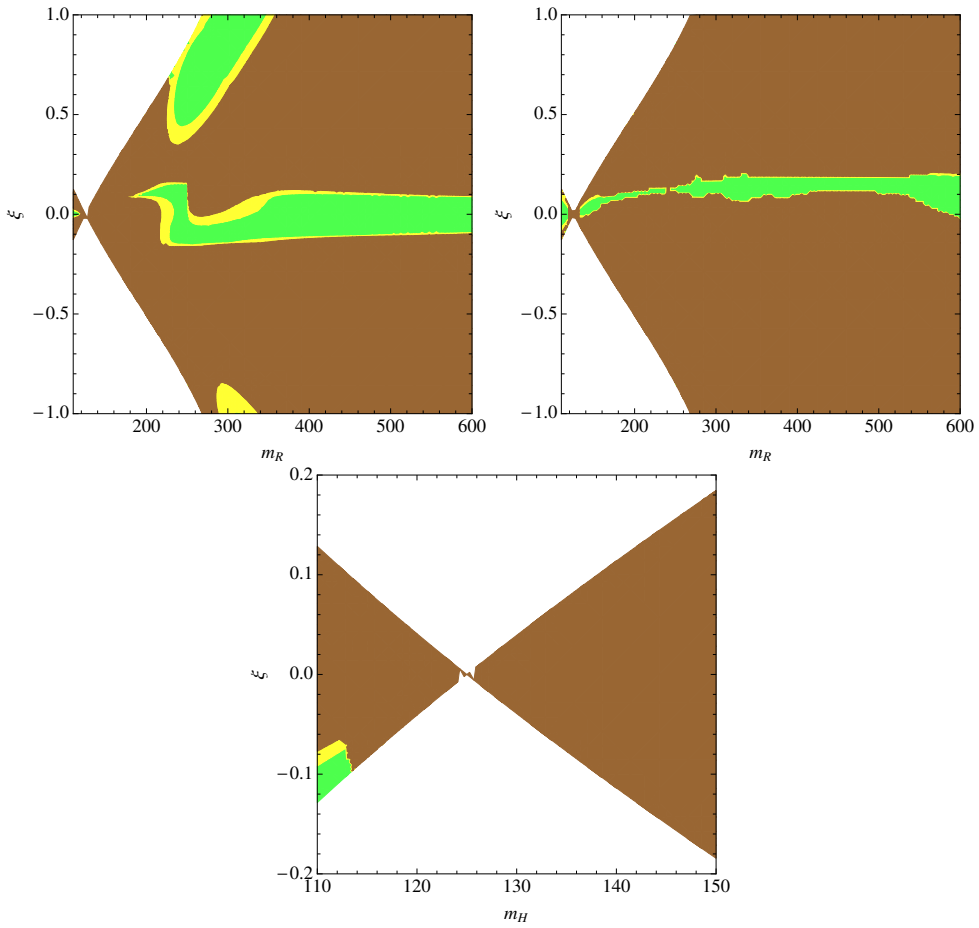

Figure 3.5: Regions that agree with current data within 68% (green) and 95.4% (yellow) for $\Lambda_\varphi = 3$ TeV. The top-left plot shows the case where no exclusions have been taken into account. The top-right side shows the change after taking exclusions into account. The bottom plot is for the case where we hold $m_R = 125$ GeV instead of m_H.

$m_R = 600$ GeV and $\xi = 0.15$ (after excl.). For 3 TeV, the numbers are (9.03, 9.08) respectively with the best-fit point at $m_R = 407$ GeV and $\xi = 0.15$ and for 5 TeV, they are (9.03, 9.04) with the best-fit point at $m_R = 383$ GeV and $\xi = -0.25$. Thus, the exclusions affect less and less as we increase Λ_φ, which is expected as the excluded parameter space also reduces. In particular, as the exclusions on negative ξ are relaxed, these values seem to give a slightly better fit. Although, as seen from the change in χ^2 with and without exclusion, the distribution is rather flat for large m_R. Also, as the best-fit value for m_R is at the edge of our scan for $\Lambda_\varphi = 1.5$ TeV, it is possible that the fit would be further improved by increasing m_R. For larger values of Λ_φ however, increasing m_R seems to increase the χ^2/dof slightly.

The chi-squared for the reverse case is decidedly worse than in the normal case. We find that the minimum values of chi-squared after exclusions are 35.6, 18.22, 52.0 for (1.5, 3, 5 TeV). Therefore, we can say that this scenario is strongly disfavoured compared to the SM.

3.4 Conclusions

We have examined the possibility that the currently observed scalar is one of the two states of a mixed radion-Higgs scenario. To perform this analysis, we have considered the contribution from both states in the $WW^{(*)}$ channel, differently affected by cuts, to calculate the signal strength. We also take into account effects of interference when both states are nearly degenerate.

We find that if the 125 GeV state is radion-dominated, only a very small region of the parameter space with a small Λ_φ is consistent with current upper limits. Even in these regions, the goodness of fit with data is decidedly worse than in the SM. Therefore, we may conclude that the idea that the discovered boson at 125 GeV is dominantly radion-like is largely disfavoured.

The second possibility, namely that the LHC has found a 125 GeV Higgs-dominated

scalar, but a radion-dominated state, too, hangs around to contribute to the observed signals (especially the $WW^{(*)}$ signal), can not be ruled out with current data. We find the scenario with small (but non-zero) mixing and an accompanying radion-dominated state with high mass results in a good fit for almost all values of Λ_φ. However, if we include exclusions on the presence of the second, radion-dominated boson that would surely accompany the Higgs-dominated state, the goodness of fit is reduced for TeV-range values of Λ_φ. We find that for Λ_φ up to 5 TeV, the SM still provides a better fit. As a special case, we find that situations where the two mass eigenstates are degenerate enough to warrant the inclusion of interference terms, are ruled out. Finally $\Lambda_\varphi = 10$ TeV is mostly indistinguishable from the SM as the modifications to signal strengths are too small to be significant.

Chapter 4

Probing light radion at the LHC

4.1 Introduction

After exploring the constraint on the Higg-radion mixing scenario from the LHC 7+8 TeV data, we have examined how the radion can be probed in a relatively difficult mass range, namely, for its mass around 100 GeV or below. In this analysis we restricted ourselves to the unmixed scenario such that the scalar resonance observed at LHC is a pure SM Higgs boson (h). We concentrated on identifying the most promising signals for an unmixed light radion ($m_\varphi < m_h$), which could provide the first observable signals for models of extra spatial dimensions with warped geometry. Our results can be very easily generalized to the mixed scenario as well, and are also applicable to extensions of the RS model where the SM fields propagate in the bulk. We focus primarily on the following interesting highlights of a light radion signal at the LHC:

- An unmixed radion lighter than the 125 GeV Higgs can have appreciable production cross section for allowed values of the vev ($2\ \mathrm{TeV} < \Lambda_\varphi < 3$ TeV), primarily through gluon fusion. A factor that contributes to this, namely, the trace anomaly contribution, boosts the loop induced decay modes of the radion into a pair of massless gauge bosons. This can partially compensate for the Λ_φ suppressions in its couplings to SM particles.

- A light radion with mass below 100 GeV is not ruled out by any experiments [89]. We show that the channel ($\gamma\gamma$) which helped discover the SM Higgs with the maximum significance would also be the most promising channel for such a light radion at the LHC.

- The radion loop-induced decay mode ($\gamma\gamma$) also acquires an enhancement from the trace anomaly (which interferes constructively with the dominant W boson mediated loop amplitude) and yields a reasonably healthy, *albeit* small diphoton branching rate for radion masses below 120 GeV.

One must note that the radion signal depends crucially on the value of Λ_φ which suppresses the effective coupling of the radion to SM fields as the couplings are inversely proportional to the value of Λ_φ. Current constraints on the KK excitations of the spin-2 graviton already put a lower bound on the value of the Λ_φ [119].

For a radion of mass $\simeq$ 100 GeV and lower, the dominant decay modes are gluon-gluon and $b\bar{b}$, while the branching ratios into WW^*/ZZ^* are suppressed (2.5.35),(2.5.38). The signal arising from $b\bar{b}$ and gg are beset with large QCD backgrounds, even if we consider various associated production channels. Thus, with the enhanced gg fusion as the production mode, $\varphi \to \gamma\gamma$ becomes the best channel for observing the light radion at the LHC. Since a peak in the diphoton invariant mass is a rather spectacular signal of new physics, the refinement of techniques to isolate two photons can be helpful in a more general context as well.

With the impressive performance of the electromagnetic calorimeter at the CMS and ATLAS experiments, and optimized event selection criteria for the diphoton signal, we have been able to observe the SM Higgs boson with large significance, even with nominal luminosities available at the 7 and 8 TeV runs. We are about to enter a regime of higher intensity running of the LHC with roughly double the center of mass energies. In view of this, the prospects of observing a light radion in the same mode are good. We demonstrate this with a detailed analysis of the radion signal and the

SM background in the $pp \to \gamma\gamma + X$ events at the 14 TeV run of LHC.

The SM backgrounds for these events are of course formidable. As for the case of Higgs signals, the $\gamma\gamma$ final state has backgrounds from not only prompt photon pairs, but also γj and jj production. Of these, the γj background can be substantial, especially for low diphoton invariant mass. We followed the cuts commonly used by ATLAS and CMS for reducing these backgrounds without compromising too much on the signal rates [120, 93].

4.2 Analysis of the radion in the two-photon channel

4.2.1 Radion production and decay at the LHC

At hadron colliders, the radion can be produced via gluon fusion or through W or Z fusion, and can also have associated production modes with W, Z bosons and $t\bar{t}$. The first of the aforementioned production modes, receives a sizable boost from trace anomaly. The radion can also be produced in association with a W or Z boson. The radion produced in association with a gauge boson can decay to $b\bar{b}$ with sizable cross section. The final state will be either dilepton plus two b-jets or single lepton plus two b-jets. But the associated production channel is not of much use, due to its suppression by Λ_φ, in contrast to the gluon-fusion channel where the trace anomaly term at least partially compensates with an enhancement (Section 2.5). We analyzed the final states for such a signal and found that the SM dilepton background and single lepton background overwhelms the signal and is roughly three to four orders of magnitude higher than the signal. Another possibility is the production of the radion via vector boson fusion and its subsequent decay to $b\bar{b}$. Here too, the suppression in couplings by the radion vev is a problem; and on the whole, the $2j + b\bar{b}$ SM background is also found to be larger than the signal by four to five orders of magnitude [121]. The most promising production channel thus remains the gluon fusion.

The production cross section of the radion in gluon fusion channel at the LHC is

illustrated in Fig 4.1(a) for 13 TeV and 14 TeV center of mass energies. Since the cross-sections are of comparable magnitudes, we present the rest of our results for 14 TeV, with the understanding that the predictions are generally valid if a part of the LHC run is at 13 TeV center of mass energy.

We used a radion vev, $\Lambda_\varphi = 2$ TeV in most of our subsequent analysis (2.5.46). The cross-section corresponding to any other Λ_φ can be obtained by simple scaling. The branching ratios of the radion to all possible final states are shown in Fig 4.1(b). Note that the different branching ratios of the radion decay are independent of Λ_φ, since all interactions of the radion with SM particles is inversely proportional to it, including the radion width.

As seen from Fig 4.1(b), when the mass of the radion is less than 100 GeV, it decays dominantly into two gluons. However the two gluon final state gets swamped by the large QCD background at the LHC, making it a very difficult channel to observe any signal for a light radion.

This leaves two potential channels in which a light radion can be probed, namely, $\gamma\gamma$ and $\tau^+\tau^-$. From the experience with the Higgs boson, various subtleties involved in the analysis of a $\tau^+\tau^-$ final state makes it more suitable as a channel which will confirm the presence of the radion, rather than one used for discovery. Furthermore, a light radion produces relatively softer τ's, which can stand in the way of efficient identification. The diphoton final state, on the other hand, is more spectacular in terms of reconstruction, in spite of the low branching ratio. Thus the diphoton channel, when it comes to uncovering a radion in the mass range 60 - 110 GeV, remains the most promising, and which we analyze next.

4.2.2 The diphoton channel: signal and backgrounds

As stated, the diphoton channel for the radion is one with very high sensitivity, and should be given priority in the explorations at the 14 TeV run of the LHC. In our study we have varied the mass of the radion from 60 GeV to 110 GeV. The status of a heavier

radion can be surmised from the 8 TeV run itself, for example, from reference [88, 90] in the zero-mixing limit. The diphoton signal for a radion of mass $m_\varphi > 100$ GeV has also been considered in [122]. However, that analysis is based on a model with gauge fields in the bulk, where the diphoton rate receives an enhancement[1]. Our study addresses a situation where (a) such enhancement is absent and (b) the radion is lighter than 100 GeV. On both counts, overcoming the backgrounds thus becomes a tougher challenge for us.

Two isolated photons in the final state can be mimicked by many SM processes. We classify the processes into two categories, reducible and irreducible.

- The irreducible background consists of two prompt photons in the final state. It originates from the tree level production via $q\bar{q}$ annihilation (Born process) as well as from the one-loop process (box diagram) in gluon fusion with quarks running in the loop. The contribution from the latter is comparable to that from the Born level process because of the high gluon flux at low-x, where x represents the energy fraction of the colliding proton energy carried by the partons. These photons are as isolated as those arising from radion decay. Such isolated photon pairs constitute an irreducible background to the signal in any search window for a mass peak [124].

- The dominant reducible background arises from a prompt photon along with a jet. A π^0, a ρ or an η decays into two collimated photons that are identified as a single electromagnetic cluster in the detector. This causes the misidentification of jets as hard isolated photons. Although the probability of this misidentification in a particular event is small, the sheer volume of the γj cross-section turns it into a serious background. We suggest ways of reducing this kind of background in the subsequent analysis.

- Similarly, as above, two jets can be misidentified as a pair of isolated photons.

[1]Other mechanisms leading to enhancement in the diphoton channel also exist [123].

The double misidentification probability, however, is small, and the dijet background is not significant in the present analysis.

- The Drell-Yan production of e^+e^- can also mimic diphotons, if the $e^\pm$ tracks are not correctly reconstructed by the inner tracking chamber. We convolute the Drell-Yan background with a typical inefficiency of 5% for the track detector at the LHC [125].

4.2.3 Signal versus background analysis

The signal events are generated in `MADGRAPH 5` [126], where the interaction vertices of the radion are included using the `FeynRules` [127, 128] package. We have used `PYTHIA 8` [110] for showering and hadronization of the signal events as well as for generating background events. We adopted CTEQ6l1 [129] as our parton density function (PDF). The renormalization and factorization scales are kept at the default value of `PYTHIA 8`. To obtain sufficient statistics for the signal as well as for the background events, we divided our whole analysis into different phase space regions distinguished by the value of the radion mass. For this purpose, we designated different region of $\hat{\mathrm{m}}$ (the invariant mass of the outgoing partons), for different mass values of the radion:

- For m_φ = 60 GeV: 45 GeV $\leq \hat{\mathrm{m}} \leq$ 75 GeV;
- For m_φ = 70 GeV: 55 GeV $\leq \hat{\mathrm{m}} \leq$ 85 GeV;
- For m_φ = 80 GeV: 65 GeV $\leq \hat{\mathrm{m}} \leq$ 95 GeV;
- For m_φ = 90 GeV: 75 GeV $\leq \hat{\mathrm{m}} \leq$ 105 GeV;
- For m_φ = 100 GeV: 85 GeV $\leq \hat{\mathrm{m}} \leq$ 115 GeV;
- For m_φ = 110 GeV: 95 GeV $\leq \hat{\mathrm{m}} \leq$ 125 GeV.

For realistic background estimations, we implemented an algorithm at the generator level, which approximates the clustering procedure in a typical electromagnetic

calorimeter (ECAL). Specifically, we used the dimension of an ECAL crystal of the Compact Muon Solenoid (CMS) detector. The ECAL at the CMS is made up of Lead Tungstate ($\mathrm{PbWO_4}$) crystals. A single crystal of the ECAL covers 0.0175×0.0175 in the $\eta - \phi$ plane. The electromagnetic shower from an unconverted photon is contained within a 5×5 crystal matrix around the seed crystal (*i.e.*, the one hit by the photon). In case of a converted photon, the typical region of energy deposit is wider. In order to make the analysis robust, we used a 10×10 crystal size for photon reconstruction, equal to $\triangle \mathrm{R} = 0.09$ (where $\triangle \mathrm{R} = \sqrt{\triangle\eta^2 + \triangle\phi^2}$) in the $\eta - \phi$ plane of the CMS detector. The momentum of the photon candidate is defined as the vector sum of the photon and electron momenta falling within the cone $\triangle \mathrm{R}$ = 0.09 around the seed, which is either a direct photon or an electron.

To account for finite detector resolutions, we smeared the photon, electron and jet energies with Gaussian functions [130]. We selected the photon seeds satisfying $|\eta| < 3.0$. The reconstructed photon candidates are then accepted if they satisfy the preselection criteria given as

- $\mathrm{p_T^{\gamma,\,leading}} > 15$ GeV and $\mathrm{p_T^{\gamma,\,subleading}} > 10$ GeV;
- $|\eta_\gamma| < 2.5$.

The $|\eta|$-interval is reduced further to emulate the inefficient tracker region. These triggered photon candidates are required to have minimal hadronic activity. Jets are reconstructed in our analysis with $|\eta| < 4.5$ and $\mathrm{p_T^j} > 10$ GeV using an anti-$\mathrm{k_t}$ algorithm [131]. Photons arising from the jets are rejected by demanding that the scalar sum of the entire transverse energy within a cone of $\triangle R = 0.4$ be less than 4 GeV[2]. Only those isolated photons which survive the above selection criteria qualify for our final analysis.

[2]This is an 'absolute isolation' criteria. One can alternatively require a relative isolation, demanding that the total visible $\mathrm{p_T}$ within $\Delta \mathrm{R} = 0.4$ is less than 10% from that of the photon. This raises the statistical significance for lower mass of m_φ.

The $\mathrm{p_T^\gamma}$ distribution for background and signal are plotted in Fig. 4.2(a), 4.2(b) for $m_\varphi = 60$ GeV, and in Fig. 4.2(c), 4.2(d) for $m_\varphi = 100$ GeV. Other kinematic variables, such as angular separations, can be used as good discriminators at the generator level. However, once the detector resolutions are taken into account the distinct features of these variables are smeared. We find that the background coming from a prompt photon and a jet dominates over the two prompt photon background in the low ($\mathrm{p_T^\gamma} < 35$ GeV) region. With increasing $\mathrm{p_T^\gamma}$, the jet-γ misidentification rate decreases and hence the γj background falls gradually. Though the Drell-Yan background is two orders of magnitude lower than the direct photon background, it increases near the Z mass pole, and is comparable to the direct photon backgrounds. We find that the two-jet background is negligible, and thus we do not consider it in our analysis. As seen in Fig. 4.2, radion mass-specific $\mathrm{p_T^\gamma}$-cuts are effective, in view of the fact that a heavier radion generally yields harder photons. For a heavier radion, the fraction of events with harder $\mathrm{p_T^\gamma}$ in the signal is large compared to the background. Thus, it is easier to separate the signal events from the background by selecting harder photon candidates. The mass dependent $\mathrm{p_T}$ cuts in our analysis are formulated as

$$\mathrm{p_{Tmin}^{leading}} = (\mathrm{m_\varphi}/2 - 5.0)\ \mathrm{GeV}; \qquad \mathrm{p_{Tmin}^{subleading}} = (\mathrm{p_{Tmin}^{leading}} - 5.0)\ \mathrm{GeV}. \tag{4.2.1}$$

We finally select only those events that fall within the invariant mass window of $\pm$3.5 GeV about the radion mass. If we consider the invariant mass window to be about 5 GeV, the background rate increases, thus reducing the signal-to-background significance ($S/\sqrt{B}$).

The cut flow for the signal with 60 GeV and 90 GeV radion mass and the corresponding SM background are presented in Table 4.1. The mass dependent cuts along with the final signal-to-background significance are shown in Table 4.2. In Fig. 4.3(a), we plot the integrated luminosity required to achieve 5σ significance level for different radion mass. In Fig. 4.3(b), we also plot the maximum vev of the radion that can

be probed with 5 σ significance level for different mass values of the radion with two choices of the integrated luminosity. Note that these results do not conflict with the recent ATLAS search [93] at $\sqrt{s} = 8$ TeV and with luminosity $\mathcal{L} = 20.3$ fb^{-1}. The data rules out signals with $\sigma_{gg} \times BR(\varphi \to \gamma\gamma)$ of 30 fb or more, while the signal rate for $\sqrt{s} = 8$ TeV in our scenario is smaller in magnitude.

m_φ	Cuts applied	$\varphi \to \gamma\gamma$	$\gamma\gamma$	$j\gamma$	e^+e^-	$b_1 + b_2 + b_3$
[GeV]		S [fb]	b_1 [pb]	b_2 [pb]	b_3 [pb]	B [pb]
60	Initial Signal	39.88	226.84	218109.90	133.78	218470.52
	Preselection	30.80	87.88	6332.58	0.67	6421.13
	Isolation	24.51	76.76	973.20	0.55	1050.51
	$p^{\gamma,l} > 27$ GeV $p_T^{\gamma,sl} > 22$ GeV $56.5 < m_{\gamma\gamma} < 63.5$ [GeV]	14.02 13.98	19.15 6.35	49.73 22.68	0.22 0.05	69.10 29.08
90	Initial Signal	30.84	48.28	46788.40	1598.90	48435.58
	Preselection	25.00	18.20	3198.46	10.60	3227.26
	Isolation	19.50	15.59	309.65	8.48	333.72
	$p^{\gamma,l} > 40$ GeV $p^{\gamma,sl} > 35$ GeV $86.5 < m_{\gamma\gamma} < 93.5$ [GeV]	9.59 9.58	3.77 1.04	7.29 2.15	3.72 2.44	14.78 5.63

Table 4.1: Cut flow table for two different values of radion mass, $m_\varphi = 60$ GeV and $m_\varphi = 90$ GeV.
.

Fig. 4.4 shows the invariant mass peak of the signal against the background, for $m_\varphi = 60$ GeV. For an efficient modeling of the background, a low-luminosity histogram for the background has been generated first. Thereafter, a fitting function has been used to improve it, thus yielding the background for a luminosity of 3000 fb^{-1}. It should also be noted that the bump corresponding to the signal is sitting on the edge of the rising part of the background. This is in contrast with the familiar figure for Higgs reconstruction, where the bump is seen against a monotonically falling back-

m_φ	$p_T^{\gamma,\,leading}$, $p_T^{\gamma,\,subleading}$	$m_{\gamma\gamma}^{min}$, $m_{\gamma\gamma}^{max}$	S	B	σ
[GeV]	[GeV]	[GeV]	[fb]	[pb]	$S/\sqrt{B}$
60	27.0, 22.0	56.5, 63.5	13.98	29.07	4.49
70	30.0, 25.0	66.5, 73.5	13.78	15.50	6.06
80	35.0, 30.0	76.5, 83.5	11.42	8.31	6.86
90	40.0, 35.0	86.5, 93.5	9.58	5.63	6.99
100	45.0, 40.0	96.5, 103.5	8.21	1.80	10.60
110	50.0, 45.0	106.5, 113.5	7.04	0.79	13.72

Table 4.2: Selection cut, background reduction and significance at 14 TeV cm energy and 3000 fb^{-1} integrated luminosity for different values of radion mass, m_φ. The signal-to-background significance, σ is defined by $S/\sqrt{B}$.

ground profile. This effect is due to the strong $\mathrm{p_T} - \mathrm{cuts}$ that we must impose on the photons, causing an additional background suppression for low $m_{\gamma\gamma}$ [3].

At this point, we should emphasize that we have carried out our analysis at the leading order (LO). To estimate how the predictions differ when including next-to-leading order (NLO) effects, one notices that the K-factor for the production of an 80 GeV Higgs is approximately 2.0 [132]. For diphotons (including the fragmentation contribution), the same K-factor is around 1.3 [133, 134]. Therefore, the inclusion of the NLO effects will, if anything, enhance our predicted significance. We also estimated the effects of varying the renormalization and factorization scales, which are set to be equal. The results presented here are based on using the default value for the renormalization scale (Q^2) of the event generator. Changing the scale to $Q^2 = {m_{\gamma\gamma}}^2$ and calculating the uncertainty by varying the scale from $Q^2/2$ to $2Q^2$, the signal as well as the background event rates change by about $\pm$ 10%.

To report the significance of a diphoton mass peak we have used a simple $S/\sqrt{(B)}$ statistic. An alternative analysis using a likelihood ratio is also possible [135, 136, 137]. While our cut-based analysis is illustrative in nature, there is scope for improving the

[3] It should be noted that we have assumed perfect identification of the vertex from where the photon is coming. In reality, due to presence of pileup vertices, photon vertex identification has a finite efficiency, which can degrade the mass resolution, and consequently the significance.

sensitivity of this channel by using more sophisticated techniques. if for example, one uses multivariate techniques, then the signal significance improves by a factor of 2. Furthermore, on splitting the sample in several categories of different purities, one expects an enhancement of about 1.5 times in signal significance.

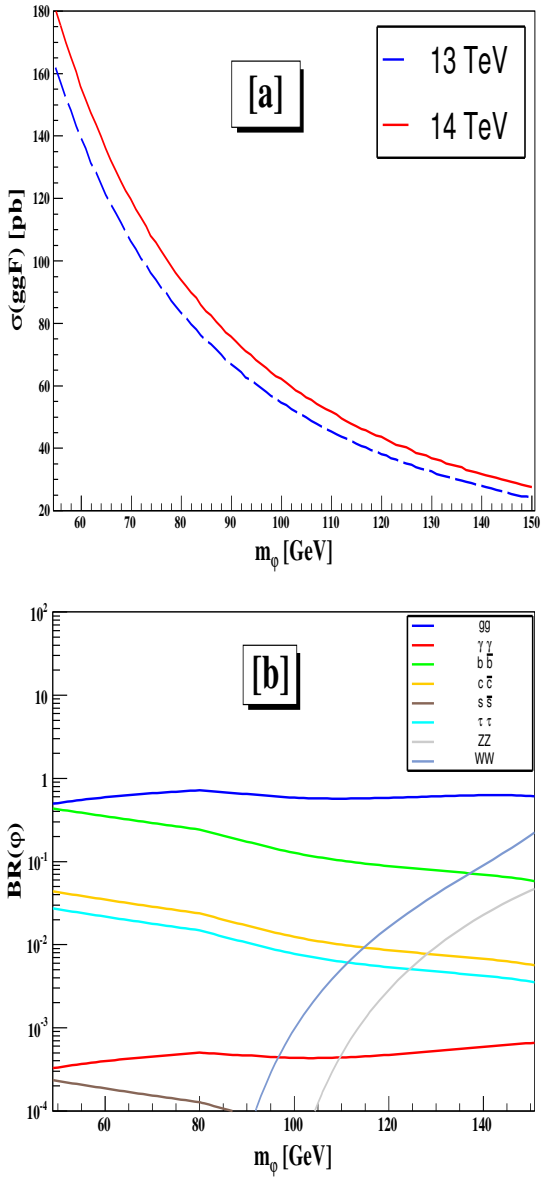

Figure 4.1: (a) Production cross section of radion via gluon fusion versus m_φ for 13 TeV and 14 TeV CM energies at the LHC. (b) Branching ratios for the radion decay modes as functions of its mass m_φ.

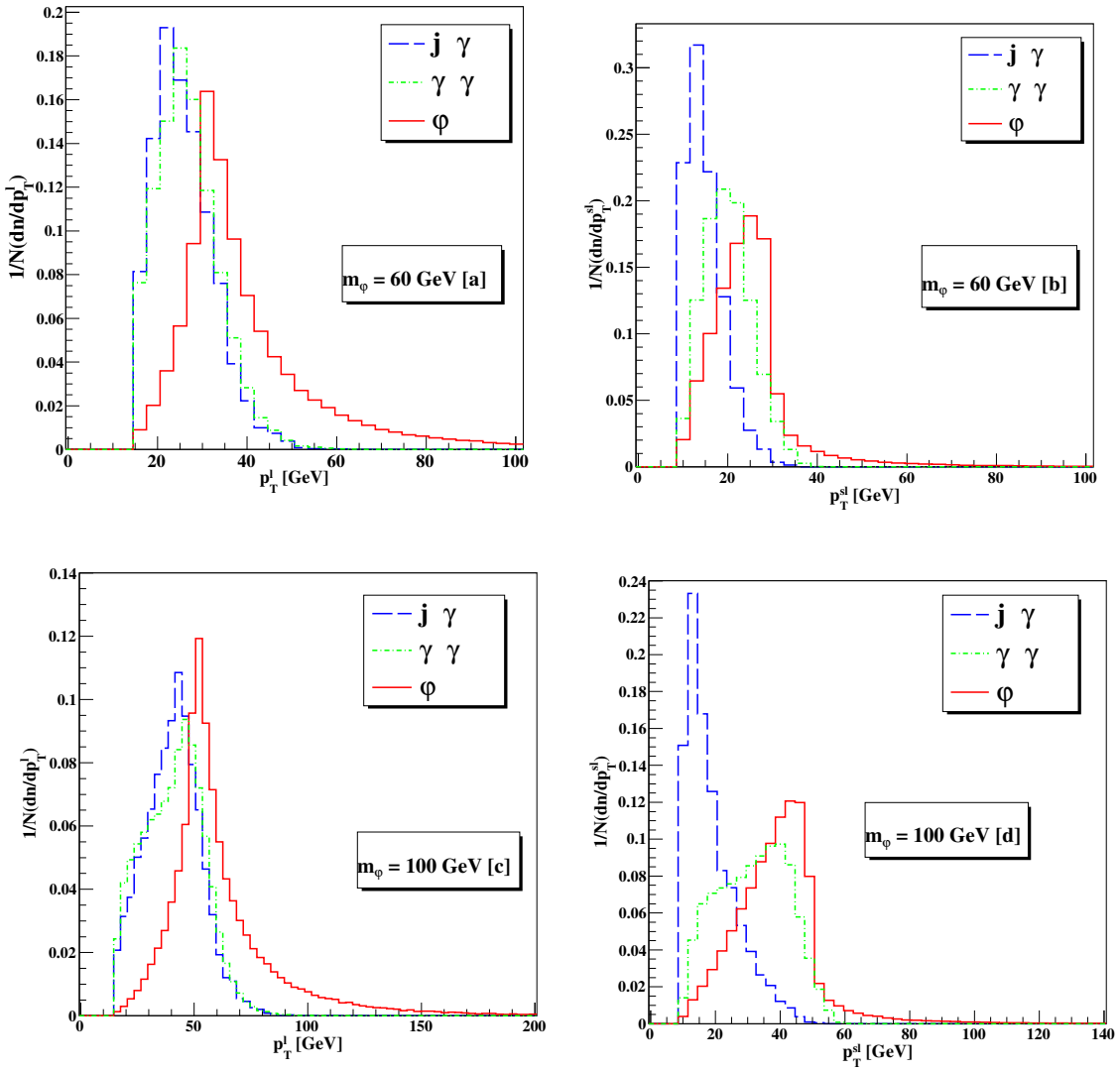

Figure 4.2: Normalized distibution of $\mathrm{p_T^{\gamma}}$ for two sample masses of radion, diphoton background and signal photon background. (a) Normalized distribution of $\mathrm{p_T^{\gamma,\,leading}}$ for $m_{\varphi} = 60$ GeV; (b) Normalized distribution of $\mathrm{p_T^{\gamma,\,subleading}}$ for $m_{\varphi} = 60$ GeV; (c) Normalized distribution of $\mathrm{p_T^{\gamma,\,leading}}$ for $m_{\varphi} = 100$ GeV; (d) Normalized distribution of $\mathrm{p_T^{\gamma,\,subleading}}$ for $m_{\varphi} = 100$ GeV.

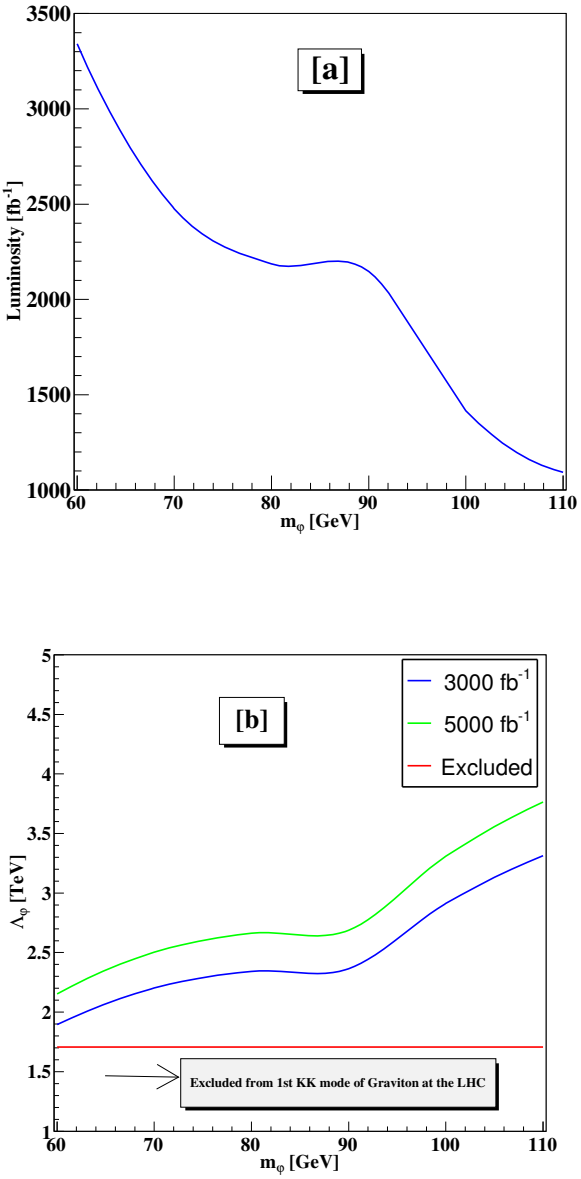

Figure 4.3: (a) Luminosity required for 5 σ discovery of radion with m_φ with $\Lambda_\varphi = 2$ TeV. (b) Maximum Λ_φ for a radion to be discovered at 5σ with m_φ.

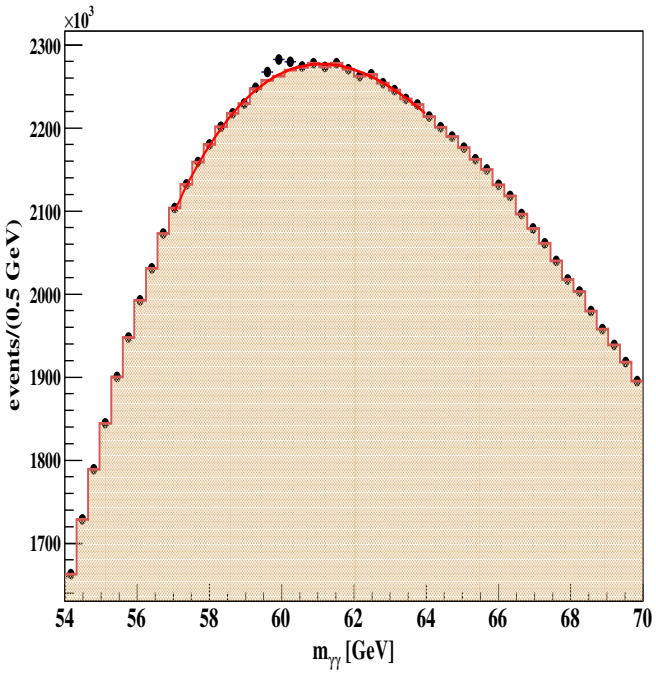

Figure 4.4: Invariant mass peak of the signal against the background, for $m_\varphi = 60$ GeV.

4.3 Summary and Conclusions

While graviton excitations are immediately recognizable signals of warped extra dimensions, spectacular as such signals can be, the limit on the mass of the lowest such excitation is increasing rather rapidly. In view of this it is important to realize that the radion, connected in a compelling way to the stabilization of the extra dimension(s), can still be quite light, consistently with data available so far.

In this work, we indicated a method for detecting the signature of a light radion, in the range 60 - 110 GeV, at the LHC. After analyzing all production and decay mechanisms, the diphoton decay channel following gluon fusion production emerges as the best and most promising signal. We thus focused on a pair of photons reconstructed to a peak at various mass windows, and applied cuts that can potentially suppress the backgrounds, where the prompt $\gamma\gamma$ production (at both the Born and box diagram levels) constitute the irreducible SM backgrounds. Event selection criteria have been suggested to reduce this as well as the (dominant) γj background, where the latter is responsible for producing a fake photon. After carrying out a detailed study using parametrized simulation and taking into account all backgrounds, we find that one can separate the signal with a significance of 5σ or more, for an integrated luminosity of up to 3000 fb^{-1}. In general, less luminosity is required for a higher radion mass, as the background falls rapidly with increasing diphoton invariant mass. The diphoton mode also avoids any problem near the Z-pole, except of course the possibility of fakes from electron-positron pairs, which is found to be small.

Notwithstanding the fact that the original RS model has gone through several extensions where SM fields have been allowed to move in the bulk, radion phenomenology has not become markedly different in such extended versions. Thus our results are valid even in extensions of the RS model that allow SM fields in the bulk. Moreover, we have studied here the case of the unmixed radion. If the radion and the Higgs boson are allowed to mix, under certain circumstances this mixing could enhance the

mixed radion-Higgs diphoton decay rate. For positive mixing parameter, the branching ratio of the light mixed radion (till 150 GeV) decaying to diphoton increases and hence can be probed with the diphoton channel at the LHC [69].

Chapter 5

An overview of two Higgs doublet models

5.1 Two Higgs doublet models

In this chapter, we will briefly discuss the minimal scalar extension of the SM, i.e adding an extra Higgs doublet [138, 47]. In order to preserve the tree-level value of the ρ-parameter at unity without extreme fine cancellations, any additional fields should be either weak isodoublets (I=1/2) with hypercharges $Y = \pm 1$. Thus, we have two complex $SU(2)_L$ doublet scalar fields ϕ_1 and ϕ_2 with the hypercharge Y = +1 or SU(2) singlets. The most general scalar potential for a two Higgs doublet scenario is

$$\begin{aligned}
\mathcal{V} &= -\mu_1^2\ \phi_1^\dagger\phi_1 - \mu_2^2\ \phi_2^\dagger\phi_2 - \mu_{12}(\phi_1^\dagger\phi_2 + \phi_2^\dagger\phi_1) \\
&+ \lambda_1\ (\phi_1^\dagger\phi_1)^2 + \lambda_2\ (\phi_2^\dagger\phi_2)^2 + \lambda_3\ (\phi_1^\dagger\phi_1)(\phi_2^\dagger\phi_2) \\
&- \lambda_4|(\phi_1^\dagger\phi_2)|^2 - \frac{1}{2}\lambda_5\left[(\phi_1^\dagger\phi_2)^2 + (\phi_2^\dagger\phi_1)^2\right] \\
&+ \lambda_6\phi_1^\dagger\phi_1\left(\phi_1^\dagger\phi_2 + \phi_2^\dagger\phi_1\right) + \lambda_7\phi_2^\dagger\phi_2\left(\phi_1^\dagger\phi_2 + \phi_2^\dagger\phi_1\right),
\end{aligned} \tag{5.1.1}$$

where all the coefficients are real. The two doublets can be written as

$$\phi_1 = \begin{pmatrix} H_1^+ \\ (v_1 + \rho_1 + i\eta_1)/\sqrt{2} \end{pmatrix},$$

and

$$\phi_2 = \begin{pmatrix} H_2^+ \\ (v_2 + \rho_2 + i\eta_2)/\sqrt{2} \end{pmatrix} \tag{5.1.2}$$

where v_1 and v_2 are the vacuum expectation value(vev) of the ϕ_1 and ϕ_2 doublets respectively. Among the eight fields, three of the fields are absorbed('eaten') to give mass of $W^\pm$ and Z^0 gauge bosons. The five remaining degrees of freedom lead to five physical scalars upon diagonalization of the neutral scalar, pseudoscalar and charged scalar mass matrices. Thus, one obtains a pair of mutually conjugate charged scalars ($H^\pm$), two neutral scalars (h, H) and one pseudoscalar A.

In a general two Higgs doublet model, a fermion can couple with both the scalar doublets. Let us consider the following Yukawa interactions for the down type quarks(Q = -1/3),

$$\mathcal{L}_Y = y_1^{ij}\bar{\psi}_i\psi_j\phi_1 + y_2^{ij}\bar{\psi}_i\psi_j\phi_2, \tag{5.1.3}$$

where i,j represents the generation index. The mass matrix is given by,

$$M_{ij} = y_1^{ij}\frac{v_1}{\sqrt{2}} + y_2^{ij}\frac{v_2}{\sqrt{2}}. \tag{5.1.4}$$

In the SM, diagonalizing the fermion mass matrices ensures the diagonalization of the Yukawa interactions. However, in the 2HDM, y_1 and y_2 can not be diagonalized simultaneously, which generates tree level flavor changing neutral currents(FCNC). These FCNCs have severe phenomenological implications [139, 140, 141, 142]. For example, if there is a $d\bar{s}\phi_1(\phi_2)$ coupling, then it contributes to $K - \bar{K}$ mixing at the tree level. Thus, it is necessary to suppress such tree level FCNCs. The Paschos-Glashow-Weinberg [143, 144] theorem states that a necessary and sufficient condition for the

absence of the FCNCs at the tree level is that all the fermions of a given charge and helicity receive their contribution of the mass matrix from a single Higgs field, i.e all the fermions of a given charge couple to only doublet. This can be arranged by implementing additional discrete symmetries in the scalar potential. Based on the Yukawa interactions of the quarks and leptons with the Higgs doublet, the 2HDMs are classified into four groups as discussed in the next section.

5.2 Types of 2HDMs

The 2HDMs with no tree level FCNCs can be classified into the following types:

- **Type I:** All the SM fermions couple to only one doublet, by convention ϕ_2. This can be enforced by adding a Z_2 symmetry and demanding that all the SM particles and the ϕ_2 doublet are even under the assigned Z_2 symmetry whereas the ϕ_1 doublet is odd under the Z_2 symmetry.

- **Type II:** The up-type quarks interact only with the ϕ_2 doublet whereas the down-type quarks and the leptons couple to the ϕ_1 doublet. In this model, the up-type quarks and the ϕ_2 doublet are even under the Z_2 symmetry and the right-handed down-type quarks, right-handed leptons and ϕ_1 are odd under the Z_2 symmetry. The Yukawa interactions of the minimal supersymmetric standard model(MSSM) and the original Peccei-Quinn models have the prototype of type II HDM.

Once the Yukawa interactions of the quarks with the two doublets are defined, we have two possibilities for the leptons to couple with the doublets. They are as follows:

- **Lepton-specific (Type X)**: All the quarks interact with the ϕ_2 doublet whereas leptons interact with the ϕ_1 doublet. Thus, all the quarks and the ϕ_2 doublet are even under the Z_2 symmetry and the right-handed leptons as well as the ϕ_1 doublet are odd under the Z_2 symmetry.

- **Flipped (Type Y)**: The up-type quarks and the leptons couple with the ϕ_2 doublet whereas down-type quarks couple with the ϕ_1 doublet. The up-type quarks, leptons and the ϕ_2 doublet are even under the Z_2 symmetry and the right-handed down-type quarks and the ϕ_1 doublet are odd under the Z_2 symmetry.

When we impose the condition of the exact Z_2 symmetry on the scalar potential, we demand that the potential should be invariant under the transformation,

$$\phi_1 \leftrightarrow -\phi_1 \ \text{ and } \ \phi_2 \leftrightarrow \phi_2.$$

As a result, the coefficients of the terms having odd numbers of ϕ_1 fields should vanish i.e $\mu_{12} = 0, \lambda_6, \lambda_7 = 0$ in (5.1.1). One can also consider a potential that softly breaks Z_2 symmetry via the term ($\mu_{12}\phi_1^\dagger\phi_2 + h.c$). If μ_{12} and λ_5 are complex numbers, then $\mathcal{V}$ has explicit CP-violating terms. However, for the sake of simplicity, we will consider a CP-conserving scenario where all the coefficients as well as the vevs are real. Thus, the CP-conserving potential has 7 parameters and is given by,

$$\begin{aligned} \mathcal{V} &= -\mu_1^2\ \phi_1^\dagger\phi_1 - \mu_2^2\ \phi_2^\dagger\phi_2 - \mu_{12}(\phi_1^\dagger\phi_2 + \phi_2^\dagger\phi_1) \\ &+ \lambda_1\ (\phi_1^\dagger\phi_1)^2 + \lambda_2\ (\phi_2^\dagger\phi_2)^2 + \lambda_3\ (\phi_1^\dagger\phi_1)(\phi_2^\dagger\phi_2) \\ &- \lambda_4|(\phi_1^\dagger\phi_2)|^2 - \frac{1}{2}\lambda_5\left[(\phi_1^\dagger\phi_2)^2 + (\phi_2^\dagger\phi_1)^2\right]. \end{aligned} \tag{5.2.5}$$

The mass matrix for the charged scalars is given by

$$\mathcal{L}_{charged} = [\mu_{12} - (\lambda_4 + \lambda_5)v_1v_2]\, C \begin{pmatrix} \frac{v_2}{v_1} & -1 \\ -1 & \frac{v_2}{v_1} \end{pmatrix} C^\dagger, \tag{5.2.6}$$

where

$$C = \left(H_1^-, H_2^-\right)$$

and the mass matrix for the pseudoscalars is given by

$$\mathcal{L}_\eta = [\mu_{12} - 2\lambda_5 v_1 v_2]\, N \begin{pmatrix} \frac{v_2}{v_1} & -1 \\ -1 & \frac{v_2}{v_1} \end{pmatrix} N^\dagger \tag{5.2.7}$$

where

$$N = (\eta_1, \eta_2)\,.$$

The two mass matrices can be diagonalized by rotating the fields with an angle β where

$$\tan\beta = v_2/v_1.$$

After the diagonalization, the neutral Goldstone boson is given by

$$G^0 = \eta_1 \cos\beta + \eta_2 \sin\beta$$

which is absorbed by the Z-boson. The field orthonormal to G^0 is the physical pseudoscalar field A, defined by

$$A = \eta_1 \sin\beta - \eta_2 \cos\beta$$

whose mass m_A is given by

$$m_A^2 = [\mu_{12}/(v_1 v_2) + 2\lambda_5]\,(v_1^2 + v_2^2). \tag{5.2.8}$$

Similarly, the charged Goldstone boson $G^\pm = H_1^\pm \cos\beta + H_2^\pm \sin\beta$ is absorbed by the $W^\pm$ boson and the field orthogonal to $G^\pm$ is the physical charged Higgs $H^\pm = H_1^\pm \sin\beta - H_2^\pm \cos\beta$ whose mass $m_{H^\pm}$ is

$$m_{H^\pm}^2 = [\mu_{12}/(v_1 v_2) + \lambda_4 + \lambda_5]\,(v_1^2 + v_2^2) \tag{5.2.9}$$

Similarly, the mass matrix for the scalars is given by

$$\mathcal{L}_\rho = -R \begin{pmatrix} \mu_{12}\frac{v_2}{v_1} + \lambda_1 v_1^2 & -\mu_{12} + \lambda_{345} v_1 v_2 \\ -\mu_{12} + \lambda_{345} v_1 v_2 & \mu_{12}\frac{v_1}{v_2} + \lambda_2 v_2^2 \end{pmatrix} R^\dagger, \tag{5.2.10}$$

where $R = (\rho_1, \rho_2)$ and $\lambda_{345} = \lambda_3 - \lambda_4 - \lambda_5$. The scalar mass matrix can be diagonalized by rotating the scalar fields with an angle α. The physical CP-even scalar fields, h and H with masses m_h and m_H respectively, are orthogonal combinations of ρ_1 and ρ_2:

$$\begin{aligned} h &= -\rho_1 \sin\alpha + \rho_2 \cos\alpha, \\ H &= \rho_1 \cos\alpha + \rho_2 \sin\alpha. \end{aligned} \tag{5.2.11}$$

It is sometimes in practice to identify the so called 'physical basis', where one doublet possess a non-vanishing vev. Once we rotate the fields to this basis, the neutral CP even scalar is given by [145]

$$H^0 = \rho_1 \cos\beta + \rho_2 \sin\beta = h \sin(\beta - \alpha) + H \cos(\beta - \alpha).$$

As v_1 and v_2 are real, so β lies in the first quadrant. In general, α can belong to either 1st quadrant or 3rd quadrant [146].

The Yukawa interactions of the fermions with the physical scalars are [147]

$$\begin{aligned} \mathcal{L}^{\text{2HDM}}_{\text{Yukawa}} &= \sum_{f=u,d,\ell} \frac{m_f}{v} \left(\xi_h^f \overline{f} f h + \xi_H^f \overline{f} f H - i \xi_A^f \overline{f} \gamma_5 f A \right) \\ &\quad - \left\{ \frac{\sqrt{2} V_{ud}}{v} \overline{u} \left(m_u \xi_A^u \mathrm{P}_L + m_d \xi_A^d \mathrm{P}_R \right) d H^+ + \frac{\sqrt{2} m_\ell \xi_A^\ell}{v} \overline{\nu_L} \ell_R H^+ \right\} \\ &\quad + \text{h.c.} \end{aligned} \tag{5.2.12}$$

where $P_{L/R}$ are projection operators for the left-/right-handed fermions, and the factors ξ are given in Table 5.1.

	Type I	Type II	Lepton-specific	Flipped
ξ_h^u	$\cos\alpha/\sin\beta$	$\cos\alpha/\sin\beta$	$\cos\alpha/\sin\beta$	$\cos\alpha/\sin\beta$
ξ_h^d	$\cos\alpha/\sin\beta$	$-\sin\alpha/\cos\beta$	$\cos\alpha/\sin\beta$	$-\sin\alpha/\cos\beta$
ξ_h^ℓ	$\cos\alpha/\sin\beta$	$-\sin\alpha/\cos\beta$	$-\sin\alpha/\cos\beta$	$\cos\alpha/\sin\beta$
ξ_H^u	$\sin\alpha/\sin\beta$	$\sin\alpha/\sin\beta$	$\sin\alpha/\sin\beta$	$\sin\alpha/\sin\beta$
ξ_H^d	$\sin\alpha/\sin\beta$	$\cos\alpha/\cos\beta$	$\sin\alpha/\sin\beta$	$\cos\alpha/\cos\beta$
ξ_H^ℓ	$\sin\alpha/\sin\beta$	$\cos\alpha/\cos\beta$	$\cos\alpha/\cos\beta$	$\sin\alpha/\sin\beta$
ξ_A^u	$\cot\beta$	$\cot\beta$	$\cot\beta$	$\cot\beta$
ξ_A^d	$-\cot\beta$	$\tan\beta$	$-\cot\beta$	$\tan\beta$
ξ_A^ℓ	$-\cot\beta$	$\tan\beta$	$\tan\beta$	$-\cot\beta$

Table 5.1: Yukawa couplings of u, d, ℓ to the neutral Higgs bosons h, H, A in the four different models.

The couplings of the neutral Higgs h(H) to the pair of massive gauge bosons WW,ZZ are modified by a factor of $\sin(\beta-\alpha)(\cos(\beta-\alpha))$. From the considerations of parity conservation, there are no tree level couplings of the pseudoscalar A, to the gauge bosons. The couplings of the charged Higgs bosons to the fermions can be derived from (5.2.12). The coefficients of the scalar potentials can be expressed in terms of the masses of the physical fields. In general, the free parameters of the theory are chosen to be the four masses$(m_h, m_H, m_A, m_{H^\pm})$ of the physical fields, the rotation angle in the neutral scalar sector α, ratio of the two vevs $\tan\beta$ and a soft Z_2 breaking parameter which is defined as $M^2 = \mu_{12}/\sin\beta\cos\beta$.

If the assigned Z_2 symmetry is not spontaneously broken in a type-I 2HDM, then the model is known as the inert Doublet model(IDM) [148]. In the inert doublet model, ϕ_1 (odd under Z_2 symmetry) doesn't develop vev and has no couplings to the SM fields whereas ϕ_2 doublet (even under Z_2) couples to the fermions and the gauge bosons. The scalar spectrum of the IDM constitutes of a SM-like Higgs (h) coming from the ϕ_2 doublet and the three inert scalars A, h and $H^\pm$ coming from the ϕ_1 doublet. As the Z_2 symmetry is unbroken, the lightest inert particle is stable and can be interpreted as a viable dark matter candidate [149, 150, 151, 152, 153, 154, 155, 156, 157, 158].

5.3 Bounds on 2HDMs

There are various constraints on the parameters of the scalar potential of 2HDMs coming from theoretical considerations, such as unitarity and vacuum stability. Constraints also arise from the experimental observations, such as electroweak precision data, flavour physics and the direct and indirect collider searches of the scalars. Some of them are briefly summarized below [159, 160, 161, 162, 163, 164].

Vacuum stability: A stable scalar potential must be bounded from below in all directions [165, 166, 167]. This is ensured by

$$\lambda_1, \lambda_2 > 0, \lambda_3 > -\sqrt{\lambda_1 \lambda_2}.$$

If the potential doesn't contain a hard Z_2 breaking term, then

$$\lambda_3 - \lambda_4 + |\lambda_5| > -\sqrt{\lambda_1 \lambda_2}.$$

Perturbativity: If the theory of the 2HDM is a perturbative theory, then all the λs and the Yukawa couplings are bounded by a maximum value i.e $|\lambda_i| < 4\pi$. This requires $\tan\beta > 0.28$ for all the 2HDMs .

S-matrix Unitarity: This is incorporated following the Lee-Quigg-Thacker(LQT) analysis [168, 169] where the J=0 partial wave(a_0) amplitudes of the scalar-scalar and the scaler-longitudinal gauge boson scatterings are required to satisfy the condition given by, $|Real(a_0)| < 1/2$. In the 2HDM, the $2 \to 2$ scattering processes involving the scalars and longitudinal gauge bosons become extremely tedious to work with. From the equivalence theorem, one can replace the scattering involving the longitudinal gauge bosons with the scattering of the Goldstone bosons at high energy($\sqrt{s} >> M_W$) [170, 171, 172]. The scattering amplitudes are encapsulated in a matrix whose elements are made up of the amplitudes between all the possible two-particle states, including the neutral channels

$(H_1^+H_1^-, H_1^+H_2^-, H_2^+H_1^-, H_2^+H_2^-, \rho_1\eta_1, \rho_1\eta_2, \rho_2\eta_2, \rho_2\eta_1, \eta_1\eta_2, \rho_1\rho_2$ and the singly charged channels $(\rho_1 H_1^+, \rho_2 H_1^+, \eta_1 H_1^+ \eta_2 H_1^+, \rho_1 H_2^+, \rho_2 H_2^+, \eta_1 H_2^+ \eta_2 H_2^+)$. The S-matrix unitarity is preserved if all the eigenvalues(E_i) of the scattering matrix follow the condition given by $E_i < 8\pi \; \forall i$. Obviously, the most stringent bound comes from the largest eigenvalue of the set [173, 174, 175, 176].

When the potential is exactly Z_2 symmetric, then the stability, perturbativity and the unitarity conditions yield $m_h < 600GeV, m_H < 870GeV, m_A < 870GeV$ and $\mathrm{m_{H^\pm}} < 780\mathrm{GeV}$. In the presence of a Z_2-breaking term, the upper limits are further increased and depends on the value of μ_{12}.

Oblique Electroweak Parameters: To ensure $\rho - \mathrm{parameter} \sim 1$, either the charged Higgs and the pseudoscalar should be close to each other or the charged Higgs should be close to either of the neutral Higgs H(h) in the limit where $\cos(\beta-\alpha)(\sin(\alpha-\beta))$ vanishes [177, 178, 179, 180].

Flavor Physics: The rare decay processes, such as $B \to X_s\gamma$ get contributions from the charged Higgs mediated diagrams in the 2HDMs. For the Type-II and Type-Y 2HDMs, these diagrams contribute at the same level as that of the SM, which is mediated by $W^\pm$. To keep the branching ratio of $B \to X_s\gamma$ close to the experimental value, charged Higgs should be heavier than 360 GeV [181]. Other than the $B \to X_s\gamma$ process, the $B_q\bar{B}_q$ mixing and the $B_u \to \tau\nu_\tau, D_s \to l\nu_l$ processes also rule out $\tan\beta < 1$ for $m_{H^\pm} < 500$ in all types of the 2HDMs. The bound on the $\tan\beta$ becomes weaker as the charged Higgs becomes heavier. For $M_{H^\pm} > 2$ TeV, the lower limit on the value of $\tan\beta$ is about 0.3 [182, 183, 184]. The rare process $B_s \to \mu^+\mu^-$ restricts type-II 2HDM models especially large $\tan\beta$ region. In the type-II 2HDM, high values of $\tan\beta \sim 50$ with $M_{H^\pm} < 500$ GeV and $M_H < 100GeV$ are excluded at 3σ confidence level [185, 186].

Collider searches: The absence of the charged Higgs signals at the LEP in the channel $e^+e^- \to H^+H^-$, imposes a lower limit of 80 GeV on the mass of the charged Higgs. This bound is derived under the assumption that the charged Higgs decays to $\tau^+\nu, c\bar{s}$

and $A, W^{\pm}$. The bound on the charged Higgs mass rises to 94 GeV, if $Br(\tau^{+}\nu) = 1$ [187]. The absence of the process $e^{+}e^{-} \rightarrow hA$ or HA (if allowed kinematically) at the LEP, leads to the condition, $m_{h(H)} + m_A > m_Z$. The higgstrahlung production of the SM Higgs $(e^{+}e^{-} \rightarrow h(H)Z)$ at the LEP, has also constrained the parameter space of the neutral Higgs sectors, which is made up of $\sin(\beta - \alpha)(\cos(\beta - \alpha))$ and $m_{h(H)}$ [188, 189].

At the LHC, a charged Higgs is produced in association with the heavy quarks [190]. If we consider a charged Higgs lighter than the top quark, then it is produced from the top quarks$(t \rightarrow H^{+}b)$ and it decays to $c\bar{s}$ or $\tau\nu$. The searches from the leptonic final states and the diquark final states have been used to draw bounds on the $Br(t \rightarrow H^{+}b, H^{+} \rightarrow \tau\nu)$. The direct searches of the light charged Higgs, rule out the possibility of a charged Higgs having its mass in the region of 100-140 GeV for all the values of $\tan\beta$. A charged Higgs heavier than the top quark, is produced in association with the top quark. A heavier charged Higgs has also been probed in the channel $\tau\nu$, as the decay $H^{+} \rightarrow tb$ has large QCD backgrounds. For $\tan\beta \sim 50$ such a scalar in the mass range $(200GeV < M_{H^{\pm}} < 300GeV)$ has been excluded from the LHC run-1 data [191, 192]. Another interesting decay channel of the charged Higgs is to the lighter neutral Higgs and $W^{\pm}$, which can be probed at the next run of the LHC with high luminosity.

The observation of the SM-like Higgs at 125 GeV [22, 21] along with the non observation of the second scalar till 1 TeV at the LHC run-1 restricts the value of α and β. Thus, we will have two possibilities. In the first situation, the lighter state (h) is discovered and there is ample scope at the next run to discover the heavier state. A second possibility is that, we have discovered the heavier state which behaves as an SM-like Higgs and the lighter state can be probed at the next run. Several analyses have been carried out in this direction [193, 194, 195, 186, 196, 197, 198]. Also, one may note that there will never be a complete exclusion of the 2HDM, as the SM can always be considered as the decoupling limit$(m_h << m_{H^{\pm},A,H})$ of the 2HDMs [199].

In addition to the four types of 2HDMs, there are models known as the neutrinophillic(neutrino-specific) 2HDMs. In these models, the SM particles are accompanied with the two Higgs doublets and three right-handed neutrinos. The SM particles couple to the ϕ_2 doublet whereas the three right-handed neutrinos couple to the ϕ_1 doublet. A Z_2 symmetry, where the SM particles along the ϕ_2 doublet are even and the right-handed neutrinos and the ϕ_1 doublet are odd, has been imposed to ensure this structure. In this model, the neutrinos have small Dirac masses in spite of O(1) Yukawa couplings. This is made possible by spontaneously(softly) breaking the Z_2 symmetry with the vev of the second doublet v_1. The vev of the second doublet is of the order of ev. The charged Higgs sector of these model offer interesting signatures.In the next chapter, we will discuss the phenomenology of the charged Higgs arising in such a scenario containing neutrinophillic doublet.

Chapter 6

Searching an elusive charged Higgs at the Large Hadron Collider

One of the principal motivations for BSM physics is to have a mechanism that explains smallness of the neutrino masses as compared to other fermions [200]. It is thus natural that efforts to unravel new physics in the Higgs sector will sometimes be guided by considerations related to neutrino masses [201, 202, 203, 204]. This chapter is based on the study carried out in [205]. In this analysis, we have considered a model which not only plays a role in the electroweak symmetry breaking mechanism, but also accounts for the tiny neutrino masses. We are interested in a two Higgs doublet model with right-handed neutrinos proposed in [202]. The essential idea is that neutrinos, like all other fermions, have Dirac masses, but are much lighter than the others because their masses come from a different Higgs doublet. The Yukawa couplings of the neutrinos can still be $\mathcal{O}(1)$. One postulates a very tiny($\sim$ eV) vacuum expectation value (vev) to the neutral component of one of the Higgs doublets, which due to a Z_2 symmetry couples only with the neutrino sector. The charged Higgs in this model therefore has very different properties when compared to other standard two Higgs doublet models (2HDM) [47]. It turns out that the main decay mode for the charged Higgs is into a W boson and a light neutral scalar present in the model. We have studied the pair

production of the charged Higgs at the LHC and considered its decay to W boson and the neutral scalar. The signal is identified by two isolated leptons and a large missing energy. We have analyzed the most dominant SM background subprocesses that affect the signal, to estimate the signal significance. The study is carried out at both the 8 TeV and 14 TeV center-of-mass energies for the LHC.

6.1 A brief review of the Model

The model under consideration is based on the symmetry group $\mathcal{G}_{SM} \times Z_2$, where $\mathcal{G}_{SM} \equiv SU(3)_c \times SU(2)_L \times U(1)_Y$. In addition to the matter fields in the SM, the model includes two scalar doublets χ and ϕ, and three $SU(2)_L$ singlet right-handed neutrinos ν_R^i, $i = 1, 2, 3$. All the SM fermions and the scalar doublet χ are even under the discrete symmetry Z_2, while the right-handed neutrinos and the scalar doublet ϕ are odd under Z_2. As a result, the SM left-handed neutrinos along with the right-handed neutrinos couple only to the Higgs doublet ϕ. The most general scalar potential and the Yukawa interaction of the fermions(leptons and quarks) with the scalar doublets which respect the $\mathcal{G}_{SM} \times Z_2$ symmetry are [202],

$$\begin{aligned}
\mathcal{V} &= -\mu_1^2\, \chi^\dagger\chi - \mu_2^2\, \phi^\dagger\phi + \lambda_1\, (\chi^\dagger\chi)^2 \\
&\quad +\lambda_2\, (\phi^\dagger\phi)^2 + \lambda_3\, (\chi^\dagger\chi)(\phi^\dagger\phi) \\
&\quad -\lambda_4|(\chi^\dagger\phi)|^2 - \frac{1}{2}\lambda_5\left[(\chi^\dagger\phi)^2 + (\phi^\dagger\chi)^2\right], \\
\mathcal{L}_Y &= y_l^{ij}\ \bar{\Psi}_L^{l,i} l_R^j \chi + y_{\nu_l}^{ij}\ \bar{\Psi}_L^{l,i} \nu_R^j \tilde{\phi} \\
&\quad +y_d^{ij} \bar{\Psi}_L^{q,i} d_R^j \chi + y_u^{ij} \bar{\Psi}_L^{q,i} u_R^j \tilde{\chi} + h.c,
\end{aligned} \tag{6.1.1}$$

where, $\bar{\Psi}_L^{l(q),i}$ and $l_R^j(u_R^j, d_R^j)$ are the usual $SU(2)_L$ lepton(quark) doublet and singlet fields, respectively and y_f^{ij} $(f \equiv l, \nu_l, u, d)$ represent the matrix elements of the lepton(quark) Yukawa matrices. The standard electroweak symmetry is broken spontaneously by giving a vev, $V_\chi \simeq 246$ GeV to the χ doublet, while the Z_2 symmetry is

broken by a vev, V_ϕ for the ϕ doublet. The spontaneous breaking of the Z_2 symmetry is arranged for generating small neutrino masses, $m_{\nu_l} \sim V_\phi$ which can be in the sub-eV/eV range for $\mathcal{O}(1)$ Yukawa couplings. We note that we are assuming lepton number conservation so that the Majorana mass terms for the right handed neutrinos, ν_R, $M\nu_R^T C^{-1}\nu_R$ are not allowed. Thus the light left-handed neutrinos cannot acquire masses via the usual see-saw mechanism [206]. Dirac mass, as obtained from Eq. 6.1.1 from the tiny vev of ϕ is the only possibility.

As a result of the symmetry breaking, the physical Higgs sector includes charged scalars $H^\pm$, two neutral CP-even scalars h and σ and a neutral pseudoscalar ρ. In the unitary gauge, the two doublets can be expressed in the following way

$$\chi = \frac{1}{\sqrt{2}} \begin{pmatrix} \sqrt{2}(V_\phi/V)H^+ \\ \\ h_0 + i(V_\phi/V)\rho + V_\chi \end{pmatrix},$$

$$\phi = \frac{1}{\sqrt{2}} \begin{pmatrix} -\sqrt{2}(V_\chi/V)H^+ \\ \\ \sigma_0 - i(V_\chi/V)\rho + V_\phi \end{pmatrix}, \tag{6.1.2}$$

The masses for these particles are given by,

$$\begin{aligned} M^2_{H^\pm} &= \frac{1}{2}(\lambda_4+\lambda_5)V^2, & M^2_\rho &= \lambda_5 V^2 \\ M^2_h &= 2\lambda_1 V^2_\chi, & M^2_\sigma &= 2\lambda_2 V^2_\phi, \end{aligned} \tag{6.1.3}$$

where, $V^2 = V^2_\chi + V^2_\phi$. We have neglected the subdominant terms in V_ϕ when deriving these relations. We note that in the case of exact Z_2 symmetry, the σ will be exactly massless. The breaking of this Z_2 symmetry with a tiny vev V_ϕ gives mass to the σ, as well as tiny Dirac masses to the observed neutrinos. Therefore in this model, the neutral scalar field σ is very light and the field h behaves like the SM Higgs boson.The CP-even scalars (h, σ) are the mass eigenstates and they are related to the weak eigen-

states (h_0, σ_0) by the mixing angle θ:

$$h = h_0 \cos\theta - \sigma_0 \sin\theta, \qquad \sigma = h_0 \sin\theta + \sigma_0 \cos\theta. \tag{6.1.4}$$

where,

$$\cos\theta = 1 + \mathcal{O}(V_\phi^2/V_\chi^2), \qquad \sin\theta = -\frac{\lambda_3 - \lambda_4 - \lambda_5}{2\lambda_1}\left(\frac{V_\phi}{V_\chi}\right) + \mathcal{O}(V_\phi^2/V_\chi^2). \tag{6.1.5}$$

This mixing can be neglected because $V_\phi << V_\chi$. It is also clear from the above equations that M_ρ lies around the electroweak scale.

In the lepton Yukawa sector the above symmetry breaking leads to neutrino masses given by, $m_{\nu_a} = y_\nu^a V_\phi/\sqrt{2}$, where y_ν^a are the eigenvalues of the neutrino Yukawa matrix. The Yukawa interaction of the charged Higgs with the leptons and quarks can then be written down following Eq. 6.1.1 as,

$$\mathcal{L}_Y \supset y_\nu^a \frac{V_\chi}{V}\, U_{ia} \bar{l}_L^i \nu_R^a H^- + y_l^i \frac{V_\phi}{V}\, U_{ia} \bar{l}_R^i \nu_L^a H^- + y_d^{ij} \bar{d}_R^i u_L^j \frac{V_\phi}{V} H^- + h.c. \tag{6.1.6}$$

In the above equation, i represents the flavour index while a is the index representing neutrino components in mass eigenstate. The $y_l^i = \sqrt{2} m_l^i/V_\chi$ are the charged lepton Yukawa couplings while U_{ia} represent the elements in the PMNS matrix [207] for the mixing of the neutrino flavours.[1] Note that the second term in Eq. 6.1.6 is clearly subdominant and negligible (suppressed by the factor V_ϕ/V) when compared to the first term and can therefore be safely neglected when considering the interaction strength of the charged Higgs with the leptons. The third term in (6.1.6) represents the couplings of the charged Higgs with the SM quarks which are also generated through terms similar to the second term. Thus, the charged Higgs is very weakly coupled to the quarks and in all practicality behaves as a "chromophobic" field. This property of the charged Higgs plays a crucial role in avoiding strong constraints on its mass, oth-

[1] $\nu^i = \sum_a U_{ia} \nu^a$.

erwise evident in other 2HDM, from low energy physics experiments such as weak meson decays and mixing. Thus in the Yukawa sector, only the decay $H^{\pm} \to l_L^{\pm}\nu_R$ becomes relevant. Other main decay modes of the charged Higgs include $H^{\pm} \to W^{\pm}\sigma$ and $H^{\pm} \to W^{\pm}\rho$ which have gauge coupling interaction strengths.

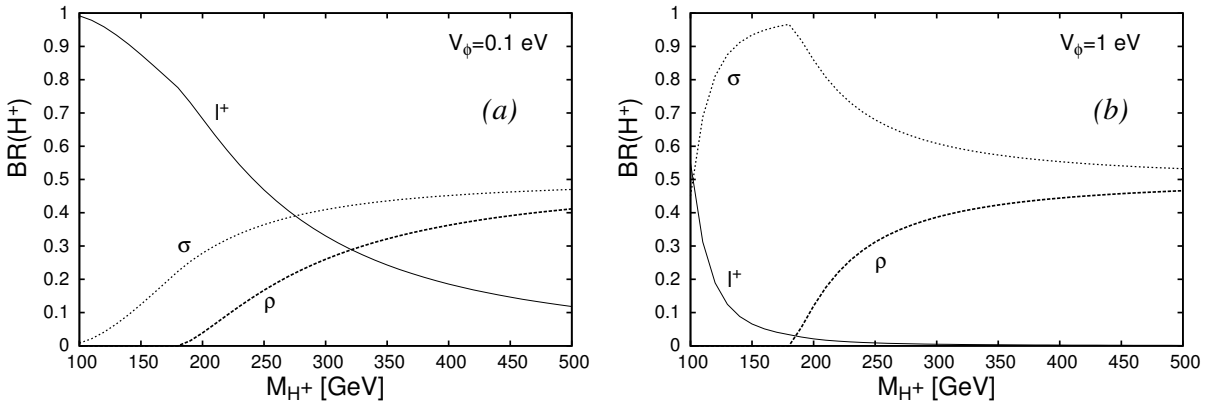

Figure 6.1: Charged Higgs branching ratios as function of its mass for (a) $V_\phi = 0.1$ eV and (b) $V_\phi = 1$ eV. The mass of σ particle is related to V_ϕ as in Eq. 6.1.3. We have chosen the other relevant variables $\lambda_2 = 1.0$ and $M_\rho = 100$ GeV for calculating the above branching ratios.

The branching ratios of charged Higgs decay is quite sensitive to the value of V_ϕ. As the leptonic channel $(l\ \nu_l)$ is dictated by the coupling strength given by $\sim m_\nu/V_\phi$ (see Eq. 6.1.6), smaller values of V_ϕ for a fixed neutrino mass increase the branching probability. To highlight this, we consider two sets of values for V_ϕ and show the branching probabilities of the charged Higgs decay as a function of its mass in Fig. 6.1. Note that the neutrino data as shown in Table 6.1 have been incorporated when calculating the partial decay widths of the charged Higgs decaying into the three generations of leptons. If V_ϕ is in the sub-eV range as shown in Fig. 6.1a, it is found to decay mostly through the leptonic mode for $M_{H^\pm} \leq 200$ GeV, while if V_ϕ is increased to about an eV (Fig. 6.1b), it decays dominantly into $W^{\pm}\sigma$. As the value of V_ϕ is increased further, we find that the leptonic channel becomes completely negligible and the $W^{\pm}\sigma$ becomes the only significant mode available for the charged Higgs decay for $M_{H^\pm} \leq 200$ GeV.

6.2 Constraints on Model Parameters

As the model under consideration is quite different from the generic 2HDM and is envisioned to account for the observed neutrino masses and mixing angles, it becomes imperative to first check how the experimental constraints affect the parameters of the model. A brief discussion on several constraints on the model parameters is already present in Ref. [202]. We choose to accommodate them with new and updated results that have modified these constraints as well as supplement them with additional constraints, if any.

Parameters	NH	IH
$\sin^2\theta_{12}$	$0.307^{+0.052}_{-0.048}$	$0.307^{+0.052}_{-0.048}$
$\sin^2\theta_{23}$	$0.386^{+0.055}_{-0.251}$	$0.392^{+0.057}_{-0.271}$
$\sin^2\theta_{13}$	$2.41^{+0.72}_{-0.72} \times 10^{-2}$	$2.42^{+0.73}_{-0.71} \times 10^{-2}$
$m^2_{\nu_2} - m^2_{\nu_1}$	$7.54^{+0.55}_{-0.64} \times 10^{-5}\text{eV}^2$	$7.54^{+0.55}_{-0.64} \times 10^{-5}\text{eV}^2$
$m^2_{\nu_3} - \frac{1}{2}(m^2_{\nu_1} + m^2_{\nu_2})$	$2.43^{+0.24}_{-0.19} \times 10^{-3}\text{eV}^2$	$-2.42^{+0.25}_{-0.19} \times 10^{-3}\text{eV}^2$

Table 6.1: Neutrino mass-mixing parameters with 3σ uncertainties [9]. The allowed ranges of parameters for the Normal Hierarchy (NH) and Inverted Hierarchy (IH) cases are shown separately.

We acknowledge that any scenario explaining neutrino masses will also need to address their mixing, and reproduce the form of the PMNS matrix as suggested by various observations [9]. The PMNS matrix is parameterized by three mixing angles and can have one phase whose value is yet unknown. The current values of these angles and the neutrino mass-squared differences are shown in Table 6.1. From the measurements on the neutrino mass-squared differences we can conclude that in both the normal and inverted hierarchy scenarios, the mass of the heaviest neutrino is $\gtrsim 0.05$ eV. We have already discussed the sensitivity of the branching ratios of the charged Higgs to the magnitude of V_ϕ. Clearly, from neutrino data, one is free to choose $\mathcal{O}(1)$ Yukawa couplings (y_ν).

However, the right-handed neutrinos are new relativistic degrees of freedom

present in our model. Due to its coupling with the charged Higgs and the leptons, they should be excessively produced in the early universe, for example, via the charged Higgs mediated $t-$channel process $l^+l^- \leftrightarrow \nu_R\bar{\nu}_R$. We can therefore put a constraint on the neutrino Yukawa coupling using the big-bang nucleosynthesis (BBN) bound on new relativistic degrees of freedom (δN_ν). The latest results combining `Planck`, `WP`, Baryon Acoustic Oscillation (`BAO`) and high multipole `CMB` data, on the upper limit of extra relativistic degrees of freedom give $\delta N_{\nu,max} \simeq 1.0$ at 95% confidence level [208] . To escape this bound, the right-handed neutrinos must be colder than the left-handed neutrinos, $T_{\nu R}/T_{\nu L} < (\delta N_{\nu,max}/3)^{1/4}$ [209]. This can be achieved if we demand that the right-handed neutrinos drop out early enough than the left-handed neutrinos. In terms of the effective number of relativistic degrees of freedom g_* at the times of decoupling of the left and right-handed neutrinos, we have $T_{\nu R}/T_{\nu L} = (g_{*L}/g_{*R})^{1/3}$. Using $g_{*L} = N_B + 7/8N_F = 43/4$ (where $N_B = 2$ and $N_F = 10, e^+, e^-$ and 3 families of ν_L), we derive $g_{*R} \geq 43/4 + 14.25$. Thus, ν_R should decouple from the thermal bath above quark-hadron transition i.e at 200-400 MeV. If we assume $T_{d,\nu R} > 300MeV$, we get an upper bound on the cross section for the production of right handed neutrino from leptons mediated by the charged Higgs using

$$\frac{T_{d,\nu R}}{T_{d,\nu L}} \sim (\frac{\sigma_R}{\sigma_L})^{-1/3} = \left(4\frac{V_\phi^4 M_H^4}{V_\chi^4 m_{\nu i}^4 |U_{li}|}\right)^{1/3} \tag{6.2.7}$$

This bound can be translated into an upper bound on the neutrino Yukawa coupling or a lower bound on V_ϕ for a given neutrino mass which is given by [204]

$$V_\phi \gtrsim 60\ m_{\nu_i}(|U_{li}|)\frac{100\ \text{GeV}}{M_{H^+}}. \tag{6.2.8}$$

The lower bound on V_ϕ is derived for the most massive neutrino labeled by l in U_{li}. The hierarchy in the neutrino masses is therefore not important here. We have considered the maximal mixing for which $|U_{li}| \simeq 1/\sqrt{2}$. A value of U_{li} consistent with the neutrino data does not alter the numerical value of the bound significantly. If $M_{H^\pm} \sim 100$ GeV,

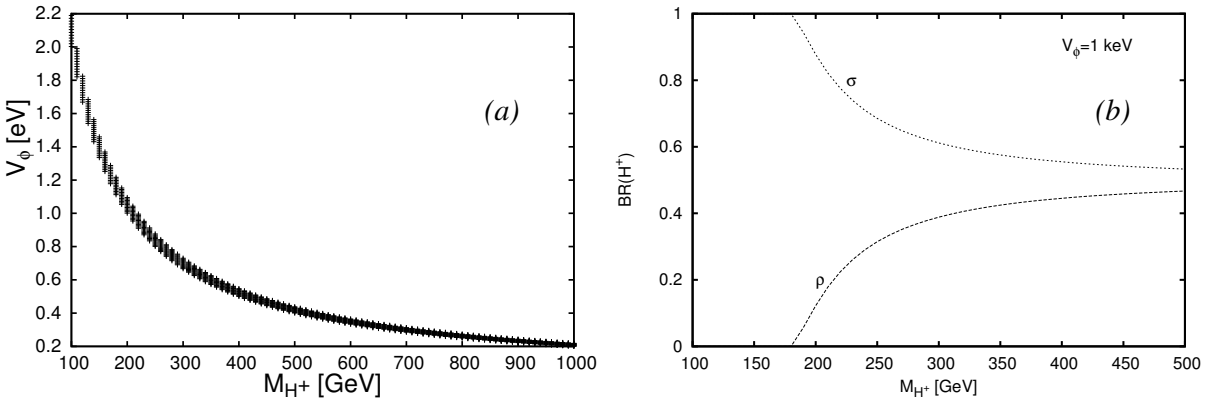

Figure 6.2: (a) The variation of the lower bound on V_ϕ as a function of M_{H^+} as defined by Eq. 6.2.8. The band represents the 3σ uncertainties shown in Table 6.1. (b) The branching ratios of the charged Higgs decay for the choice of $V_\phi = 1$ keV.

the above bound implies $V_\phi \gtrsim 2$ eV. In Fig. 6.2a, we have shown the variation of the lower bound on V_ϕ as a function of $M_{H^\pm}$ consistent with the neutrino data. For a fixed value of $M_{H^\pm}$, the range of V_ϕ illustrates 3σ uncertainty in neutrino data. This, when considered with the decay properties of the charged Higgs illustrated in Fig. 6.1 shows that for a light charged Higgs (100-200 GeV), the dominant decay is to $W\sigma$ as $V_\phi > 1$ eV.

In addition to that, if the supernova neutrino observations and the energy-loss argument for supernova cores are also considered, the lower bound on V_ϕ can be pushed to $V_\phi \gtrsim 1$ keV [210]. This also takes care of the excessive production of neutrinos through the σ boson mediated process $\nu_i + \bar{\nu}_i \to \nu_j + \bar{\nu}_j$, in the early Universe. Since $\Gamma(H^\pm \to l_L^\pm \nu_R) \propto m_\nu^2/V_\phi^2$, the leptonic decay mode of the charged Higgs will be extremely suppressed as the Yukawa couplings are further suppressed ($y_\nu \sim m_\nu/V_\phi$). Instead, it will decay overwhelmingly via the modes $H^\pm \to W^\pm\sigma$ and $W^\pm\rho$ (see Fig. 6.2b) , thus behaving more like a "fermiophobic" field.

The values of coupling parameters $\lambda_1, \lambda_2, \lambda_4$ and λ_5 appearing in the scalar potential (Eq. 6.1.1) can be fixed once we make a choice for the scalar masses M_h, M_σ, M_ρ and $M_{H^\pm}$ (see Eq. 6.1.3). To incorporate the recently discovered SM-like Higgs boson in our model, we would like to have $M_h \sim 125 - 126$ GeV, which fixes λ_1. We can choose

any value for λ_2 which is not very large so that $M_\sigma \simeq V_\phi \sim$ keV. Note that a 1 keV σ particle will decay into neutrinos in about 10^{-9} seconds. Although $\mathcal{O}(1)$ values of λ_3 do not affect the scalar mass spectrum, it appears in various interaction vertices. We find that by choosing $\lambda_3 = \lambda_4 + \lambda_5$ we can suppress large contributions to the invisible decay width of the SM-like Higgs via the decay mode $h \to \sigma\sigma$. As the present LHC data allows a maximum of 20% branching ratio for any invisible decay mode(s) of the Higgs boson at the 95 % C.L. [211, 212], allowing $BR(h \to \sigma\sigma) = 20\%$ puts a condition on λ_3 which is given by,

$$\begin{aligned} \lambda_3 &= 0.0133 + \lambda_5 + \lambda_4, \\ &= 0.0133 + 0.3305 \times \left(\frac{M_{H^\pm}}{100 \text{ GeV}}\right)^2, \end{aligned} \tag{6.2.9}$$

where we have used Eq. 6.1.3 and $V \simeq V_\chi = 246$ GeV. Even with the above choice of λ_3, a light enough ρ may further contribute to the Higgs invisible decay width. We may therefore choose M_ρ sufficiently large so that this situation is avoided. The pseudoscalar ρ, belonging to the doublet ϕ has no significant interaction with charged leptons and quarks, and decays mostly into a neutrino-antineutrino pair. Since the decay $Z \to \rho\sigma$ contributes to the invisible decay width of the Z boson, the experimental measurements require $M_\rho \gtrsim 78$ GeV [181]. For $M_\rho > m_Z$, one also needs to consider the LEP2 data for the signal from the process $e^+e^- \to Z^* \to \rho\sigma$. Non observation of any such signal puts a lower bound on the ρ mass of 95 GeV [202]. Note that if we take $M_\rho = 100$ GeV, $\Gamma(h \to \rho\rho^*) \sim$ eV which will have negligible contribution to the Higgs invisible decay width.

The only bound on the mass of the charged Higgs in our model comes from the direct searches for the pair production at the LEP experiments. Due to very suppressed coupling of the charged Higgs with quarks, the constraints from rare processes such as $b \to s\gamma$ do not put any additional bound on the charged Higgs mass. Thus it is enough to have $m_{H^\pm} \geq 79.3$ GeV [181].

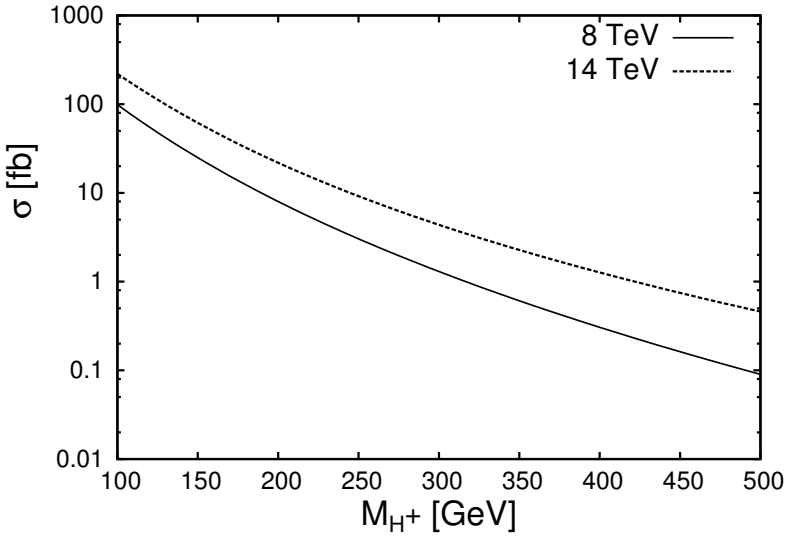

Figure 6.3: Charged Higgs pair production cross section as function of charged Higgs mass at 8 TeV and 14 TeV LHC center-of-mass energies.

6.3 Prospects of the charged Higgs at the LHC: Signal background analysis

Since the chromophobic nature of the charged Higgs in this scenario disallows its production in association with a top (anti-top) quark, one has to rely on electroweak subprocesses for its pair production. Thus the $H^{\pm}$ pair is produced via Drell-Yan process through the exchange of photon and Z boson in the s-channel. It can also be produced at the LHC through vector boson fusion (VBF), namely, $qq \to qqV^*V^* \to qqH^+H^-$ where $V = \gamma, Z, W^{\pm}$. However, the VBF production cross section is quite suppressed when compared to Drell-Yan. The pair production cross section for the charged Higgs at the LHC at center-of-mass energies of 8 TeV and 14 TeV is shown in Fig. 6.3. The cross sections have been computed using `CTEQ6L1` parton distribution functions (PDF) [129]. Since the coupling of SM-like Higgs boson with the charged Higgs is not negligible, the charged Higgs pair production may also receive additional contributions via a Higgs (h) mediated gluon fusion process. For our choice of λ_3 and $M_{H^{\pm}} = 150$ GeV, the $gg \to h^* \to H^+H^-$, we find the gluon mediated cross section

is about 1.86 fb for the 14 TeV run of the LHC. For larger values of $M_{H^\pm}$, one expects this contribution to grow, as λ_3 also increases (Eq. 6.2.9). But the s-channel mediated process receives a significant propagator suppression (as the effective $\hat{s} > 2M_{H^\pm}$ for pair production), making it quite small for larger $M_{H^\pm}$. The charged Higgs can also be produced singly in association with a ρ or σ in the channel $qq' \to \rho H^\pm, \sigma H^\pm$. These production modes lead to single $H^\pm$ along with large missing energy when ρ and σ decay to $\nu\bar{\nu}$. Although the rate of single charged Higgs production is comparable to that of pair produced charged Higgs, the single-$W^\pm$ background is very large compared to that from W^+W^-. So we study the signals for the charged Higgs via pair production. As illustrated in Fig. 6.2b when $V_\phi \sim$ keV, $H^\pm \to W^\pm\sigma$ is the most favourable decay channel as compared to other decays. As σ decays to neutrinos with 100% branching probability, we will be focusing on events with large transverse missing energy ($\not{E}_T$). The W produced from the charged Higgs, decays into $(l\ \nu_l)$. Thus, the signature of charged Higgs in this model is $pp \to H^+H^- \to W^+W^-\sigma\sigma \to l^+l^- + \not{E}_T$.

For our analysis, we have used the package `MadGraph 5` [111] to generate events for the signal as well as the SM background processes. To generate the events for the signal, we have included the interaction vertices of the new model in `MadGraph 5` using the publicly available package `Feynrules` [127]. We have kept the factorization and renormalization scales same as the default event-by-event `MadGraph 5` value which happens to be the transverse mass of the pair produced particle [111]. A full simulation of the generated events has been carried out by including fragmentation and hadronization effects using `PYTHIA 8` [110]. We also include the initial and final state radiations. In order to get a real assessment of the signal and the background at the detector level we have considered isolated leptons and jets. The event selection criteria that we use is consistent with that of the ATLAS detector [213]. However, a 100% lepton identification (for e and μ) efficiency is assumed. To account for the detector resolutions we have smeared the energies/transverse momenta of leptons and jets with Gaussian functions as shown in Table 6.2 [214].

	Electrons $\frac{\sigma(E)}{E}$	**Muons** $\frac{\sigma(p_T)}{p_T}$	**Jets** $\frac{\sigma(E)}{E}$	**Uncl. Energy** $\sigma(E)$
Formula	$\frac{a}{\sqrt{E}} \oplus b \oplus \frac{c}{E}$	a if $p_T < 100$ else $a + b\log(\frac{p_T}{100})$	$\frac{a}{\sqrt{E}} \oplus b \oplus \frac{c}{E}$	$\alpha\sqrt{\sum_i E_T^{uncl}}$
$\lvert\eta\rvert < 1.5$	$a = 0.11,\ b = 0.007,$ $c = 0.25$	$a = 0.02,\ b = 0.08$	$a = 0.65,\ b = 0.027,$ $c = 4$	$\alpha = 0.55$
$1.5 < \lvert\eta\rvert < 2.5$	$a = 0.13,\ b = 0.007,$ $c = 0.25$	$a = 0.03,\ b = 0.06$	$a = 1.10,\ b = 0.01,$ $c = 6.5$	$\alpha = 0.55$
$2.5 < \lvert\eta\rvert < 3.0$	—	—	$a = 1.10,\ b = 0.01,$ $c = 6.5$	$\alpha = 0.55$
$3.0 < \lvert\eta\rvert < 4.5$	—	—	$a = 1.00,\ b = 0.05,$ $c = 1.0$	$\alpha = 0.55$

Table 6.2: Functional form and parameters of the resolution functions of different physics objects. These parameterizations give the value of σ parameter of the gaussian functions used. The first and second column of the last two rows are kept blank as the leptons are identified within $|\eta| < 2.5$.

The model parameters used in our analysis are

$$\begin{aligned}
&\lambda_1 = 0.13, && \lambda_2 = 1.0, && \lambda_3 = 0.0133 + \lambda_4 + \lambda_5,\\
&\lambda_4 = 2\frac{M_{H^+}^2}{V^2} - \lambda_5, && \lambda_5 = \frac{M_\rho^2}{V^2}, && V_\phi = 1 \text{ keV},\\
&M_\rho = 100 \text{ GeV}, && M_\sigma = \sqrt{2}V_\phi, && M_h = 126 \text{ GeV}.
\end{aligned} \tag{6.3.10}$$

It is worth pointing out that we have chosen neutrino masses (normal hierarchy) which are consistent with the neutrino data. In our analysis, however, neutrino masses and their hierarchy are of no consequence because the leptonic decay mode of the charged Higgs for $V_\phi = 1$ keV is highly suppressed. The major subprocesses in the SM that contribute as background to our signal are $pp \to t\bar{t}$, W^+W^-, ZZ and also $pp \to h \to WW^*/ZZ^*$. Note that we have identified the Higgs (h) mediated subprocesses separately. As the Higgs production through gluon-fusion is a loop mediated process, we have included it in `Madgraph 5` via an effective operator. The $t\bar{t}$ background is a reducible background which can be ignored by selecting zero jet events. By removing the Z-peak (selecting a narrow window of 30 GeV

around the peak in the invariant mass distribution of the dileptonic system) we can also suppress the ZZ background. This invariant mass cut partially takes care of the $pp \to h \to ZZ^*$ background when the on-shell Z decays into charged lepton pair. As we shall explain in the next section, a large missing transverse energy ($\not{E}_T$) cut is essential for our signal-background analysis. We find that on applying a large $\not{E}_T$ cut the $pp \to h \to WW^*/ZZ^*$ backgrounds become negligible. Thus the $pp \to W^+W^-$ is the major irreducible background to our signal.

Note that we have performed a leading order analysis here. Since the production of the charged Higgs takes place via a Drell-Yan process, QCD corrections are not expected to make any significant difference to the kinematic distributions, to be discussed later, on which our conclusions hinge so crucially.

6.4 Results

In this section, we present our results for charged Higgs masses of 150 GeV and 200 GeV as benchmark values. For $M_{H^\pm} = 150$ (200) GeV, the pair production ($pp \to H^+H^-$) cross sections at 8 TeV and 14 TeV LHC center-of-mass energies are 21.48 (6.86) fb and 53.05 (18.73) fb respectively. The dominant decay mode of the charged Higgs for our choice of parameters is $W^\pm\sigma$. The branching fraction of this decay mode for the charged Higgs mass of 150 GeV is close to 100%. Since we have taken $M_\rho = 100$ GeV, for 200 GeV charged Higgs the $W^\pm\rho$ decay mode is also allowed and $H^\pm \to W^\pm\sigma$ branching probability reduces to about 88% (see Fig. 6.2b). Thus for the 200 GeV charged Higgs, $W\sigma$ mode still remains the most dominant channel. However, even the $W^\pm\rho$ mode might contribute to our signal, since the ρ can also decay invisibly. For $M_\rho = 100$ GeV, there are two possible decay modes, *viz.* $\rho \to Z\sigma$ and $\rho \to \nu\bar{\nu}$. But much like the charged Higgs, the choice of $V_\phi = 1$ keV suppresses the invisible decay of ρ and it decays to $Z\sigma$ with 100% branching probability. The decay of the charged Higgs is followed by the leptonic decay of W boson. Since we have isolated both the

leptons and jets, the events with isolated jets are removed and we select the signal and background events consisting of two isolated charged leptons and missing energy.

The basic acceptance cuts for the signal as well as background include,

$$p_T^l > 20 \text{ GeV},\ |\eta_l| < 2,\ \Delta R_{ll} > 0.4,\ |m_{ll} - m_Z| > 15 \text{ GeV and } \not{E}_T > 50 \text{ GeV}. \quad (6.4.11)$$

With these cuts at 8 TeV center-of-mass energy, the signal cross section for 150 GeV charged Higgs mass is quite small (~ 0.13 fb) whereas the background cross section is 64.12 fb. We note that the signal has additional sources of missing energy due to the presence of σ particles which completely decay to neutrinos. Thus, selecting events with high missing transverse energy is expected to be helpful in distinguishing the signal from the background. However, when the mass of charged Higgs is close to m_W the effect of large missing transverse energy cut is not very helpful. As the mass of the charged Higgs increases, the fraction of events with higher transverse momentum (p_T) as well as higher missing transverse energy ($\not{E}_T$) is larger in the signal as compared to the background. Thus, the effect of harder missing energy cut becomes evident. This feature is illustrated in Fig. 6.4. The background, therefore, can be further reduced by raising the minimum missing energy cut. We find that the signal and background cross sections after applying 100 GeV minimum $\not{E}_T$ cut become 0.04 fb and 2.11 fb respectively. This means, with the available luminosity of $\simeq 25$ fb^{-1} at 8 TeV, for one signal event the number of background events is about 52. Therefore, it is very difficult to see the signal excess over such a large background at the 8 TeV LHC. The situation gets worse for $M_{H^\pm}$ = 200 GeV due to its smaller production cross section at 8 TeV. However, with larger center-of-mass energy (Fig. 6.3) there is a significant increase in the pair production cross section. At $\sqrt{s} = 14$ TeV the signal cross section is much larger and the data will be collected at much higher luminosity. Thus one expects to achieve greater signal significance at $\sqrt{s} = 14$ TeV run of the LHC.

The event section criteria and basic acceptance cuts for the $\sqrt{s} = 14$ TeV analy-

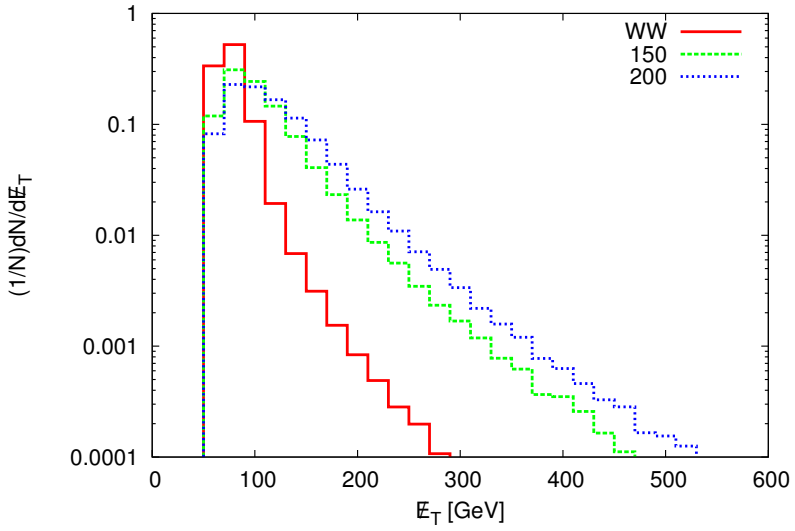

Figure 6.4: A comparison of the missing energy distributions for the signal and the W^+W^- background at 8 TeV. Both the 150 GeV and 200 GeV charged Higgs mass cases of the signal is considered.

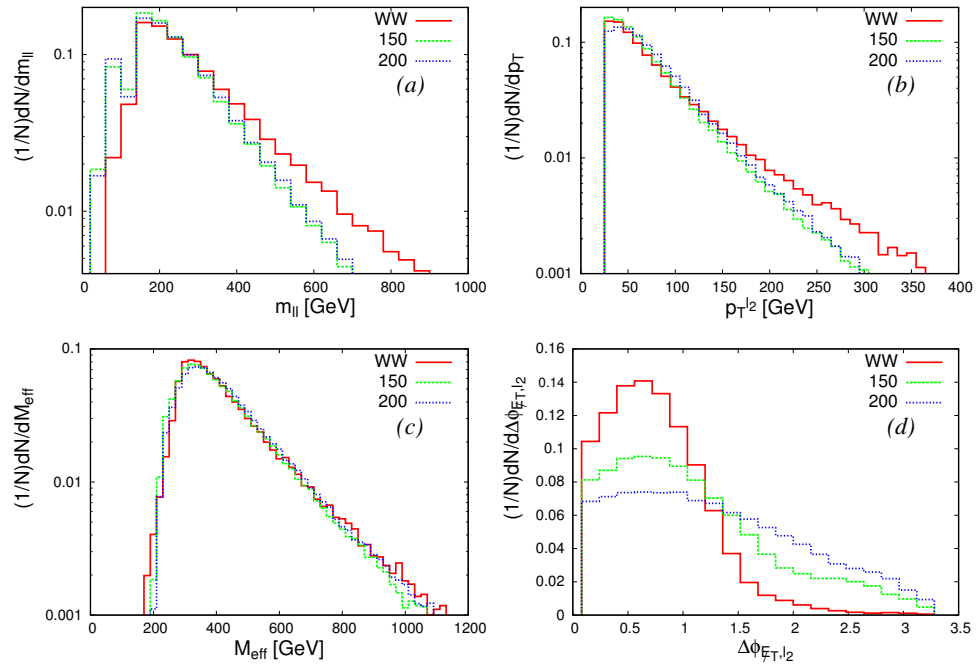

Figure 6.5: Kinematic distributions for the ($2l+\not{E}_T$) signal with $M_{H^\pm}$=150, 200 GeV and background (W^+W^-). The events satisfy the $\not{E}_T > 110$ GeV cut and the acceptance cuts listed in Eq. 6.4.11.

sis are kept same, as shown in Eq. 6.4.11. The cross sections for the ($2l + \not{E}_T$) signal ($M_{H^\pm} = 150$ GeV) and background are respectively, 0.25 fb and 96.21 fb after apply-

ing the acceptance cuts. Motivated by the observation in the $\sqrt{s} = 8$ TeV analysis, we apply a minimum $\not{E}_T$ cut of about 110 GeV to enhance the signal significance to ~ 2. However, we note that raising the $\not{E}_T$ cut beyond 110 GeV does not improve the situation and we need to construct suitable kinematic variables which can help in reducing the background further. In Fig. 6.5 we display kinematic distributions for the invariant mass (m_{ll}), the transverse momentum of the sub-leading lepton ($p_T^{l_2}$), the effective mass (M_{eff})[2] and the angle between the directions of missing energy and the subleading lepton in the transverse plane ($\Delta\phi_{\not{E}_T,l_2}$). These distributions are plotted after applying the large $\not{E}_T$ cut. Quite clearly, it is the angle $\Delta\phi_{\not{E}_T,l_2}$ (Fig. 6.5d) which turns out to be the most effective kinematic variable in separating the signal from the background. We also note that this cut is more promising for the $M_{H^\pm} = 200$ GeV. Based on this we have applied a minimum cut of 1.6 on the angle $\Delta\phi_{\not{E}_T,l_2}$. This improves the signal-to-background ratio significantly.

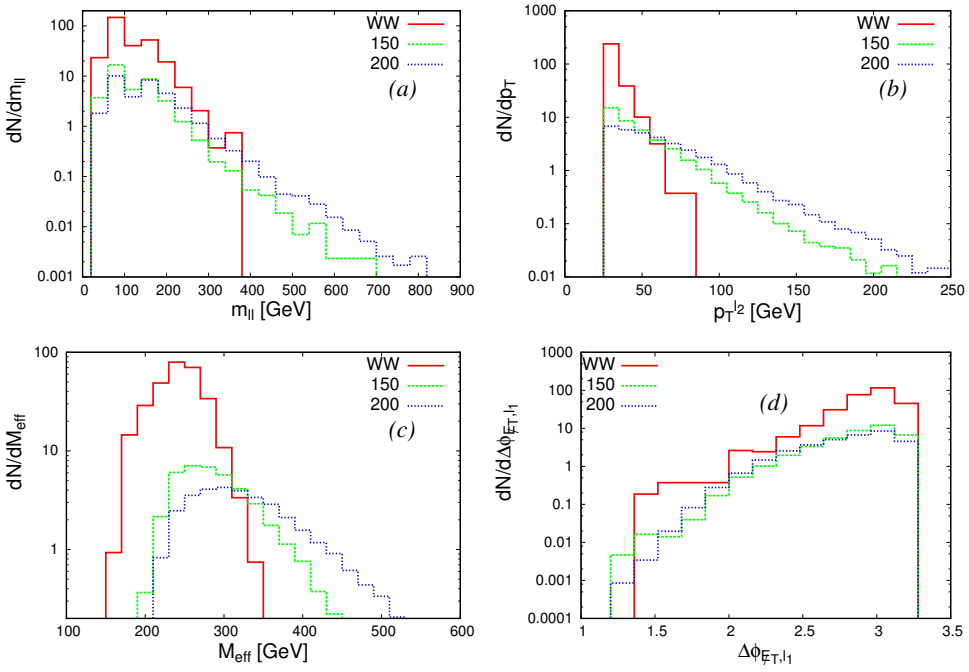

Figure 6.6: Kinematic distributions for the ($2l + \not{E}_T$) signal with $M_{H^\pm}$=150, 200 GeV and background (W^+W^-). The events satisfy the $\Delta\phi_{\not{E}_T,l_2} > 1.6$, $\not{E}_T > 110$ GeV cut and the acceptance cuts listed in Eq. 6.4.11.

[2] $M_{eff} = \sum p_T^{visible} + \sum p_T^{missing}$

The kinematic distributions shown in Fig. 6.6 have been plotted after applying the $\Delta\phi_{\not{E}_T,l_2}$ cut. If we compare the distributions for m_{ll}, $p_T^{l_2}$ and M_{eff} in Fig. 6.5 after the application of $\Delta\phi_{\not{E}_T,l_2}$ cut, as shown in Fig. 6.6, we find that this cut affects the background events quite significantly. In our case, the additional source of missing energy reduces the correlation between the leptons and the $\not{E}_T$, which is so crucially present in the W^+W^- background. This causes events of background events with high p_T to be removed once the above azimuthal angle cut is applied. We can see from these distributions that the cut on the angle $\Delta\phi_{\not{E}_T,l_2}$ followed by a suitable cut on $p_T^{l_2}$ / M_{eff} looks very promising in enhancing the signal significance. The kinematic distribution displayed in Fig. 6.6d indicates that a minimum cut on $\Delta\phi_{\not{E}_T,l_1}$[3] may also help in improving the significance slightly. We have chosen a minimum cut of 55 GeV on $p_T^{l_2}$ and a minimum cut of 1.8 on the angle $\Delta\phi_{\not{E}_T,l_1}$ in our present analysis. With the help of these optimal values of cuts, a signal significance of about 4.6 can be achieved assuming an integrated luminosity $L = 3000$ fb^{-1}, for the case of $M_{H^\pm} = 150$ GeV.

Cuts applied	**No of events**			**S/B**		**Significance** (S_σ)	
	H^+H^-**(S)**		W^+W^-**(B)**				
	$M_{H^\pm}$=150	(200) GeV		$M_{H^\pm}$=150	(200) GeV	$M_{H^\pm}$=150	(200) GeV
Initial Signal	2331.8	(855.3)	931500.0	0.002	(0.001)	2.3	(0.9)
Isolation + 0j	943.7	(321.3)	431865.4	0.002	(0.001)	1.4	(0.5)
Acceptance cut	739.5	(263.9)	288626.8	0.002	(0.001)	1.4	(0.5)
$\not{E}_T > 110$ GeV	201.6	(107.9)	7423.1	0.028	(0.014)	2.3	(1.2)
$\Delta\phi_{\not{E}_T,l_2} > 1.6$	40.0	(33.5)	292.1	0.130	(0.115)	2.3	(1.9)
$p_T^{l_2} > 55$ GeV	8.6	(13.6)	1.9	4.382	(7.301)	4.3	(6.2)
$\Delta\phi_{\not{E}_T,l_1} > 1.8$	8.5	(13.5)	1.5	5.415	(9.020)	4.6	(6.5)

Table 6.3: Cut flow table at 14 TeV center-of-mass energy and 3000 fb^{-1} integrated luminosity for $M_{H^\pm}$ =150 GeV and 200 GeV. The significance (S_σ) is defined in Eq. 6.4.12.

The effects of applying various cuts on the signal and background events have been summarized as a cut flow scheme in Table 6.3 for the two benchmark values of the charged Higgs mass of 150 GeV and 200 GeV. We have selected only those cuts that

[3]Angle between the missing energy and the leading lepton in the transverse plane

increase the signal significance (S_σ) defined as

$$S_\sigma = \sqrt{2(S+B)\ln(1+S/B) - 2S}, \tag{6.4.12}$$

where S and B are number of signal and background events respectively. This significance estimator is useful for events with low statistics [136]. When the background is large, the formula for S_σ reduces to the more familiar $S/\sqrt{B}$ form used for estimating the signal significance. Although the number of events that satisfy all the applied cuts are low, the significance is nevertheless promising. With the 3000 fb^{-1} integrated luminosity, the same set of cuts lead to a signal significance of about 6.5 for $M_{H^\pm} = 200$ GeV. We can further improve the significance by optimizing various cuts. For example, pushing the minimum $\not{E}_T$ cut on the higher side does help in achieving better significance. As mentioned before, a suitable large cut on M_{eff} instead of the cut on $p_T^{l_2}$ can also be used to suppress the background efficiently. However, in that case the minimum $\not{E}_T$ cut should be relaxed slightly to maintain a high signal significance.

As both $\Delta\phi_{\not{E}_T,l_2}$ and $p_T^{l_2}$ play an important role in enhancing the signal significance, it will be useful to study a possible correlation between the minimum cuts that can be applied on these kinematic variables. We have shown this correlation in Fig. 6.7 using the contour plots for $M_{H^\pm}$=150, 200 GeV. The plots are shown for two values of the integrated luminosity, *viz* $L = 3000$ fb^{-1} and $L = 5000$ fb^{-1}. The contour plots have been obtained after applying the minimum $\not{E}_T > 110$ GeV cut along with the acceptance cuts. In these plots we show the minimum cuts on $p_T^{l_2}$ and $\Delta\phi_{\not{E}_T,l_2}$ required to achieve a signal significance $S_\sigma \geq 2$, keeping the total number of events $S + B \geq 5$. The signal significance is clearly seen to increase substantially with more optimal choices of cuts for the two correlated kinematic variables. The variation in the signal significance is represented with different color codes. With the help of these plots it is easier to find the optimal values of the cuts on $\Delta\phi_{\not{E}_T,l_2}$ and $p_T^{l_2}$ which can maximize the significance. We should also point out that our analysis for the two benchmark val-

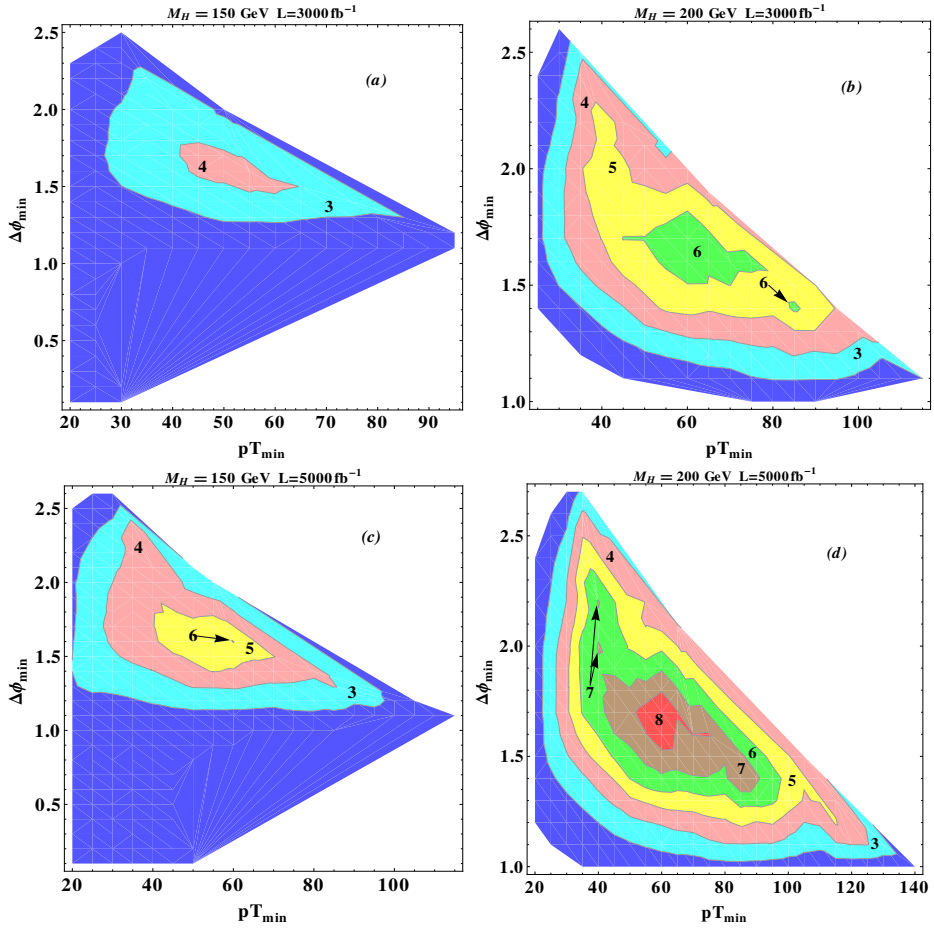

Figure 6.7: Contour plots for the significance (S_σ) as a function of minimum cuts on $\Delta\phi_{\not{E}_T,l_2}$ (y-axis) and $p_T^{l_2}$ (x-axis) for (a) $M_{H^\pm} = 150$ GeV, $L = 3000$ fb^{-1}, (b) $M_{H^\pm} = 200$ GeV, $L = 3000$ fb^{-1}, (c) $M_{H^\pm} = 150$ GeV, $L = 5000$ fb^{-1}, and, (d) $M_{H^\pm} = 200$ GeV, $L = 5000$ fb^{-1}. The blue shaded regions in the above plots refer to 2σ statistical significance.

ues of the charged Higgs mass achieved a signal significance in accordance with the contour plots shown in Fig. 6.7a and 6.7b. However, the efficiency of these correlated cuts for the case of $M_{H^\pm} = 200$ GeV which is clearly visible in Fig. 6.7b, suggests that a significance, as high as 5σ, should be well within the reach with more optimal choices of the cuts when compared to those listed in Table 6.3. As expected, with higher integrated luminosity, much better signal significance can be achieved (see Figs. 6.7c and 6.7d). It is worth pointing out that in Fig. 6.7, the constraint $S + B \geq 5$ plays a major role in modifying the shape of common significance contours. As the discrete cut-off for events will not be uniform for both $L = 3000$ fb^{-1} and $L = 5000$ fb^{-1}, it gives an

impression of a non trivial scaling at different luminosities.

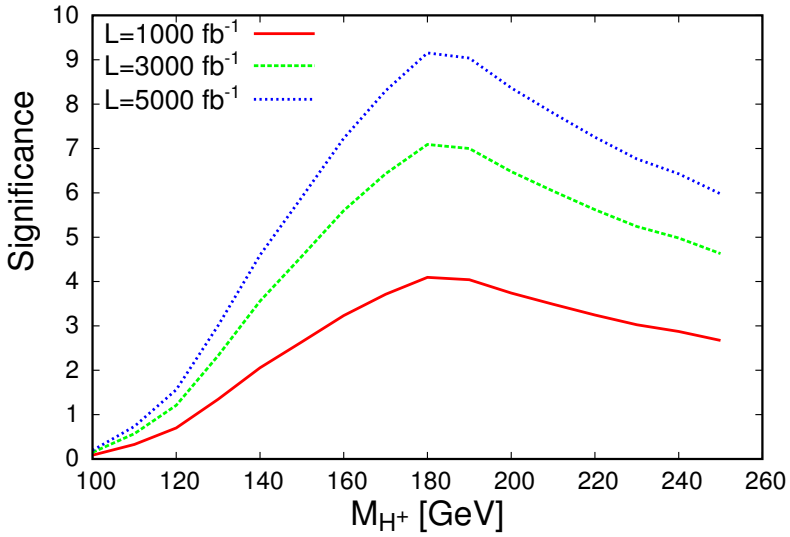

Figure 6.8: Illustrating the signal significance for different charged Higgs masses and integrated luminosities. The kinematic cuts are the same as given in Table 6.3.

In Fig. 6.8, we estimate the signal significance for various charged Higgs masses assuming 1000, 3000 and 5000 fb^{-1} integrated luminosities at the LHC with $\sqrt{s} = 14$ TeV. We have applied the same set of cuts as listed in Table 6.3. Since we have applied a large missing energy cut, the significance increases for higher charged Higgs masses. However, beyond a certain value of charged Higgs mass, the significance goes down. This is mainly due to the small pair production cross section of the charged Higgs. We note that for $M_{H^\pm} = 180$ GeV the significance is seen to become maximum in Fig. 6.8. This is just the artifact of the choice of $\not{E}_T$ cut, which is more effective at that charged Higgs mass. Note that beyond the charged Higgs mass of about 180 GeV, the $H^\pm \to W^\pm \rho$ decay channel is also open for $M_\rho = 100$ GeV. This reduces the charged Higgs branching ratio in the $W\sigma$ decay mode and hence reduces the signal cross section further for $M_{H^\pm} > 180$ GeV. The upper bound on M_ρ which is related to an upper bound on the coupling λ_5 can be about 470 GeV [202]. It means, by considering heavier ρ mass we can ensure a 100% branching ratio of the charged Higgs decay to $W^\pm\sigma$ for the heavier charged Higgs masses. It is needless to say that optimization of kine-

matic cuts is required to estimate the actual signal significance for different charged Higgs masses. For example, despite larger signal cross section for $M_{H^\pm} = 120$ GeV, the significance is maximized for a minimum $\not{E}_T$ cut of 90 GeV. On the other hand, for $M_{H^\pm} = 220$ GeV we have smaller signal cross section but a minimum cut of 130 GeV on $\not{E}_T$ is more helpful in achieving a larger signal significance. We note that $(\Delta\phi_{\not{E}_T,l_2}, p_T^{l_2})$ combination which we have used to discriminate the signal from the background for $M_{H^\pm} = 150,\ 200$ GeV is not very useful in increasing the significance for lower $M_{H^\pm}$ values. This is related to the fact that the efficiency of these cuts is closely related to the high $\not{E}_T$ cut which in turn is related to the mass difference between the charged Higgs and the W boson. When the mass difference between the charged Higgs and the W boson is not large enough, the application of high $\not{E}_T$ cut also kills the signal along with the background. It is also worth pointing out that for larger charged Higgs masses a suitable $\Delta\phi_{\not{E}_T,l_2}$ cut with large enough $\not{E}_T$ cut is sufficient. In other words, if it is possible to apply a very high $\not{E}_T$ cut, the additional $p_T^{l_2}$ cut becomes less relevant.

6.5 Summary and Conclusion

We have studied the signatures of charged Higgs boson at the LHC in a two Higgs doublet model with right-handed neutrinos. The model, aiming to derive neutrino masses via preferential Yukawa couplings $\mathcal{O}(1)$ with an additional Higgs doublet, also implies large Yukawa coupling of the charged Higgs with the light leptons and neutrinos. However, if cosmological constraints are taken into account, the leptonic decay mode of the charged Higgs is highly suppressed and $H^\pm \to W^\pm\sigma$ is the dominant decay mode. In this study, the charged Higgs pair production via the Drell-Yan process and its further decay leading to opposite sign di-leptons+missing energy in the final state is considered as the signal. The major SM background to the signal comes from the process, $pp \to W^+W^-$. We have done a complete signal-background cut based analysis for both the 8 TeV and 14 TeV center-of-mass energies at LHC. The charged

Higgs masses of 150 GeV and 200 GeV serve as the benchmark points for our study. Since the signal has additional sources of missing energy, we find that a large $\not{E}_T$ cut helps in suppressing the SM background. Also, a combination of minimum cuts on the angle $\Delta\phi_{\not{E}_T,l_2}$ and $p_T^{l_2}$ plays an important role in enhancing the signal significance. Due to the lack of sufficient data and the low signal cross section as compared to the background, the observability of the signal is not possible at the LHC with $\sqrt{s} = 8$ TeV and we therefore carry out our analysis for the 14 TeV run of the LHC. We find that even at the 14 TeV run of LHC, a charged Higgs with the characteristics of a "fermiophobic" field will prove elusive without a very optimized kinematic selection of events even with high integrated luminosity. We show this by identifying the kinematic variables sensitive to specific selection cuts which with a large (3000 fb^{-1}) integrated luminosity yields a signal significance of 4.6σ for $M_{H^\pm} = 150$ GeV. For the case of $M_{H^\pm} = 200$ GeV, a signal significance of 5σ can be easily achieved with better statistics. We highlight the significance of the optimized cuts in the analysis through a correlation plot for event selection that enhances the signal significance in a very robust way. Our analysis indicates that the observation of this otherwise elusive fermiophobic charged Higgs boson is rather promising at the high energy and high luminosity run of the LHC, provided that proper event selection criteria are applied.

Chapter 7

Summary and conclusions

In this thesis, we have carried out a detailed probe of the fact that the LHC data can still accommodate additional scalars along with the recently discovered Higgs boson. In particular we have studied two specific scenarios beyond the standard model, with a view to possible outcomes in the high energy run.

- The radion coming from the RS model: We have explored the constraints on the parameter space of a Randall-Sundrum warped geometry scenario, where a radion field arises out of the attempt to stabilise the radius of the extra compact spacelike dimension, using the LHC-run1 data and all other experimental data such as Tevatron. We have calculated contributions from both the scalar mass eigenstates arising from radion-higgs kinetic mixing in all important search channels. We found that the most important channel to be affected is the decay via WW*, where no invariant mass peak can discern the two distinct physical states. We have performed a full cut based analysis in the WW* channel, taking into account the effect of various cuts and interference when the two scalar are closely spaced. We examined both cases where the experimentally discovered scalar is either 'higgs-like' or 'radion-like'. The implications of a relatively massive scalar decaying into a pair of 125 GeV scalars is also included. We found that the discovered scalar can be a Higgs-like scalar with a heavy(~ 400 GeV)

radion-like scalar.

- The existing LHC data do not rule out the possibility of a light radion-like scalar(< 100 GeV) along with Higgs-like scalar at 125 GeV. However, LHC data exclude the possibility that the scalar discovered at 125 GeV is a radion. As the LHC-run1 data can accommodate a light radion(<100 GeV) along with the SM Higgs, so we have studied the prospect of such light radion in the next run of LHC. We found that two-photon mode of decay can enable us to probe a radion in the mass range 60 - 110 GeV. Our conclusion is that, with an integrated luminosity of 3000 fb^{-1} or less, the next run of the Large Hadron Collider should be able to detect a radion in this mass range, with a significance of 5 standard deviations or more.

- We have also studied the signals for a "fermiophobic" charged Higgs boson present in an extension of the standard model with an additional Higgs doublet and right handed neutrinos, responsible for generating Dirac-type neutrino masses. We have studied the pair production of the charged Higgs at the Large Hadron Collider (LHC), which can be relatively light and still allowed by experimental data. The charged Higgs decays dominantly into a W boson and a very light neutral scalar present in the model, which decays invisibly and passes undetected. We find that the signal for such a charged Higgs is overwhelmed by the standard model background and will prove elusive at the 8 TeV run of the LHC. We have considered a cut-flow based analysis to pinpoint a search strategy at the 14 TeV run of the LHC which can achieve a signal significance of about 5σ.

Bibliography

[1] "Atlas higgs result." https://atlas.web.cern.ch/Atlas/GROUPS/PHYSICS/CombinedSummaryPlots/HIGGS/.

[2] **CMS** Collaboration, V. Khachatryan *et al.*, *Precise determination of the mass of the Higgs boson and tests of compatibility of its couplings with the standard model predictions using proton collisions at 7 and 8 TeV*, *Eur. Phys. J.* **C75** no. 5, (2015) 212, arXiv:1412.8662 [hep-ex].

[3] K.-m. Cheung, *Phenomenology of radion in Randall-Sundrum scenario*, *Phys.Rev.* **D63** (2001) 056007, arXiv:hep-ph/0009232 [hep-ph].

[4] **ATLAS Collaboration** Collaboration, G. Aad *et al.*, *Search for the Standard Model Higgs boson in the $H \to WW(*) \to \ell\nu\ell\nu$ decay mode with 4.7 /fb of ATLAS data at $\sqrt{s} = 7$ TeV*, *Phys.Lett.* **B716** (2012) 62–81, arXiv:1206.0756 [hep-ex].

[5] **ATLAS Collaboration** Collaboration, G. Aad *et al.*, *Measurements of the properties of the higgs-like boson in the $ww^{(*)} \to \ell\nu\ell\nu$ decay channel with the atlas detector using 25 fb^{-1} of proton-proton collision data*, Tech. Rep. ATLAS-CONF-2013-030, CERN, Geneva, Mar, 2013.

[6] **ATLAS Collaboration** Collaboration, G. *et al.*, *Combined measurements of the mass and signal strength of the higgs-like boson with the atlas detector using up to 25 fb^{-1} of proton-proton collision data*, Tech. Rep. ATLAS-CONF-2013-014, CERN, Geneva, Mar, 2013.

[7] **CMS Collaboration** Collaboration, S. Chatrchyan *et al.*, *Combination of standard model higgs boson searches and measurements of the properties of the new boson with a mass near 125 gev*, Tech. Rep. CMS-PAS-HIG-13-005, CERN, Geneva, 2013.

[8] **CDF Collaboration, D0 Collaboration** Collaboration, T. Aaltonen *et al.*, *Evidence for a particle produced in association with weak bosons and decaying to a*

bottom-antibottom quark pair in Higgs boson searches at the Tevatron, *Phys.Rev.Lett.* **109** (2012) 071804, arXiv:1207.6436 [hep-ex].

[9] G. Fogli, E. Lisi, A. Marrone, D. Montanino, A. Palazzo, *et al.*, *Global analysis of neutrino masses, mixings and phases: entering the era of leptonic CP violation searches*, *Phys.Rev.* **D86** (2012) 013012, arXiv:1205.5254 [hep-ph].

[10] M. Gell-Mann, *A Schematic Model of Baryons and Mesons*, *Phys.Lett.* **8** (1964) 214–215.

[11] D. J. Gross and F. Wilczek, *Ultraviolet Behavior of Nonabelian Gauge Theories*, *Phys.Rev.Lett.* **30** (1973) 1343–1346.

[12] H. D. Politzer, *Reliable Perturbative Results for Strong Interactions?*, *Phys.Rev.Lett.* **30** (1973) 1346–1349.

[13] S. Glashow, *Partial Symmetries of Weak Interactions*, *Nucl.Phys.* **22** (1961) 579–588.

[14] S. Weinberg, *A Model of Leptons*, *Phys.Rev.Lett.* **19** (1967) 1264–1266.

[15] A. Salam, *Weak and Electromagnetic Interactions*, *Conf.Proc.* **C680519** (1968) 367–377.

[16] P. W. Higgs, *Broken Symmetries and the Masses of Gauge Bosons*, *Phys.Rev.Lett.* **13** (1964) 508–509.

[17] P. W. Higgs, *Spontaneous Symmetry Breakdown without Massless Bosons*, *Phys.Rev.* **145** (1966) 1156–1163.

[18] F. Englert and R. Brout, *Broken Symmetry and the Mass of Gauge Vector Mesons*, *Phys.Rev.Lett.* **13** (1964) 321–323.

[19] G. Guralnik, C. Hagen, and T. Kibble, *Global Conservation Laws and Massless Particles*, *Phys.Rev.Lett.* **13** (1964) 585–587.

[20] T. Kibble, *Symmetry breaking in nonAbelian gauge theories*, *Phys.Rev.* **155** (1967) 1554–1561.

[21] **CMS Collaboration** Collaboration, S. Chatrchyan *et al.*, *Observation of a new boson at a mass of 125 GeV with the CMS experiment at the LHC*, *Phys.Lett.* **B716** (2012) 30–61, arXiv:1207.7235 [hep-ex].

[22] **ATLAS Collaboration** Collaboration, G. Aad *et al.*, *Observation of a new particle in the search for the Standard Model Higgs boson with the ATLAS detector at the LHC*, *Phys.Lett.* **B716** (2012) 1–29, arXiv:1207.7214 [hep-ex].

[23] M. Gonzalez-Garcia, M. Maltoni, and J. Salvado, *Updated global fit to three neutrino mixing: status of the hints of theta13 > 0*, *JHEP* **1004** (2010) 056, arXiv:1001.4524 [hep-ph].

[24] M. Gonzalez-Garcia, M. Maltoni, and T. Schwetz, *Updated fit to three neutrino mixing: status of leptonic CP violation*, *JHEP* **1411** (2014) 052, arXiv:1409.5439 [hep-ph].

[25] A. Strumia and F. Vissani, *Neutrino masses and mixings and...*, arXiv:hep-ph/0606054 [hep-ph].

[26] R. Mohapatra, S. Antusch, K. Babu, G. Barenboim, M.-C. Chen, *et al.*, *Theory of neutrinos: A White paper*, *Rept.Prog.Phys.* **70** (2007) 1757–1867, arXiv:hep-ph/0510213 [hep-ph].

[27] **WMAP** Collaboration, C. Bennett *et al.*, *Nine-Year Wilkinson Microwave Anisotropy Probe (WMAP) Observations: Final Maps and Results*, *Astrophys.J.Suppl.* **208** (2013) 20, arXiv:1212.5225 [astro-ph.CO].

[28] A. Borriello and P. Salucci, *The Dark matter distribution in disk galaxies*, *Mon.Not.Roy.Astron.Soc.* **323** (2001) 285, arXiv:astro-ph/0001082 [astro-ph].

[29] H. Hoekstra, H. Yee, and M. Gladders, *Current status of weak gravitational lensing*, *New Astron.Rev.* **46** (2002) 767–781, arXiv:astro-ph/0205205 [astro-ph].

[30] F. Zwicky, *Die Rotverschiebung von extragalaktischen Nebeln*, *Helv.Phys.Acta* **6** (1933) 110–127.

[31] D. Hooper, *TASI 2008 Lectures on Dark Matter*, arXiv:0901.4090 [hep-ph].

[32] M.-C. Chen, *TASI 2006 Lectures on Leptogenesis*, arXiv:hep-ph/0703087 [HEP-PH].

[33] C. J. Copi, D. N. Schramm, and M. S. Turner, *Big bang nucleosynthesis and the baryon density of the universe*, *Science* **267** (1995) 192–199, arXiv:astro-ph/9407006 [astro-ph].

[34] S. P. Martin, *A Supersymmetry primer*, *Adv.Ser.Direct.High Energy Phys.* **21** (2010) 1–153, arXiv:hep-ph/9709356 [hep-ph].

[35] S. Dawson, *Introduction to electroweak symmetry breaking*, arXiv:hep-ph/9901280 [hep-ph].

[36] L. Randall and R. Sundrum, *A Large mass hierarchy from a small extra dimension*, *Phys.Rev.Lett.* **83** (1999) 3370–3373, arXiv:hep-ph/9905221 [hep-ph].

[37] W. D. Goldberger and M. B. Wise, *Modulus stabilization with bulk fields*, *Phys.Rev.Lett.* **83** (1999) 4922–4925, arXiv:hep-ph/9907447 [hep-ph].

[38] W. D. Goldberger and M. B. Wise, *Phenomenology of a stabilized modulus*, *Phys.Lett.* **B475** (2000) 275–279, arXiv:hep-ph/9911457 [hep-ph].

[39] W. D. Goldberger, B. Grinstein, and W. Skiba, *Distinguishing the Higgs boson from the dilaton at the Large Hadron Collider*, *Phys.Rev.Lett.* **100** (2008) 111802, arXiv:0708.1463 [hep-ph].

[40] B. Grinstein and P. Uttayarat, *A Very Light Dilaton*, *JHEP* **1107** (2011) 038, arXiv:1105.2370 [hep-ph].

[41] B. Bellazzini, C. Csaki, J. Hubisz, J. Serra, and J. Terning, *A Higgslike Dilaton*, *Eur.Phys.J.* **C73** no. 2, (2013) 2333, arXiv:1209.3299 [hep-ph].

[42] J. D. Wells, *Lectures on Higgs Boson Physics in the Standard Model and Beyond*, arXiv:0909.4541 [hep-ph].

[43] C. Burgess, M. Pospelov, and T. ter Veldhuis, *The Minimal model of nonbaryonic dark matter: A Singlet scalar*, *Nucl.Phys.* **B619** (2001) 709–728, arXiv:hep-ph/0011335 [hep-ph].

[44] H. Davoudiasl, R. Kitano, T. Li, and H. Murayama, *The New minimal standard model*, *Phys.Lett.* **B609** (2005) 117–123, arXiv:hep-ph/0405097 [hep-ph].

[45] J. D. Wells, *How to Find a Hidden World at the Large Hadron Collider*, arXiv:0803.1243 [hep-ph].

[46] S. Gopalakrishna, S. J. Lee, and J. D. Wells, *Dark matter and Higgs boson collider implications of fermions in an abelian-gauged hidden sector*, *Phys.Lett.* **B680** (2009) 88–93, arXiv:0904.2007 [hep-ph].

[47] G. Branco, P. Ferreira, L. Lavoura, M. Rebelo, M. Sher, *et al.*, *Theory and phenomenology of two-Higgs-doublet models*, *Phys.Rept.* **516** (2012) 1–102, arXiv:1106.0034 [hep-ph].

[48] R. Peccei, *The Strong CP problem and axions*, *Lect.Notes Phys.* **741** (2008) 3–17, arXiv:hep-ph/0607268 [hep-ph].

[49] J. M. Cline, *Baryogenesis*, arXiv:hep-ph/0609145 [hep-ph].

[50] T. Cheng and L.-F. Li, *Neutrino Masses, Mixings and Oscillations in SU(2) x U(1) Models of Electroweak Interactions*, *Phys.Rev.* **D22** (1980) 2860.

[51] P. Bhupal Dev, D. K. Ghosh, N. Okada, and I. Saha, *125 GeV Higgs Boson and the Type-II Seesaw Model*, *JHEP* **1303** (2013) 150, arXiv:1301.3453 [hep-ph].

[52] H. Georgi and M. Machacek, *DOUBLY CHARGED HIGGS BOSONS*, *Nucl.Phys.* **B262** (1985) 463.

[53] M. S. Chanowitz and M. Golden, *Higgs Boson Triplets With M (W) = M (Z) $\cos\theta\omega$*, *Phys.Lett.* **B165** (1985) 105.

[54] C. Englert, E. Re, and M. Spannowsky, *Triplet Higgs boson collider phenomenology after the LHC*, *Phys.Rev.* **D87** no. 9, (2013) 095014, arXiv:1302.6505 [hep-ph].

[55] "LHC website." http://home.web.cern.ch/topics/large-hadron-collider.

[56] T. Han, *Collider phenomenology: Basic knowledge and techniques*, arXiv:hep-ph/0508097 [hep-ph].

[57] A. Djouadi, *The Anatomy of electro-weak symmetry breaking. I: The Higgs boson in the standard model*, *Phys.Rept.* **457** (2008) 1–216, arXiv:hep-ph/0503172 [hep-ph].

[58] N. Arkani-Hamed, S. Dimopoulos, and G. Dvali, *The Hierarchy problem and new dimensions at a millimeter*, *Phys.Lett.* **B429** (1998) 263–272, arXiv:hep-ph/9803315 [hep-ph].

[59] T. Appelquist, H.-C. Cheng, and B. A. Dobrescu, *Bounds on universal extra dimensions*, *Phys.Rev.* **D64** (2001) 035002, arXiv:hep-ph/0012100 [hep-ph].

[60] H. Davoudiasl, J. Hewett, and T. Rizzo, *Phenomenology of the Randall-Sundrum Gauge Hierarchy Model*, *Phys.Rev.Lett.* **84** (2000) 2080, arXiv:hep-ph/9909255 [hep-ph].

[61] H. Davoudiasl, J. Hewett, and T. Rizzo, *Experimental probes of localized gravity: On and off the wall*, *Phys.Rev.* **D63** (2001) 075004, arXiv:hep-ph/0006041 [hep-ph].

[62] S. Chang and M. Yamaguchi, *Fate of gravitons in warped extra dimension*, arXiv:hep-ph/9909523 [hep-ph].

[63] *Search for high-mass dilepton resonances in 20 fb^{-1} of pp collisions at $\sqrt{s} = 8$ tev with the atlas experiment*, Tech. Rep. ATLAS-CONF-2013-017, CERN, Geneva, Mar, 2013.

[64] C. Csaki, M. Graesser, L. Randall, and J. Terning, *Cosmology of brane models with radion stabilization*, *Phys.Rev.* **D62** (2000) 045015, arXiv:hep-ph/9911406 [hep-ph].

[65] C. Csaki, M. L. Graesser, and G. D. Kribs, *Radion dynamics and electroweak physics*, *Phys.Rev.* **D63** (2001) 065002, arXiv:hep-th/0008151 [hep-th].

[66] U. Mahanta and S. Rakshit, *Some low-energy effects of a light stabilized radion in the Randall-Sundrum model*, *Phys.Lett.* **B480** (2000) 176–180, arXiv:hep-ph/0002049 [hep-ph].

[67] J. F. Gunion, M. Toharia, and J. D. Wells, *Precision electroweak data and the mixed Radion-Higgs sector of warped extra dimensions*, *Phys.Lett.* **B585** (2004) 295–306, arXiv:hep-ph/0311219 [hep-ph].

[68] M. Toharia, *Precision electroweak constraints on the mixed radion Higgs sector*, arXiv:hep-ph/0402092 [hep-ph].

[69] M. Toharia, *Higgs-Radion Mixing with Enhanced Di-Photon Signal*, *Phys.Rev.* **D79** (2009) 015009, arXiv:0809.5245 [hep-ph].

[70] M. Frank, B. Korutlu, and M. Toharia, *Saving the fourth generation Higgs with radion mixing*, *Phys.Rev.* **D85** (2012) 115025, arXiv:1204.5944 [hep-ph].

[71] T. G. Rizzo, *Effects on Higgs boson properties from radion mixing*, arXiv:hep-ph/0207113 [hep-ph].

[72] K. Cheung, C. Kim, and J. Song, *Probing the radion-Higgs mixing at photon colliders*, *Phys.Rev.* **D72** (2005) 115015, arXiv:hep-ph/0509017 [hep-ph].

[73] T. Han, G. D. Kribs, and B. McElrath, *Radion effects on unitarity in gauge boson scattering*, *Phys.Rev.* **D64** (2001) 076003, arXiv:hep-ph/0104074 [hep-ph].

[74] M. Chaichian, A. Datta, K. Huitu, and Z.-h. Yu, *Radion and Higgs mixing at the LHC*, *Phys.Lett.* **B524** (2002) 161–169, arXiv:hep-ph/0110035 [hep-ph].

[75] M. Battaglia, S. De Curtis, A. De Roeck, D. Dominici, and J. F. Gunion, *On the complementarity of Higgs and radion searches at LHC*, *Phys.Lett.* **B568** (2003) 92–102, arXiv:hep-ph/0304245 [hep-ph].

[76] B. Bhattacherjee and S. Raychaudhuri, *Tevatron Signal for an Unmixed Radion*, arXiv:1104.4749 [hep-ph].

[77] V. Goncalves and W. Sauter, *Radion production in exclusive processes at CERN LHC*, *Phys.Rev.* **D82** (2010) 056009, arXiv:1007.5487 [hep-ph].

[78] V. Barger, M. Ishida, and W.-Y. Keung, *Differentiating the Higgs boson from the dilaton and the radion at hadron colliders*, *Phys.Rev.Lett.* **108** (2012) 101802, arXiv:1111.4473 [hep-ph].

[79] K. Cheung and T.-C. Yuan, *Could the excess seen at 124-126 GeV be due to the Randall-Sundrum Radion?*, *Phys.Rev.Lett.* **108** (2012) 141602, arXiv:1112.4146 [hep-ph].

[80] H. Davoudiasl, T. McElmurry, and A. Soni, *The Radion as a Harbinger of Deca-TeV Physics*, *Phys.Rev.* **D86** (2012) 075026, arXiv:1206.4062 [hep-ph].

[81] I. Low, J. Lykken, and G. Shaughnessy, *Have We Observed the Higgs (Imposter)?*, *Phys.Rev.* **D86** (2012) 093012, arXiv:1207.1093 [hep-ph].

[82] D. Soa, T. Tham, N. Thao, D. Thuy, D. Thuy, *et al.*, *Radion production in gamma-electron collisions*, *Mod.Phys.Lett.* **A27** (2012) 1250126, arXiv:1207.6471 [hep-ph].

[83] Z. Chacko, R. Franceschini, and R. K. Mishra, *Resonance at 125 GeV: Higgs or Dilaton/Radion?*, *JHEP* **1304** (2013) 015, arXiv:1209.3259 [hep-ph].

[84] V. Barger and M. Ishida, *Randall-Sundrum Reality at the LHC*, *Phys.Lett.* **B709** (2012) 185–191, arXiv:1110.6452 [hep-ph].

[85] B. Grzadkowski, J. F. Gunion, and M. Toharia, *Higgs-Radion interpretation of the LHC data?*, *Phys.Lett.* **B712** (2012) 70–80, arXiv:1202.5017 [hep-ph].

[86] H. de Sandes and R. Rosenfeld, *Radion-Higgs mixing effects on bounds from LHC Higgs Searches*, *Phys.Rev.* **D85** (2012) 053003, arXiv:1111.2006 [hep-ph].

[87] H. Kubota and M. Nojiri, *Radion-higgs mixing state at the LHCwith the KK contributions to the production and decay*, arXiv:1207.0621 [hep-ph].

[88] Y. Ohno and G.-C. Cho, *Production and decay of a heavy radion in Rundall-Sundrum model at the LHC*, *EPJ Web Conf.* **49** (2013) 18003, arXiv:1301.7514 [hep-ph].

[89] G.-C. Cho, D. Nomura, and Y. Ohno, *Constraints on radion in a warped extra dimension model from Higgs boson searches at the LHC*, arXiv:1305.4431 [hep-ph].

[90] N. Desai, U. Maitra, and B. Mukhopadhyaya, *An updated analysis of radion-higgs mixing in the light of LHC data*, *JHEP* **1310** (2013) 093, arXiv:1307.3765 [hep-ph].

[91] U. Mahanta and A. Datta, *Production of light stabilized radion at high-energy hadron collider*, *Phys.Lett.* **B483** (2000) 196–202, arXiv:hep-ph/0002183 [hep-ph].

[92] **LEP Working Group for Higgs boson searches, ALEPH, DELPHI, L3, OPAL** Collaboration, R. Barate *et al.*, *Search for the standard model Higgs boson at LEP*, *Phys.Lett.* **B565** (2003) 61–75, arXiv:hep-ex/0306033 [hep-ex].

[93] **ATLAS** Collaboration, G. Aad *et al.*, *Search for Scalar Diphoton Resonances in the Mass Range* $65 - 600$ *GeV with the ATLAS Detector in* pp *Collision Data at* $\sqrt{s} = 8$ TeV, *Phys.Rev.Lett.* **113** no. 17, (2014) 171801, arXiv:1407.6583 [hep-ex].

[94] S. Bhattacharya, M. Frank, K. Huitu, U. Maitra, B. Mukhopadhyaya, *et al.*, *Probing the light radion through diphotons at the Large Hadron Collider*, *Phys.Rev.* **D91** (2015) 016008, arXiv:1410.0396 [hep-ph].

[95] W. D. Goldberger and M. B. Wise, *Bulk fields in the Randall-Sundrum compactification scenario*, *Phys.Rev.* **D60** (1999) 107505, arXiv:hep-ph/9907218 [hep-ph].

[96] H. Davoudiasl, J. Hewett, and T. Rizzo, *Bulk gauge fields in the Randall-Sundrum model*, *Phys.Lett.* **B473** (2000) 43–49, arXiv:hep-ph/9911262 [hep-ph].

[97] A. Pomarol, *Gauge bosons in a five-dimensional theory with localized gravity*, *Phys.Lett.* **B486** (2000) 153–157, arXiv:hep-ph/9911294 [hep-ph].

[98] K. Agashe, A. Belyaev, T. Krupovnickas, G. Perez, and J. Virzi, *LHC Signals from Warped Extra Dimensions*, *Phys.Rev.* **D77** (2008) 015003, arXiv:hep-ph/0612015 [hep-ph].

[99] K. Agashe, G. Perez, and A. Soni, *B-factory signals for a warped extra dimension*, *Phys.Rev.Lett.* **93** (2004) 201804, arXiv:hep-ph/0406101 [hep-ph].

[100] K. Agashe, G. Perez, and A. Soni, *Flavor structure of warped extra dimension models*, *Phys.Rev.* **D71** (2005) 016002, arXiv:hep-ph/0408134 [hep-ph].

[101] K. Agashe, A. Delgado, M. J. May, and R. Sundrum, *RS1, custodial isospin and precision tests*, *JHEP* **0308** (2003) 050, arXiv:hep-ph/0308036 [hep-ph].

[102] C. Csaki, J. Hubisz, and S. J. Lee, *Radion phenomenology in realistic warped space models*, *Phys.Rev.* **D76** (2007) 125015, arXiv:0705.3844 [hep-ph].

[103] G. F. Giudice, R. Rattazzi, and J. D. Wells, *Graviscalars from higher dimensional metrics and curvature Higgs mixing*, *Nucl.Phys.* **B595** (2001) 250–276, arXiv:hep-ph/0002178 [hep-ph].

[104] Y. Tang, *Implications of LHC Searches for Massive Graviton*, *JHEP* **1208** (2012) 078, arXiv:1206.6949 [hep-ph].

[105] J. E. Kim, B. Kyae, and H. M. Lee, *Effective Gauss-Bonnet interaction in Randall-Sundrum compactification*, *Phys.Rev.* **D62** (2000) 045013, arXiv:hep-ph/9912344 [hep-ph].

[106] J. E. Kim, B. Kyae, and H. M. Lee, *Various modified solutions of the Randall-Sundrum model with the Gauss-Bonnet interaction*, *Nucl.Phys.* **B582** (2000) 296–312, arXiv:hep-th/0004005 [hep-th].

[107] T. G. Rizzo, *Warped phenomenology of higher-derivative gravity*, *JHEP* **0501** (2005) 028, arXiv:hep-ph/0412087 [hep-ph].

[108] S. Choudhury and S. Sengupta, *Features of warped geometry in presence of Gauss-Bonnet coupling*, *JHEP* **1302** (2013) 136, arXiv:1301.0918 [hep-th].

[109] U. Maitra, B. Mukhopadhyaya, and S. SenGupta, *Reconciling small radion vacuum expectation values with massive gravitons in an Einstein-Gauss-Bonnet warped geometry scenario*, arXiv:1307.3018 [hep-ph].

[110] T. Sjostrand, S. Mrenna, and P. Z. Skands, *A Brief Introduction to PYTHIA 8.1*, *Comput.Phys.Commun.* **178** (2008) 852–867, arXiv:0710.3820 [hep-ph].

[111] J. Alwall, M. Herquet, F. Maltoni, O. Mattelaer, and T. Stelzer, *MadGraph 5 : Going Beyond*, *JHEP* **1106** (2011) 128, arXiv:1106.0522 [hep-ph].

[112] **LHC Higgs Cross Section Working Group** Collaboration, S. Dittmaier *et al.*, *Handbook of LHC Higgs Cross Sections: 1. Inclusive Observables*, arXiv:1101.0593 [hep-ph].

[113] A. Denner, S. Heinemeyer, I. Puljak, D. Rebuzzi, and M. Spira, *Standard Model Higgs-Boson Branching Ratios with Uncertainties*, *Eur.Phys.J.* **C71** (2011) 1753, arXiv:1107.5909 [hep-ph].

[114] **CMS Collaboration** Collaboration, S. Chatrchyan *et al.*, *Evidence for a particle decaying to w+w- in the fully leptonic final state in a standard model higgs boson search in pp collisions at the lhc*, Tech. Rep. CMS-PAS-HIG-13-003, CERN, Geneva, 2013.

[115] *Properties of the higgs-like boson in the decay h to zz to 4l in pp collisions at sqrt s =7 and 8 tev*, Tech. Rep. CMS-PAS-HIG-13-002, CERN, Geneva, 2013.

[116] *Measurements of the properties of the higgs-like boson in the four lepton decay channel with the atlas detector using 25 fbâĹŠ1 of proton-proton collision data*, Tech. Rep. ATLAS-CONF-2013-013, CERN, Geneva, Mar, 2013.

[117] *Updated measurements of the higgs boson at 125 gev in the two photon decay channel*, Tech. Rep. CMS-PAS-HIG-13-001, CERN, Geneva, 2013.

[118] *Observation and study of the higgs boson candidate in the two photon decay channel with the atlas detector at the lhc*, Tech. Rep. ATLAS-CONF-2012-168, CERN, Geneva, Dec, 2012.

[119] **ATLAS** Collaboration, G. Aad *et al.*, *Search for high-mass dilepton resonances in pp collisions at* $\sqrt{s} = 8$*âĂL'âĂL'TeV with the ATLAS detector*, *Phys.Rev.* **D90** no. 5, (2014) 052005, arXiv:1405.4123 [hep-ex].

[120] M. Pieri, S. Bhattacharya, I. Fisk, J. Letts, V. A. Litvine, *et al.*, *Inclusive search for the Higgs boson in the H —> gamma gamma channel*, .

[121] *Higgs to bb in the vbf channel*, Tech. Rep. CMS-PAS-HIG-13-011, CERN, Geneva, 2013.

[122] H. Davoudiasl, T. McElmurry, and A. Soni, *Precocious Diphoton Signals of the Little Radion at Hadron Colliders*, *Phys.Rev.* **D82** (2010) 115028, arXiv:1009.0764 [hep-ph].

[123] Z. Chacko, R. K. Mishra, and D. Stolarski, *Dynamics of a Stabilized Radion and Duality*, arXiv:1304.1795 [hep-ph].

[124] T. Binoth, J. Guillet, E. Pilon, and M. Werlen, *A Full next-to-leading order study of direct photon pair production in hadronic collisions*, *Eur.Phys.J.* **C16** (2000) 311–330, arXiv:hep-ph/9911340 [hep-ph].

[125] "Private communication with Bhawna Gombar.".

[126] J. Alwall, R. Frederix, S. Frixione, V. Hirschi, F. Maltoni, *et al.*, *The automated computation of tree-level and next-to-leading order differential cross sections, and their matching to parton shower simulations*, *JHEP* **1407** (2014) 079, arXiv:1405.0301 [hep-ph].

[127] N. D. Christensen and C. Duhr, *FeynRules - Feynman rules made easy*, *Comput.Phys.Commun.* **180** (2009) 1614–1641, arXiv:0806.4194 [hep-ph].

[128] N. D. Christensen, P. de Aquino, C. Degrande, C. Duhr, B. Fuks, *et al.*, *A Comprehensive approach to new physics simulations*, *Eur.Phys.J.* **C71** (2011) 1541, arXiv:0906.2474 [hep-ph].

[129] J. Pumplin, D. Stump, J. Huston, H. Lai, P. M. Nadolsky, *et al.*, *New generation of parton distributions with uncertainties from global QCD analysis*, *JHEP* **0207** (2002) 012, arXiv:hep-ph/0201195 [hep-ph].

[130] *Electromagnetic calorimeter calibration with 7 tev data*, Tech. Rep. CMS-PAS-EGM-10-003, CERN, Geneva, 2013.

[131] M. Cacciari, G. P. Salam, and G. Soyez, *The Anti-k(t) jet clustering algorithm*, *JHEP* **0804** (2008) 063, arXiv:0802.1189 [hep-ph].

[132] "Private communication with V. Ravindran.".

[133] **CMS** Collaboration, V. Khachatryan *et al.*, *Search for excited quarks in the γ+jet final state in protonâĂŞproton collisions at $\sqrt{s} = 8$ TeV*, *Phys.Lett.* **B738** (2014) 274–293, arXiv:1406.5171 [hep-ex].

[134] Z. Bern, L. J. Dixon, and C. Schmidt, *The Diphoton background to a light Higgs boson at the LHC*, *Nucl.Phys.Proc.Suppl.* **116** (2003) 178–182, arXiv:hep-ph/0211216 [hep-ph].

[135] M. Pieri, S. Bhattacharya, I. Fisk, J. Letts, V. Litvin, and J. G. Branson, *Inclusive Search for the Higgs Boson in the $H \to \gamma\gamma$ Channel*, Tech. Rep. CMS-NOTE-2006-112, CERN, Geneva, Jun, 2006. http://cds.cern.ch/record/973112.

[136] G. Cowan, K. Cranmer, E. Gross, and O. Vitells, *Asymptotic formulae for likelihood-based tests of new physics*, *Eur.Phys.J.* **C71** (2011) 1554, arXiv:1007.1727 [physics.data-an].

[137] S. Bhattacharya, S. S. Chauhan, B. C. Choudhary, and D. Choudhury, *Search for excited quarks in $q\bar{q} \to \gamma\gamma$ at the cern lhc*, *Phys. Rev. D* **76** (Dec', publisher =, 2007) 115017.

[138] J. F. Gunion, H. E. Haber, G. L. Kane, and S. Dawson, *The Higgs Hunter's Guide*, *Front.Phys.* **80** (2000) 1–448.

[139] B. McWilliams and L.-F. Li, *Virtual Effects of Higgs Particles*, *Nucl.Phys.* **B179** (1981) 62.

[140] O. U. Shanker, *Flavor Violation, Scalar Particles and Leptoquarks*, *Nucl.Phys.* **B206** (1982) 253.

[141] A. Arhrib, *Top and Higgs flavor changing neutral couplings in two Higgs doublets model*, *Phys.Rev.* **D72** (2005) 075016, arXiv:hep-ph/0510107 [hep-ph].

[142] A. Dery, A. Efrati, G. Hiller, Y. Hochberg, and Y. Nir, *Higgs couplings to fermions: 2HDM with MFV*, *JHEP* **1308** (2013) 006, arXiv:1304.6727.

[143] E. Paschos, *Diagonal Neutral Currents*, *Phys.Rev.* **D15** (1977) 1966.

[144] S. L. Glashow and S. Weinberg, *Natural Conservation Laws for Neutral Currents*, *Phys.Rev.* **D15** (1977) 1958.

[145] H. E. Haber and D. O'Neil, *Basis-independent methods for the two-higgs-doublet model. iii. the cp-conserving limit, custodial symmetry, and the oblique parameters s, t, u*, *Phys. Rev. D* **83** (Mar, 2011) 055017. http://link.aps.org/doi/10.1103/PhysRevD.83.055017.

[146] M. Carena and H. E. Haber, *Higgs boson theory and phenomenology*, *Prog.Part.Nucl.Phys.* **50** (2003) 63–152, arXiv:hep-ph/0208209 [hep-ph].

[147] M. Aoki, S. Kanemura, K. Tsumura, and K. Yagyu, *Models of Yukawa interaction in the two Higgs doublet model, and their collider phenomenology*, *Phys.Rev.* **D80** (2009) 015017, arXiv:0902.4665 [hep-ph].

[148] E. Ma, *Verifiable radiative seesaw mechanism of neutrino mass and dark matter*, *Phys.Rev.* **D73** (2006) 077301, arXiv:hep-ph/0601225 [hep-ph].

[149] R. Barbieri, L. J. Hall, and V. S. Rychkov, *Improved naturalness with a heavy Higgs: An Alternative road to LHC physics*, *Phys.Rev.* **D74** (2006) 015007, arXiv:hep-ph/0603188 [hep-ph].

[150] H. Martinez, A. Melfo, F. Nesti, and G. Senjanovic, *Three Extra Mirror or Sequential Families: A Case for Heavy Higgs and Inert Doublet*, *Phys.Rev.Lett.* **106** (2011) 191802, arXiv:1101.3796 [hep-ph].

[151] E. Ma, *Common origin of neutrino mass, dark matter, and baryogenesis*, *Mod.Phys.Lett.* **A21** (2006) 1777–1782, arXiv:hep-ph/0605180 [hep-ph].

[152] D. Majumdar and A. Ghosal, *Dark Matter candidate in a Heavy Higgs Model - Direct Detection Rates*, *Mod.Phys.Lett.* **A23** (2008) 2011–2022, arXiv:hep-ph/0607067 [hep-ph].

[153] L. Lopez Honorez, E. Nezri, J. F. Oliver, and M. H. Tytgat, *The Inert Doublet Model: An Archetype for Dark Matter*, *JCAP* **0702** (2007) 028, arXiv:hep-ph/0612275 [hep-ph].

[154] M. Gustafsson, E. Lundstrom, L. Bergstrom, and J. Edsjo, *Significant Gamma Lines from Inert Higgs Dark Matter*, *Phys.Rev.Lett.* **99** (2007) 041301, arXiv:astro-ph/0703512 [ASTRO-PH].

[155] N. Sahu and U. Sarkar, *Predictive model for dark matter, dark energy, neutrino masses and leptogenesis at the TeV scale*, *Phys.Rev.* **D76** (2007) 045014, arXiv:hep-ph/0701062 [hep-ph].

[156] M. Lisanti and J. G. Wacker, *Unification and dark matter in a minimal scalar extension of the standard model*, arXiv:0704.2816 [hep-ph].

[157] E. Lundstrom, M. Gustafsson, and J. Edsjo, *The Inert Doublet Model and LEP II Limits*, *Phys.Rev.* **D79** (2009) 035013, arXiv:0810.3924 [hep-ph].

[158] A. Arhrib, Y.-L. S. Tsai, Q. Yuan, and T.-C. Yuan, *An Updated Analysis of Inert Higgs Doublet Model in light of the Recent Results from LUX, PLANCK, AMS-02 and LHC*, *JCAP* **1406** (2014) 030, arXiv:1310.0358 [hep-ph].

[159] J. Bijnens, J. Lu, and J. Rathsman, *Constraining General Two Higgs Doublet Models by the Evolution of Yukawa Couplings*, *JHEP* **1205** (2012) 118, arXiv:1111.5760 [hep-ph].

[160] S. Kanemura, T. Kasai, and Y. Okada, *Mass bounds of the lightest CP even Higgs boson in the two Higgs doublet model*, *Phys.Lett.* **B471** (1999) 182–190, arXiv:hep-ph/9903289 [hep-ph].

[161] N. Chakrabarty, U. K. Dey, and B. Mukhopadhyaya, *High-scale validity of a two-Higgs doublet scenario: a study including LHC data*, *JHEP* **1412** (2014) 166, arXiv:1407.2145 [hep-ph].

[162] A. Barroso, P. Ferreira, I. Ivanov, and R. Santos, *Metastability bounds on the two Higgs doublet model*, *JHEP* **1306** (2013) 045, arXiv:1303.5098 [hep-ph].

[163] A. Broggio, E. J. Chun, M. Passera, K. M. Patel, and S. K. Vempati, *Limiting two-Higgs-doublet models*, *JHEP* **1411** (2014) 058, arXiv:1409.3199 [hep-ph].

[164] I. Chakraborty and A. Kundu, *Two-Higgs doublet models confront the naturalness problem*, *Phys.Rev.* **D90** no. 11, (2014) 115017, arXiv:1404.3038 [hep-ph].

[165] K. Kannike, *Vacuum Stability Conditions From Copositivity Criteria*, *Eur.Phys.J.* **C72** (2012) 2093, arXiv:1205.3781 [hep-ph].

[166] S. Nie and M. Sher, *Vacuum stability bounds in the two Higgs doublet model*, *Phys.Lett.* **B449** (1999) 89–92, arXiv:hep-ph/9811234 [hep-ph].

[167] P. Ferreira and D. Jones, *Bounds on scalar masses in two Higgs doublet models*, *JHEP* **0908** (2009) 069, arXiv:0903.2856 [hep-ph].

[168] B. W. Lee, C. Quigg, and H. Thacker, *Weak Interactions at Very High-Energies: The Role of the Higgs Boson Mass*, *Phys.Rev.* **D16** (1977) 1519.

[169] D. A. Dicus and V. S. Mathur, *Upper bounds on the values of masses in unified gauge theories*, *Phys. Rev. D* **7** (May, 1973) 3111–3114. http://link.aps.org/doi/10.1103/PhysRevD.7.3111.

[170] M. S. Chanowitz and M. K. Gaillard, *The TeV Physics of Strongly Interacting W's and Z's*, *Nucl.Phys.* **B261** (1985) 379.

[171] G. Gounaris, R. Kogerler, and H. Neufeld, *Relationship Between Longitudinally Polarized Vector Bosons and their Unphysical Scalar Partners*, *Phys.Rev.* **D34** (1986) 3257.

[172] C. Vayonakis, *Born Helicity Amplitudes and Cross-Sections in Nonabelian Gauge Theories*, *Lett.Nuovo Cim.* **17** (1976) 383.

[173] J. Horejsi and M. Kladiva, *Tree-unitarity bounds for THDM Higgs masses revisited*, *Eur.Phys.J.* **C46** (2006) 81–91, arXiv:hep-ph/0510154 [hep-ph].

[174] I. Ginzburg and I. Ivanov, *Tree-level unitarity constraints in the most general 2HDM*, *Phys.Rev.* **D72** (2005) 115010, arXiv:hep-ph/0508020 [hep-ph].

[175] A. G. Akeroyd, A. Arhrib, and E.-M. Naimi, *Note on tree level unitarity in the general two Higgs doublet model*, *Phys.Lett.* **B490** (2000) 119–124, arXiv:hep-ph/0006035 [hep-ph].

[176] S. Kanemura, T. Kubota, and E. Takasugi, *Lee-Quigg-Thacker bounds for Higgs boson masses in a two doublet model*, *Phys.Lett.* **B313** (1993) 155–160, arXiv:hep-ph/9303263 [hep-ph].

[177] W. Grimus, L. Lavoura, O. Ogreid, and P. Osland, *A Precision constraint on multi-Higgs-doublet models*, *J.Phys.* **G35** (2008) 075001, arXiv:0711.4022 [hep-ph].

[178] W. Grimus, L. Lavoura, O. Ogreid, and P. Osland, *The Oblique parameters in multi-Higgs-doublet models*, *Nucl.Phys.* **B801** (2008) 81–96, arXiv:0802.4353 [hep-ph].

[179] M. E. Peskin and T. Takeuchi, *Estimation of oblique electroweak corrections*, *Phys.Rev.* **D46** (1992) 381–409.

[180] G. Funk, D. O'Neil, and R. M. Winters, *What the Oblique Parameters S, T, and U and Their Extensions Reveal About the 2HDM: A Numerical Analysis*, *Int.J.Mod.Phys.* **A27** (2012) 1250021, arXiv:1110.3812 [hep-ph].

[181] **Particle Data Group** Collaboration, J. Beringer *et al.*, *Review of Particle Physics (RPP)*, *Phys.Rev.* **D86** (2012) 010001.

[182] **BaBar** Collaboration, M. Margoni, *B —> X(s/d) gamma and B —> X(s/d) l+ l-*, *PoS* **KRUGER2010** (2011) 048.

[183] F. Mahmoudi and O. Stal, *Flavor constraints on the two-Higgs-doublet model with general Yukawa couplings*, *Phys.Rev.* **D81** (2010) 035016, arXiv:0907.1791 [hep-ph].

[184] T. Hermann, M. Misiak, and M. Steinhauser, *$\bar{B} \to X_s\gamma$ in the Two Higgs Doublet Model up to Next-to-Next-to-Leading Order in QCD*, *JHEP* **1211** (2012) 036, arXiv:1208.2788 [hep-ph].

[185] **LHCb** Collaboration, R. Aaij *et al.*, *First Evidence for the Decay $B_s^0 \to \mu^+\mu^-$*, *Phys.Rev.Lett.* **110** no. 2, (2013) 021801, arXiv:1211.2674 [hep-ex].

[186] C.-Y. Chen and S. Dawson, *Exploring Two Higgs Doublet Models Through Higgs Production*, *Phys.Rev.* **D87** (2013) 055016, arXiv:1301.0309 [hep-ph].

[187] **ALEPH, DELPHI, L3, OPAL, LEP** Collaboration, G. Abbiendi *et al.*, *Search for Charged Higgs bosons: Combined Results Using LEP Data*, *Eur.Phys.J.* **C73** (2013) 2463, arXiv:1301.6065 [hep-ex].

[188] **ALEPH, DELPHI, L3, OPAL, LEP Working Group for Higgs Boson Searches** Collaboration, S. Schael *et al.*, *Search for neutral MSSM Higgs bosons at LEP*, *Eur.Phys.J.* **C47** (2006) 547–587, arXiv:hep-ex/0602042 [hep-ex].

[189] E. Keith, E. Ma, and D. Roy, *Lower bound on the pseudoscalar mass in the minimal supersymmetric standard model*, *Phys.Rev.* **D56** (1997) 5306–5309, arXiv:hep-ph/9707512 [hep-ph].

[190] M. Aoki, R. Guedes, S. Kanemura, S. Moretti, R. Santos, *et al.*, *Light Charged Higgs bosons at the LHC in 2HDMs*, *Phys.Rev.* **D84** (2011) 055028, arXiv:1104.3178 [hep-ph].

[191] *Search for charged Higgs bosons in the τ+jets final state with pp collision data recorded at $\sqrt{s} = 8$ TeV with the ATLAS experiment*, Tech. Rep. ATLAS-CONF-2013-090, CERN, Geneva, Aug, 2013. http://cds.cern.ch/record/1595533.

[192] **CMS** Collaboration, C. Collaboration, *Search for H+ to cs-bar decay*, .

[193] B. Dumont, J. F. Gunion, Y. Jiang, and S. Kraml, *Constraints on and future prospects for Two-Higgs-Doublet Models in light of the LHC Higgs signal*, *Phys.Rev.* **D90** (2014) 035021, arXiv:1405.3584 [hep-ph].

[194] B. Coleppa, F. Kling, and S. Su, *Constraining Type II 2HDM in Light of LHC Higgs Searches*, *JHEP* **1401** (2014) 161, arXiv:1305.0002 [hep-ph].

[195] P. Ferreira, R. Santos, M. Sher, and J. P. Silva, *Implications of the LHC two-photon signal for two-Higgs-doublet models*, *Phys.Rev.* **D85** (2012) 077703, arXiv:1112.3277 [hep-ph].

[196] A. Celis, V. Ilisie, and A. Pich, *Towards a general analysis of LHC data within two-Higgs-doublet models*, *JHEP* **1312** (2013) 095, arXiv:1310.7941 [hep-ph].

[197] O. Eberhardt, U. Nierste, and M. Wiebusch, *Status of the two-Higgs-doublet model of type II*, *JHEP* **1307** (2013) 118, arXiv:1305.1649 [hep-ph].

[198] J. Bernon, J. F. Gunion, Y. Jiang, and S. Kraml, *Light Higgs bosons in Two-Higgs-Doublet Models*, *Phys.Rev.* **D91** no. 7, (2015) 075019, arXiv:1412.3385 [hep-ph].

[199] H. E. Haber and Y. Nir, *Multi-scalar models with a high-energy scale*, *Nuclear Physics B* **335** no. 2, (1990) 363 – 394.

[200] M. Gonzalez-Garcia and Y. Nir, *Neutrino masses and mixing: Evidence and implications*, *Rev.Mod.Phys.* **75** (2003) 345–402, arXiv:hep-ph/0202058 [hep-ph].

[201] E. Ma, *Naturally small seesaw neutrino mass with no new physics beyond the TeV scale*, *Phys.Rev.Lett.* **86** (2001) 2502–2504, arXiv:hep-ph/0011121 [hep-ph].

[202] S. Gabriel and S. Nandi, *A New two Higgs doublet model*, *Phys.Lett.* **B655** (2007) 141–147, arXiv:hep-ph/0610253 [hep-ph].

[203] F. Wang, W. Wang, and J. M. Yang, *Split two-Higgs-doublet model and neutrino condensation*, *Europhys.Lett.* **76** (2006) 388–394, arXiv:hep-ph/0601018 [hep-ph].

[204] S. M. Davidson and H. E. Logan, *Dirac neutrinos from a second Higgs doublet*, *Phys.Rev.* **D80** (2009) 095008, arXiv:0906.3335 [hep-ph].

[205] U. Maitra, B. Mukhopadhyaya, S. Nandi, S. K. Rai, and A. Shivaji, *Searching for an elusive charged Higgs boson at the Large Hadron Collider*, *Phys.Rev.* **D89** no. 5, (2014) 055024, arXiv:1401.1775 [hep-ph].

[206] R. N. Mohapatra and G. Senjanovic, *Neutrino Mass and Spontaneous Parity Violation*, *Phys.Rev.Lett.* **44** (1980) 912.

[207] Z. Maki, M. Nakagawa, and S. Sakata, *Remarks on the unified model of elementary particles*, *Prog.Theor.Phys.* **28** (1962) 870–880.

[208] **Planck** Collaboration, P. Ade *et al.*, *Planck 2013 results. I. Overview of products and scientific results*, *Astron.Astrophys.* **571** (2014) A1, arXiv:1303.5062 [astro-ph.CO].

[209] G. Steigman, K. A. Olive, and D. Schramm, *Cosmological Constraints on Superweak Particles*, *Phys.Rev.Lett.* **43** (1979) 239–242.

[210] S. Zhou, *Comment on astrophysical consequences of a neutrinophilic 2HDM*, *Phys.Rev.* **D84** (2011) 038701, arXiv:1106.3880 [hep-ph].

[211] **ATLAS** Collaboration, *Search for invisible decays of a Higgs boson produced in association with a Z boson in ATLAS*, .

[212] **CMS** Collaboration, *Search for the Higgs boson decaying to invisible particles produced in association with Z bosons decaying to bottom quarks*, .

[213] **ATLAS** Collaboration, G. Aad *et al.*, *Measurement of W^+W^- production in pp collisions at $\sqrt{s}$=7âĂĽâĂĽTeV with the ATLAS detector and limits on anomalous WWZ and WWÎş couplings*, *Phys.Rev.* **D87** no. 11, (2013) 112001, arXiv:1210.2979 [hep-ex].

[214] **ATLAS** Collaboration, G. Aad *et al.*, *Expected Performance of the ATLAS Experiment - Detector, Trigger and Physics*, arXiv:0901.0512 [hep-ex].